EXPERIMENTAL INVESTIGATION OF CO_2 ADSORPTION ON SELECT TURKISH LIGNITE COALS

A THESIS SUBMITTED TO
THE BOARD OF GRADUATE PROGRAMS
OF
MIDDLE EAST TECHNICAL UNIVERSITY, NORTHERN CYPRUS CAMPUS

BY

SYED MUHAMMAD HUSSAIN TURAB ALVI

IN PARTIAL FULFILLMENT OF THE REQUIREMENTS
FOR
THE DEGREE OF MASTER OF SCIENCE
IN SUSTAINABLE ENVIRONMENT AND ENERGY SYSTEMS PROGRAM

AUGUST 2023

Approval of the Board of Graduate Programs

Prof. Dr. Cumali Sabah

Chairperson

I certify that this thesis satisfies all the requirements as a thesis for the degree of Master of Science

Asst. Prof. Dr. Canras Batunlu

Program Coordinator

This is to certify that we have read this thesis and that in our opinion it is fully adequate, in scope and quality, as a thesis for the degree of Master of Science.

Dr.-Ing. Aykut Argönül	Asst. Prof. Dr. Doruk Alp
Co-Supervisor	Supervisor

Examining Committee Members

Prof. Dr. Salih Saner	NEU/PGE	
Asst. Prof. Dr. Canras Batunlu	METU NCC/EEE	
Asst. Prof. Dr. Doruk Alp	METU NCC/PNGE	

I hereby declare that all information in this document has been obtained and presented in accordance with academic rules and ethical conduct. I also declare that, as required by these rules and conduct, I have fully cited and referenced all material and results that are not original to this work.

Name, Last Name: Syed Muhammad Hussain Turab, Alvi

Signature:

ABSTRACT

EXPERIMENTAL INVESTIGATION OF CO_2 ADSORPTION ON SELECT TURKISH LIGNITE COALS

Alvi, Syed Muhammad Hussain Turab
Master of Science, Sustainable Environment and Energy Systems Program
Supervisor: Asst. Prof. Dr. Doruk Alp
Co-Supervisor: Dr.-Ing. Aykut Argönül

August 2023, 116 pages

Rapid industrialization and fossil fuel consumption are major contributors to greenhouse gas (GHG) emissions and ensuing global climate change. The concentration of CO_2, a GHG, in Earth's atmosphere has reached unprecedented levels. Contemporary studies assert that geological storage of CO_2 is among the most effective ways to curb GHG emissions to the atmosphere, with the aim of mitigating global climate change.

In this study we experimentally investigate CO_2 adsorption on three distinct Turkish lignite coals—namely, Çankırı, Elazığ–Sivrice, and Amasya–Merzifon. The volumetric method is employed to ascertain the CO_2 adsorption capacity at a constant temperature of 313.15 K (40 ^oC) and incremental pressures up to 85 bars. A compression setup is employed for compressing CO_2 gas above 60 bars, to achieve supercritical state. Data acquired from experiments is used to develop excess adsorption isotherms through Gibbs excess adsorption equation, facilitating observation of the interaction between CO_2 and the coal samples.

The study utilizes four adsorption models, (1) Langmuir modified, (2) Langmuir modified +k, (3) D-R modified, and (4) D-R modified +k, to fit the experimental results. The function of correction term ‘k’ is to account for and mitigate various measurement uncertainties. The Average Relative Error (ARE%) function is harnessed to compare model performances. All the sorption models fit the data with an ARE of less than ±9 %. Notably, the D-R modified model demonstrates the best fit. Furthermore, it has been observed that the drying of the samples before the experiment leads to moisture loss, resulting in visible shrinkage within the range of approximately 4 % - 9 % by volume.

Finally, the storage potential of the three coal seams is approximated using seam volume data from literature. Elazığ–Sivrice exhibits a maximum CO_2 storage potential of 6.28 Mt despite its relatively modest reserves. Çankırı follows with a storage capacity of 5.15 Mt, while Amasya–Merzifon showcases the least storage capacity with 1.08 Mt. The storage capacities are also estimated based on the CO_2 emissions from a typical 100 MW coal-fired powerplant as 10 years for Elazığ–Sivrice, 8 years for Çankırı, and 2 years for Amasya–Merzifon.

Keywords: Carbon dioxide, CO_2, Adsorption, Kinetics, Isotherms, Lignite, Coal, Sequestration.

ÖZ

SEÇİLİ TÜRK LİNYİT KÖMÜRLERİNDE CO_2 YÜZE TUTUNMASININ DENEYSEL İNCELEMESİ

Alvi, Syed Muhammad Hussain Turab
Yüksek Lisans, Sürdürülebilir Çevre ve Enerji Sistemleri Programı
Tez Yöneticisi: Dr. Öğr. Üyesi Doruk Alp
Ortak Tez Yöneticisi: Dr. Aykut Argönül

Ağustos 2023, 116 sayfa

Hızlı sanayileşme ve fosil yakıt tüketimi sera gazı (GHG) olan CO2'nun atmosferdeki yoğunluğunu daha önce görülmemiş seviyelere çıkarmıştır. Güncel çalışmaların ortaya koyduğu üzere, CO2'nin jeolojik olarak (yeraltındaki kayalarda) depolanması, küresel iklim değişikliğinin önünü alabilmek için sera gazı salınımını dizginlemenin en etkili yollarından biridir.

Bu çalışma, Çankırı, Elazığ-Sivrice ve Amasya-Merzifon bölgeleri olmak üzere Türkiye'de bulunan üç farklı linyit kömürü üstünde CO2 yüze tutunmasının (adsorpsiyonunun) deneysel incelemesini ele almaktadır. Linyit örneklerinin CO2 yüze tutunma sığası (adsorpsiyon kapasitesi) 313.15 K (40 ^{o}C) sabit sıcaklıkta ve 85 bara kadar artan farklı basınçlarda hacimsel yöntem ile saptanmıştır. CO2 gazının 60 bar üstüne çıkarak superkritik faza geçmesi için deney düzeneğine el pompası eklenmiştir. Deneyde toplanan basınç verileri Gibbs'in ilgili denklemine konularak aşırı yüzey tutunum eğrileri çizmekte kullanılmıştır. Böylece, gaz ve süperkritik fazda CO2 ile kömür örnekleri arasındaki etkileşim incelenmiştir.

(1) Modifiye Langmuir, (2) modifiye Langmuir +k, (3) modifiye D-R ve (4) modifiye D-R +k olmak üzere dört adsorpsiyon denklemi deney verilerini

modellemek üzere kullanılmıştır. Düzeltme terimi olan 'k', deneysel belirsizlikleri hesaba katmak için modellere eklenmiştir. Modelleri karşılaştırmak için Ortalama Göreceli Hata (ARE %) hesaplanmıştır. 4 Adsorpsiyon modelinde de ± % 9'dan az ARE gözlenmiştir. Özellikle modifiye D-R modeli en az ARE göstermiştir. Ayrıca, deney öncesi numunelerin kurutulmasının nem kaybına yol açarak yaklaşık % 4 - % 9 aralığında gözle görülür bir büzülmeye neden olduğu gözlemlenmiştir.

Çalışma sonunda bu üç kömür damarının depolama potansiyeli hesaplanmıştır. Elazığ-Sivrice, nispeten mütevazı rezervlerine rağmen 6.28 Mt azami CO2 depolama potansiyeli sergilemektedir. Ardından Çankırı 5.15 Mt depolama kapasitesiyle gelirken, Amasya-Merzifon 1.08 Mt ile en az depolama kapasitesine sahiptir. Buna göre, Elazığ-Sivrice 10 yıl, Çankırı 8 yıl ve Amasya-Merzifon 2 yıl süre ile 100 MW'lık bir kömür termik santralinin CO2 salınımını depolayabilir.

Anahtar Kelimeler: Karbondioksit, CO2, Yüzeye tutunma, Kinetik, İzoterm, Linyit, Kömür, Saklama.

This thesis is dedicated to my parents, Syed M. Asghar Abbas Alvi and Dr. Tahira Tehseen, and to my beloved siblings, Naiha Fatima, and Zara Rubab. Their unwavering love, encouragement, and sacrifices have been my guiding light throughout this academic journey.

ACKNOWLEDGMENTS

First and foremost, my deepest appreciation goes to my thesis supervisor, Dr. Doruk Alp, for his unwavering support and guidance throughout my academic journey. Dr. Alp has been a constant source of inspiration since our first meeting seven years ago during my undergraduate studies. From course advising to thesis supervision, he has played a pivotal role in shaping my academic and professional growth. His mentorship and motivation have been invaluable, and I am profoundly thankful for his care and concern, which extended beyond academic matters.

I extend my heartfelt thanks to my co-supervisor, Dr.-Ing. Aykut Argonul, for his trust in me to contribute to the research in the field of CO_2 adsorption on coals. Working under his mentorship has been a privilege, and his guidance has been crucial in developing my critical thinking skills in research. Despite our limited time together, Dr. Argonul's dedication to his students has left an indelible mark, and I am grateful for his unwavering support.

I am indebted to Mr. Hasan Okaygun, in-charge for the laboratory, and Mr. Ozan Asilkan, in charge of the machine lab, for their unwavering assistance and support during my research. Their patience and willingness to accommodate my needs and challenges were instrumental in the successful completion of my work. Their guidance, access to essential labs and equipment, and unwavering support have been indispensable.

To my friends and fellow students, I extend my thanks for being a significant part of my academic journey. Your companionship and support have turned these years into cherished memories. You are not just friends; you are family, and I will always hold you close in my heart.

Last but certainly not least, my profound gratitude goes to my parents for their unwavering trust and support. Their sacrifices and love have been the driving force behind my achievements in life. I owe my success to their enduring belief in me.

“Praise be to Allah, who blessed us to be among -those who cling and hold to the "Wilayaat" (love, friendship, and authority) of Ameer Al Momineen and all the Imams, peace be on them all.”

TABLE OF CONTENTS

LIST OF TABLES

TABLES

LIST OF FIGURES

FIGURES

LIST OF ABBREVIATIONS

ABBREVIATIONS

ARE	Average Relative Error
ASTM	American Society for Testing Materials
BET	Brunauer, Emmett, and Teller Equation
CCS	Carbon Capture and Storage
D-R	Dubinin-Radushkevich
Daf	Dry, Ash Free Basis
DOE	Department of Energy
ECBM	Enhanced Coal Bed Methane
EU	European Union
FC	Fixed Carbon
GHGs	Greenhouse Gasses
HR	Huminite Reflectance
IEA	International Energy Agency
IPCC	Intergovernmental Panel on Climate Change
IUPAC	International Union of Pure and Applied Chemistry
MTA	General Directorate of Mineral Research and Exploration
Mt	Metric Ton
NOAA	National Oceanic and Atmospheric Administration
pm	Pico meter
ppm	Parts per million
SGGs	Sustainable Development Goals
SEM	Scanning Electron Microscopy
TKI	General Directorate of Turkish Coal Enterprises
TVFM	Theory of Volume Filling of Micropores
UNFCCC	United Nations Framework Convention on Climate Chang

LIST OF SYMBOLS

SYMBOLS

ρ_a	Adsorbed phase density	mol/cc
ρ_g	Free gas phase density	mol/cc
ρ_{coal}	Coal density	g/cc
ρ_w	Water density	g/cc
ρ_o	Organic fraction density	g/cc
Ø	Cleat porosity	
Γ	Total amount of gas per unit area	mol/m^2
β	Affinity coefficient	
R	Universal gas constant	$cc.bar.K^{-1}.mol^{-1}$
M_∞	Total amount of CO_2 adsorbed at infinite time.	mmol/g
M_t	Total amount of CO_2 adsorbed at time 't'.	mmol/g
P_{RC}	Pressure in reference cell	bars
P_{SC}	Pressure in sample cell	bars
P_o	Saturation vapor pressure of the adsorbate	bars
P_L	Langmuir pressure	bars
V_{RC}	Volume in in reference cell	cc
V_{SC}	Volume in sample cell	cc
V_{coal}	Volume of coal seam	m^3
V_{Void}	Void volume in sample cell	cc
V_{ske}	Volume of coal sample	cc
V_L	Langmuir volume	cc/g
E_o	Characteristic heat of adsorption	kJ/mole
Z	Compressibility factor for gas	

CHAPTER 1

INTRODUCTION

The Earth is currently confronted with a significant and urgent challenge about global climate change, primarily attributed to the escalating levels of greenhouse gases present in the Earth's atmosphere. The greenhouse effect is a naturally occurring phenomenon characterized by the absorption and re-emission of solar radiation within the thermal infrared range of 0.75-15μm by specific gases referred to as "greenhouse gases." These gases function like a thermal blanket, trapping heat in the lower atmosphere (Perera et al., 2011). This phenomenon contributes to the escalation of earth's surface temperatures, commonly known as "global warming," a subject that has been extensively discussed and analyzed by researchers on a global scale (Green, 1992).

The ramifications of global warming have reached a critical level, as evidenced by numerous reports highlighting its detrimental effects on the natural environment and the well-being of humans (Izrael et al., 2007; Perera, 2018). The primary contributors to the increased concentrations of atmospheric carbon dioxide are human activities, specifically the combustion of fossil fuels and deforestation (Kaliyavaradhan & Ling, 2017). In the past century, there has been an observed increase in the average global temperature by approximately 1 °C due to global warming. This ongoing trend is further exacerbated by the rapid growth in industrial activities (Perera et al., 2011).

1.1 CO_2 emissions leading to climate change

The increase in CO_2 concentrations is a matter of significant concern due to its status as the predominant greenhouse gas in the Earth's atmosphere. This rise in CO_2 levels

is primarily attributed to various industrial activities, such as the generation of electricity through the combustion of coal (Hanak et al., 2015). The share of fossil fuels in the energy portfolio continues to account for over 80% and research indicates that fossil fuels will retain their position as the dominant energy source for the foreseeable future, spanning few decades (Ediger, 2019). Apart from the use of fossil fuels, deforestation is another cause for the increased concentration of CO_2 in the atmosphere. As a result, considerable attention has been directed towards the mitigation of global warming by targeting the reduction of atmospheric CO_2 levels, given the significant quantities of CO_2 that are emitted into the atmosphere on a daily basis through several human activities (Perera, 2018).

According to the annual report published by the National Oceanic and Atmosphere Administration (NOAA) global monitoring lab, the average global atmospheric concentration of CO_2 reached 417 ppm in 2022, establishing a new record peak, (Figure 1.1). Notably, there was an increase of 2.13 ppm between 2021 and 2022, marking the 11^{th} consecutive year with a rise of more than 2 ppm in atmospheric CO_2 levels (NOAA, 2023; NASA, 2023). The consequences of exceeding the critical threshold of 450 ppm of CO_2, known as the point-of-no-return, can be very serious. Scientists predict that this event could result in a significant increase in the Earth's mean temperature, approximately by 2 °C (Den Elzen & Meinshausen, 2006; IEA, 2013). The potential consequences of such a rise are alarming and could have far-reaching implications. The current environmental issues that we face include the rapid melting of glaciers causing rise in sea levels, a significant reduction in biodiversity, heightened health risks, extreme weather conditions, and the devastating disruption of ecosystems (Donnelly et al., 2017).

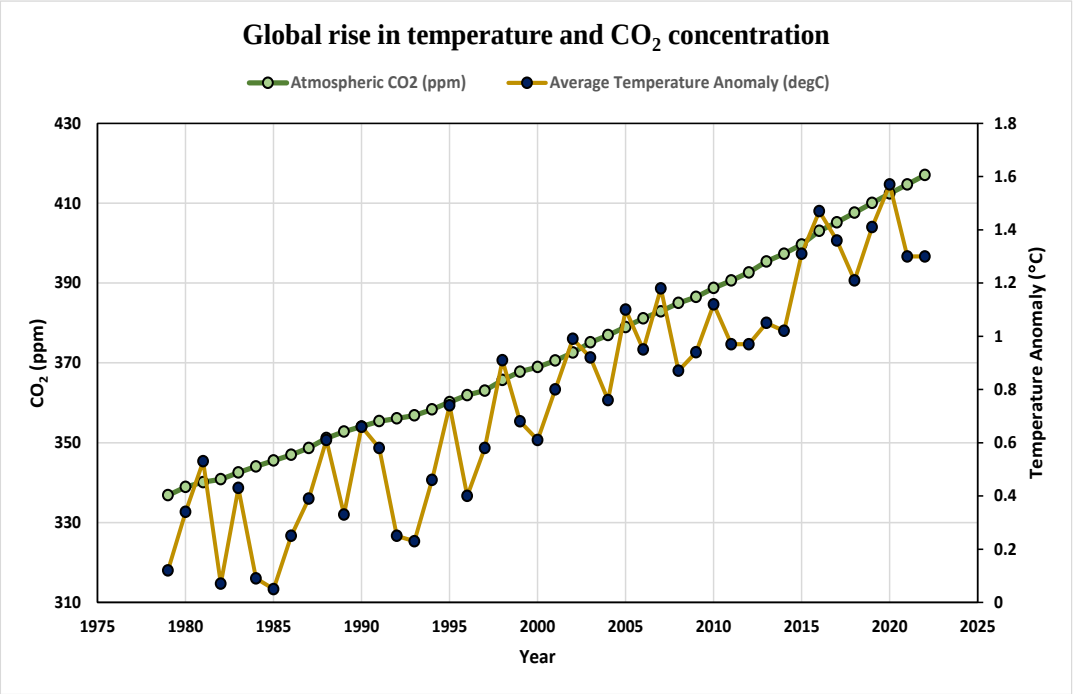

Figure 1.1. Atmospheric CO_2 concentration.

Numerous strategies for mitigating these emissions and controlling global warming have been extensively investigated in response to the pressing imperative of reducing greenhouse gas emissions. The significance of maintaining the average global temperature increase below 2 °C by the year 2100 has been underscored to mitigate extreme climate change events (Metz & Intergovernmental Panel on Climate Change, 2005). The European Union and the G8 have established specific objectives to substantially reduce greenhouse gas emissions by 2050 (International Energy Agency, 2009). In a similar way, the Paris Agreement of 2015 aimed to constrain the rise in global temperatures to a level below 2° above pre-industrial levels (Hulme, 2016).

1.2 Sustainable development goals and SDG 7-Climate Action

The year 2015 was a significant milestone in the endeavor for sustainable development, as it witnessed the adoption of the United Nations' Sustainable Development Goals (SDGs) within the framework of the agenda 2030 for Sustainable Development, Figure 1.2. Simultaneously, the Paris Agreement, a global climate accord established within the framework of the United Nations Framework Convention on Climate Change (UNFCCC), was designed to constrain the rise in global temperatures to a level below 2°C (United Nations, 2015). The interconnection between climate action and sustainable development is emphasized in this integration, leading scholars, and policymakers to investigate the ways in which climate actions can contribute to the attainment of Sustainable Development Goals (Fuso Nerini et al., 2019).

Figure 1.2. SDGs and climate action (Modified from Martin, 2015).

SDG-13 encompasses the objective of Climate action, focusing on the United Nations Framework Convention on Climate Change (UNFCCC) as the principal international forum for tackling climate change worldwide. The importance of SDG-13 goes beyond its main aim of dealing with climate change. By using climate actions together with sustainable production and consumption, energy, industry, and infrastructure in a strategic manner, it is possible to address other significant Sustainable Development Goals (SDGs) at the same time (United Nations, 2018; Nilsson et al., 2018). Researchers have investigated various potential solutions to

reduce atmospheric CO_2 levels originating from both industrial sources and natural processes. These solutions encompass a spectrum of strategies, including enhancing energy efficiency, promoting the adoption of renewable energy sources, bio-sequestration and exploring geoengineering techniques for CO_2 mitigation (Dutta et al., 2008; Leung et al., 2014).

Among the various alternatives considered, **Carbon Capture and Storage** (CCS) stands out as a viable and auspicious approach. CCS plays a crucial role in deep decarbonization scenarios by effectively mitigating CO_2 emissions from primary point sources, such as power generation utilities and energy-intensive industries like cement kiln plants (Leung et al., 2014). According to estimates, implementing CCS technology alone can achieve a nearly 20% reduction in emissions by the year 2050. Conversely, the absence of CCS could lead to a substantial 70% increase in the global cost required to attain emission reduction targets. (Aminu et al., 2017).

CCS can significantly contribute to SDG-7, which focuses on ensuring access to affordable and clean energy, and SDG-9, which emphasizes the importance of industry, innovation, and infrastructure (Coenen et al., 2022). As such, CCS plays a crucial role in the broader climate action agenda, working in harmony with sustainable development objectives.

1.3 Carbon Capture and Storage (CCS) options

Carbon capture and storage (CCS) encompasses a comprehensive process involving the collection, transportation, and secure disposal of CO_2 emissions from various sources, including industrial facilities, before permanently storing them in underground reservoirs. These geological formations, such as deep saline aquifers, depleted oil and gas reservoirs, methane hydrate reservoirs, shales, and coal seams, have emerged as potential storage sites for sequestering CO_2 (Corum et al., 2013; Aminu et al., 2017).

Geological storage projects worldwide have primarily focused on saline aquifers and depleted oil and gas reservoirs. Nevertheless, the integration of CCS projects into sustainable development agendas is crucial for effectively addressing climate change. In this context, the United States Department of Energy has invested significantly in CCS initiatives known as the carbonSAFE projects with a primary focus on developing geological storage options capable of storing over 50 megatons (Mt) of carbon dioxide from industrial sources across the nation. Such projects stand as a testament to the ongoing commitment towards addressing the pressing concern of climate change and the pursuit of attaining carbon neutrality (Sullivan et al., 2020).

The process of CCS involves distinct stages, including carbon capture, transportation, and final sequestration in geological formations as illustrated in Figure 1.3. Carbon capture techniques encompass cryogenic separation, adsorption/abstraction, and membrane separation, enabling the extraction of CO_2 from flue gases emitted by power plants. The captured CO_2 is subsequently compressed and transported through either pipelines or ships to a nearby geological storage site, where it is injected into the chosen formation through a deep borehole for permanent sequestration. This technique, known as sequestration or storage, relies on various geological sinks, such as deep saline formations, depleted oil and gas reservoirs, and non-mineable coal seams (Figueroa et al., 2008; Al Hameli et al., 2022). The phase envelope of CO_2 and the corresponding pressure-temperature (P-T) ranges for both transportation and geological storage are depicted in Figure 1.4.

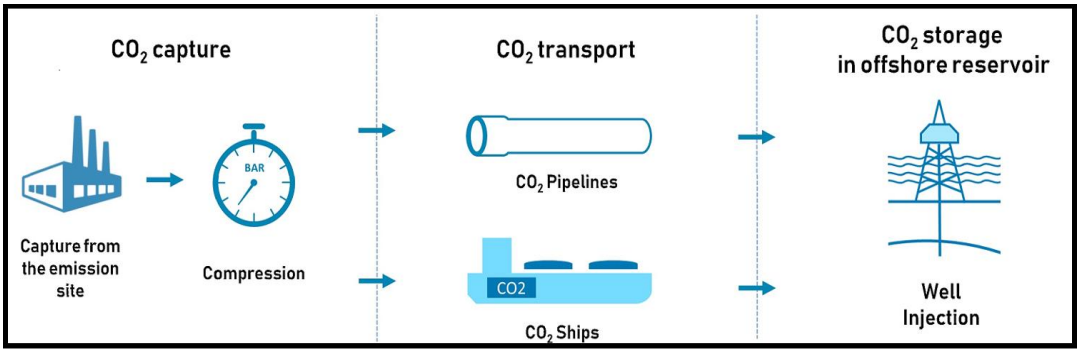

Figure 1.3. CCS stages. (Modified from Ansaloni et al., (2020))

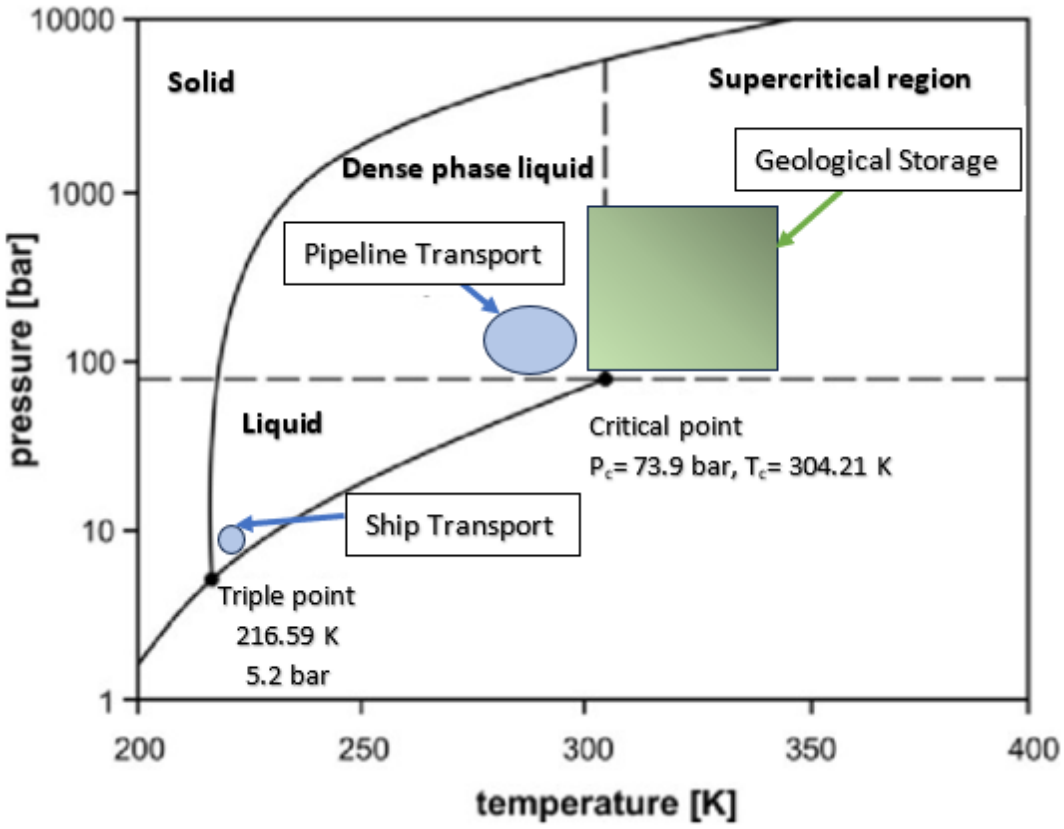

Figure 1.4. Phase envelope of CO_2 and range for CCS application (Modified from Witkowski et al., (2014)).

There is huge potential for carbon dioxide (CO_2) sequestration in non-mineable coal seams, making them an attractive option among geological sinks. These coal beds tend to absorb CO_2 more readily than methane, which is beneficial for enhanced coal bed methane recovery (ECBM) and as a storage medium for CO_2 (Talapatra, 2020). Implementing carbon capture and storage (CCS) technology in coal seams has the potential to improve methane production while effectively sequestering CO_2. Additionally, the proximity of many power plants to coal seams makes this approach even more feasible and cost-effective (Ozdemir, 2004; Corum et al., 2013).

1.3.1 CO_2 storage in coal seams

Investigating CO_2 adsorption in coal seams has emerged as a promising approach for carbon storage, contributing to developing sustainable energy solutions and mitigating climate change. Coalbeds, known for their dual role as both source and reservoir rocks for coalbed methane (CBM), offer potential as storage sites for anthropogenic CO_2. The CO_2 storage process in coal beds depends on various mechanisms, including adsorption within micropores, free gas in cleats or fractures, and the dissolution of gas in groundwater within coal fractures. Adsorbed gas molecules within micropores are the predominant mechanism accountable for more than 90% of gas storage in coalbeds (Gray, 1987).

Non-mineable coal seams, which may be economically unfeasible due to factors such as thickness, depth, sulfur content, or calorific value, present a particularly attractive option for CO_2 sequestration. The fundamental concept of carbon dioxide sequestration in coal beds is predicated on the higher affinity of coal to gaseous CO_2 relative to methane. The process of enhanced coalbed methane (ECBM) recovery involves the injection of CO_2 into the coal matrix, which results in the displacement of adsorbed methane in a competitive manner. This displacement leads to the permanent storage of CO_2 and simultaneously enhances methane production (Shukla et al., 2010).

The sorption behavior of CO_2 in coal is influenced by several factors, including coal type, environmental conditions, and adsorption energy (Cui et al., 2004). The adsorption capacity and retention ability of coal for CO_2 play pivotal roles in determining the success of CO_2 storage in coal seams. Experimental evidence indicates that CO_2 molecules exhibit a preferential adsorption over methane, with the adsorption ratio varying across different coal types. In general, the coal matrix is composed of **macropores**, commonly known as cleats, and **micropores** that enable the diffusion and the storage of gases. Cleats act as the natural fractures in coal to enhance the permeability and gas flow within the coal. Whereas micropores contribute as an important site for gas adsorption and storage. The matrix has a dual-

porosity system, macro-porosity in large cleats or fractures, and microporosity in small pores. Movement of gases in the coal seam occurs through the fractured porous network, with gases being adsorbed in the micropores and trapped in the cleat system (Hadi Mosleh et al., 2018). Understanding the transformational processes that transpire when CO_2 is injected into coal seams is essential for comprehending the storage and transport characteristics of CO_2.

CHAPTER 2

COAL STRUCTURE AND COMPOSITION

Understanding the structure and composition of coal is of vital importance in the fields of sustainable energy and environmental science. Coal, as an essential fossil fuel, holds considerable importance in worldwide energy generation. (Burnard, 2003). There has been a growing concern in contemporary society regarding climate change and its direct correlation with the release of GHG, specifically carbon dioxide, primarily attributed to the combustion of fossil fuels such as coal (Edwards, 2020). To effectively develop strategies for reducing CO_2 emissions and improving CCS technology, it is imperative to get a comprehensive understanding of the microscopic and macroscopic characteristics of coal, as well as its distribution of pore sizes. Variations in coal ranks, lithotypes, and mineral matter result in varying CO_2 adsorption capacities, which can affect the effectiveness of the sequestration process. Thus, it is important to have a complete understanding of coal's structural properties to determine its ability to adsorb CO_2 (Klunk et al., 2018). The objective of this chapter is to provide a detailed analysis of the complex characteristics of coal structure and composition, with a particular focus on their relevance to the study of CO_2 adsorption.

2.1 The geological genesis of coal

The formation of coal is a complex and captivating geological process that extends over millions of years and is intricately connected to the Earth's history. The process of coal formation begins with the accumulation of plant debris in wetlands such as swamps, fens, and bogs, where the complete decomposition of organic material is impeded by the presence of water and sediments (Haenel, 1992). In these wetland plants, leaves and stems die and fall into the water and they undergo anaerobic

bacterial action and transform into peat (Stracher et al., 2015). Over time, the accumulated peat experiences a process of burial under new sediments, resulting in pressure, temperature, and exposure to tectonic stresses. These factors are responsible for inducing chemical and physical changes that give rise to a phenomenon commonly referred to as “coalification” (Liu et al., 2018). During coalification, peat undergoes a series of geochemical transformations leading to the formation of various coal ranks, including lignite, sub-bituminous, bituminous, semi-anthracite, and anthracite. These ranks are determined by the extent of diagenesis experienced by peat, as expressed below (Mathews & Sharma, 2012). 'Brown coal' refers to low-rank coals such as lignite and sub-bituminous coal, while 'black' or 'hard' coal refers to higher-rank coals such as bituminous, semi-anthracite, and anthracite.

Peat ⟶ Lignite ⟶ Subbituminous coal ⟶ Bituminous coal ⟶ Anthracite

The coalification process, as shown in Table 2.1, encompasses a series of consecutive reactions originating from the primary material, which is the live plant serving as the fundamental constituent of coal.

Table 2.1. Coalification process of different ranks of coal (Miller, 2017).

Materials	Partial Processes	Main chemical reactions
1. Vegetation	Peatification	Bacterial and fungal life cycles
2. Peat	Lignitification	Air oxidation, followed by decarboxylation and dehydration
3. Lignite	Bituminization	Decarboxylation and hydrogen disproportioning
4. Bituminous coal	Preanthracitization	Condensation in small aromatic ring systems

5.	**Semi anthracite**	Anthracitization	Condensation of small aromatic rings into larger ones; dehydrogenation
6.	**Anthracite**	Graphtization	Complete carbonification

2.2 Coal maceral

A maceral refers to the fundamental composition of coal that is discernible and identifiable when observed through a microscope. Macerals are organic substances originating from plant tissues that have become part of the sedimentary layers and undergone decomposition, compaction, and chemical transformations due to geological stresses. This organic material exhibits significant heterogeneity, prompting the development of a comprehensive classification system to categorize its various constituents (Bustin et al., 1985).

The macerals are classified into three distinct groups, namely **vitrinite**, **liptinite** (also referred to as exinite), and **inertinite**, in a systematic manner. The categorizations primarily rely on visual attributes, chemical composition, and optical properties. The vitrinite maceral group observed in low-rank coals, such as lignite and subbituminous coals, is referred to as '**huminite**'. It is considered to be equivalent to and the precursor of the vitrinite macerals present in higher rank coals (Thomas, 2013). Macerals are further divided into sub-macerals based on their diverse morphologies and origins. Table 2.2 presents a comprehensive overview of the specific characteristics of the sub-macerals obtained from McCabe (1984).

Table 2.2. Classification of macerals based on morphology and origin (McCabe, 1984).

Maceral Group	Maceral types, their morphology, and origin
Vitrinite or Huminite	Telinite: Obtained from cellular structures of trunks, branches, roots, and leaves.
	Collinite: Structureless form, arises from the precipitation of dissolved organic matter.
	Vitrodetrinite: Fragments of vitrinite, tracing back to the initial stages of degradation of plant matter and humic peat.
	Spronite: Type of fossilized material consists of mega-micropores and their associated structures.
	Cutinite: Composed of bands with possible appendages, derived from the outer layer of leaves and shoots.
Liptinite	Resinite: Commonly found in cell filling layers or dispersed material from plant resins and waxes.
	Alganite: Fossilized form of algae.
Inertinite	Liptodetrinite: Consists of fragments of Exinite, which are formed due to the degradation of organic residues.
	Fusinite: Characterized by a cellular structure that is either empty or filled with minerals. Composed of plant material that has undergone oxidation.
	Semifusinite: Plant material that undergoes partial oxidation
	Macrinite: An amorphous cement-like structure originating from oxidized gel material.
	Inertodetinite: Consists of small patches of fusinite, semi-fusinite, or macrinite.

2.2.1 Various ranks of coal

The classification of coals based on rank relies on the degree of coalification, which represents progressive changes from the original peat precursor. However, various countries may adopt different classification systems due to the diverse causes of coalification and specific application requirements. The classification process serves different purposes, such as geological assessment, mining and development, commercial transactions, and industrial applications. The American Society for Testing Materials (ASTM) sets standards that are widely used to rank coal. These standards include tests to analyze how metamorphism changed properties like calorific value, volatile matter, moisture, ash, and fixed carbon (ASTM, 2011).

As coals mature from peat to anthracite, significant changes occur in their physical and chemical properties. Low-rank coals, like lignite and subbituminous coals, are softer with higher moisture and lower carbon content, resulting in limited energy production and applications. In contrast, higher-rank coals are harder, stronger, and have more carbon and less moisture, making them valuable for diverse applications. Anthracite, the highest rank, boasts the highest carbon and energy content and the lowest moisture, rendering it the most calorific (Flores, 2014).

Coal ranks are identified using vitrinite reflectance (R%), fixed carbon content (FC), and volatile matter percentage (VM%) for higher-rank coals, while calorific value and moisture content may distinguish lower-rank coals. With increasing rank, coal experiences changes in carbon, oxygen, and hydrogen content, as well as volatile matter, calorific value, aromaticity, and vitrinite reflectance (Bratek et al., 2002; Li et al., 2013). These variations in coal properties have significant implications for its applications and utilization.

2.2.2 Structure and Pore distribution of coal

Coal possesses a dual porosity system consisting of micropores and macropores (cleats), with the former representing the void volume within the coal matrix. Cleats or the natural fractures will be used as a terminology for the macropores to avoid confusion with the ‘macropore’ relating to the largest pore of the micropores. Cleats, the primary and dominant fracture system, include face and butt cleats, with face cleats being continuous and widely spaced, while butt cleats are less continuous and often terminate at face cleats, as depicted in Figure 2.1 (Laubach et al., 1998).

The coal matrix contains pores of various sizes, classified into four categories, mentioned in Table 2.3. Sub-micropores, characterized by diameters smaller than 0.8nm; micropores, which have diameters ranging from 0.8 to 2nm; mesopores, exhibiting diameters ranging from 2 to 50nm; and macropores, possessing diameters exceeding 50nm. The presence of smaller pores facilitates a significant internal surface area, enabling coal to serve as a potential reservoir for CO_2 and CH_4 adsorption (White et al., 2005; Thomas, 2013). According to Grey (1987), a significant proportion of the gas present in coal is contained within micropores. Various techniques, including mercury intrusion, thin section analysis, image analysis, and gas adsorption, are employed to analyze pore size and distribution. The fluid probe method is commonly utilized in laboratories, using gases like He, CO_2, N_2, and CH_4 to observe the porosity. Helium gas, is however, preferred for coalbeds containing micropores due to its small molecular size and inert nature (Laubach et al., 1998). The estimated range for cleat-fracture porosity in coal is between 0.5% and up to 2.5% (Purl et al., 1991).

Table 2.3. Pore size distribution in coal

Pore Types	Size (width), nm
Sub-micropores	< 0.8 nm
Micropores	0.8-2 nm
Mesopores	2-50 nm
Macropores	>50 nm

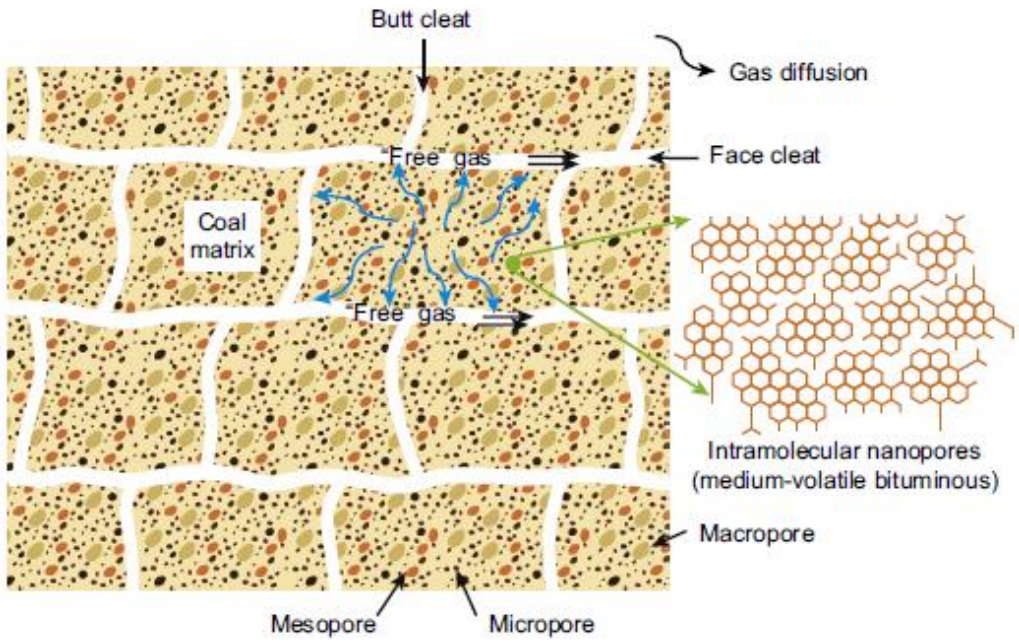

Figure 2.1. Dual-porosity coal matrix showing cleats and pores of various sizes (Flores, 2014)

The composition of porosity varies with coal rank, with lignite and subbituminous coals exhibiting sparse and poorly developed cleats, while bituminous coals possess well-ordered face and butt cleats. Anthracitic coals have fewer, widely spaced cleats due to matrix metamorphosis. Micropores make up a significant portion of coal porosity, but their accessibility to gas adsorption may be limited. The permeability of coal-bed methane extraction is affected by the density and size of cleats, while the spacing between cleats varies depending on the rank of the coal (Seidle, 2011).

The complex interplay between pore size distribution, coal structure, and gas adsorption behavior is essential for effectively utilizing coal as a storage medium for gases and developing sustainable energy and environmental solutions (Klunk et al., 2018).

CHAPTER 3

ADSORPTION OF CO2 ON COAL: CONCEPT AND MECHANISM

Adsorption is a phenomenon that occurs when the molecules or atoms from a gaseous or liquid state adhere to the surface of a solid material due to attractive forces between the two. The process is exothermic in nature and occurs due to the intermolecular forces of attraction between the adsorbate, which refers to the substance being adsorbed, and the adsorbent, which pertains to the material onto which adsorption takes place. Adsorption processes are crucial in various scientific and industrial applications, including gas separation, catalysis, wastewater treatment, and environmental remediation such as carbon capture and storage (Zhou et al., 2019; Gbenou et al., 2021). The adsorption phenomenon can be classified into four distinct categories, which are determined by the interface between the adsorbent and the adsorbate. These categories include solid/gas, solid/liquid, liquid/liquid, and liquid/gas. Solid-gas adsorption has been the subject of extensive study and research, making significant contributions to the field of interface chemistry. Therefore, when discussing adsorption or solid adsorption, the term solid-gas adsorption is commonly utilized (Wang & Hao, 2017).

3.1 Gas adsorption

Gas adsorption is a complex process that occurs when a solid substance is subjected to a gas or vapor, leading to the accumulation of gas molecules on the surface of the adsorbent. The term used to describe gas adsorption can be interchangeable and may vary depending on the context. The term “Adsorption’ is commonly used to refer to the phenomenon of gases condensing on the surfaces that are exposed. On the other hand, ‘absorption’ or ‘imbibition’ are terms used to describe the process by which gas molecules penetrate the interior of the solid material that absorbs them (Ozdemir,

2004). To provide clarity, the International Union of Pure and Applied Chemistry (IUPAC) has established a universally acknowledged definition of ‘adsorption’ as the process by which one or more constituents are concentrated within an interfacial layer (IUPAC, 1976). Adsorption can be categorized into two distinct forms based on the strength of interaction between the two phases: physical adsorption and chemical adsorption.

3.1.1 Physical adsorption

Physical adsorption, also known as physisorption, occurs due to the presence of weak intermolecular forces between adsorbent and adsorbate such as van der Waals and electrostatic interactions. These forces are caused by transient dipoles formed in the adsorbate and the corresponding induced dipoles in the adsorbent. Physical adsorption usually takes place at relatively low temperatures and pressures. The forces involved are relatively weak and can easily be desorbed from the surface when conditions change, making it a reversible process. The term desorption refers to the removal of previously adsorbed molecules from the solid surface (Steele, 1993). In physisorption of gases, monolayer coverage occurs at low pressures but under high pressure and temperature conditions, the gas molecules can be adsorbed in excess through multi-layers or filling of micro pores (IUPAC, 1976).

3.1.2 Chemical adsorption

Chemical adsorption, also known as chemisorption, entails the formation of more robust chemical bonds between the adsorbate and adsorbent. The process of bonding frequently involves the transfer or sharing of electrons, resulting in a much stronger and more permanent attachment. The bonding which can be covalent, hydrogen, or ionic, typically takes place under high temperatures and pressures and is generally considered as an irreversible process in comparison to physical adsorption. Generally monolayer structure is formed in chemical adsorption, wherein the adsorption

process terminates once all the active sites on the surface are completely occupied (IUPAC, 1976; Choi et al., 2001).

3.2 Adsorption isotherms

The process of adsorption can be characterized by the adsorption isotherm, which depicts the correlation between the quantity of adsorbate present on the adsorbent and its equilibrium concentration in the surrounding medium against pressure, while maintaining a constant temperature (Dąbrowski, 2001). The amount of gas adsorbed by a solid sample is contingent upon several factors, including the mass, temperature, pressure, and the characteristics of both the solid and the gas. There are several types of adsorption isotherms that have been identified and categorized based on their characteristics.

The classification of adsorption isotherms holds significant importance in understanding the dynamic adsorption behavior. The international Union of Pure and Applied Chemistry (IUPAC) has developed a widely utilized classification system that encompasses six primary types of adsorption isotherms (Figure 3.1): Type I, Type II, Type III, Type IV, Type V, Type VI.

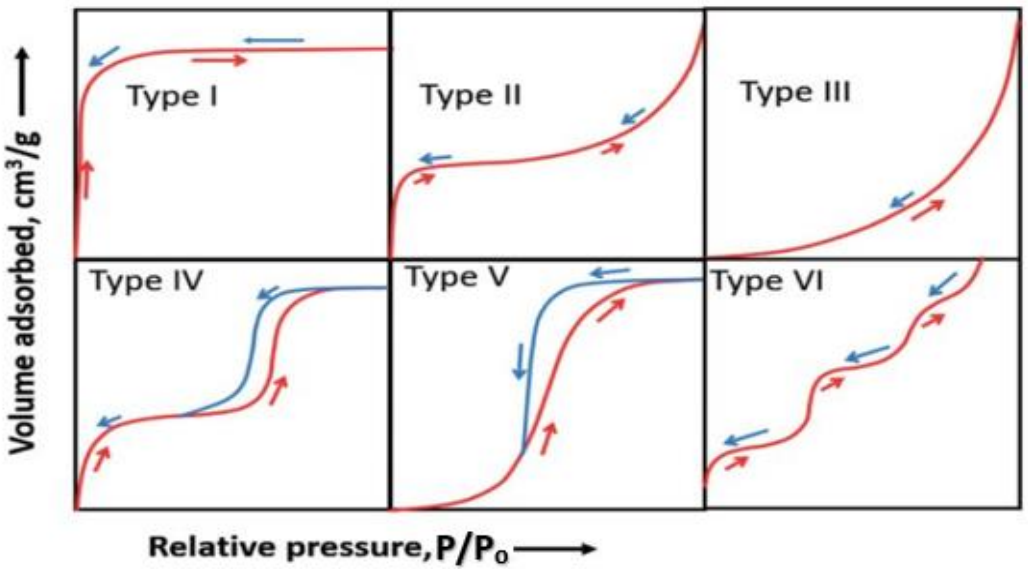

Figure 3.1. IUPAC classification for adsorption isotherms (Kumar et al., 2019).

Type I isotherm is observed when a layer of adsorbate molecules forms on a solid surface that has micropores, or when the adsorption process is primarily influenced by the filling of micropores. The isotherm is commonly referred to as the Langmuir type. The assumption is made that the molecules are being adsorbed to form a monolayer that covers the entire surface, a phenomenon commonly observed in microporous solids such as CO_2 adsorption isotherms (Haul, 1982; Dąbrowski, 2001).

Type II isotherm is observed in adsorbents that are nonporous or macroporous. It is distinguished by the presence of an inflection point, which indicates the saturation of the monolayer and the initiation of the formation of multiple layers (Donohue & Aranovich, 1998).

Type III isotherm is commonly observed in situations involving non-porous or macroporous adsorbents, where there are weak interactions between the adsorbent and adsorbate (Donohue & Aranovich, 1998).

Type IV isotherm, which is commonly observed in mesoporous adsorbents, exhibits a hysteresis loop caused by capillary condensation, similar to the Type II isotherm (Andersen, 1968).

Type V isotherm is commonly observed in situations involving non-porous or macroporous adsorbents, where the interactions between the adsorbent and adsorbate are relatively weak (Andersen, 1968).

Type VI isotherms are rarely observed and is characterized by a series of stepped isotherms. It is classified according to the IUPAC classification (Haul, 1982).

3.2.1 Adsorption kinetics

The term “adsorption kinetics” pertains to the rate at which the substance binds or adheres to the surface of another material, which is commonly referred to as an adsorbent. Adsorption kinetics plays an important role in comprehending the

mechanism of adsorption and optimizing the rate at which gas molecules engage with the surface of a solid adsorbent and subsequently undergo adsorption (Zhang et al., 2016). Several scholarly investigations have examined the kinetics of CO_2 adsorption on coal and its associated materials. The adsorption rate of CO_2 onto coal is contingent upon various factors, including temperature, pressure, surface area, porosity of the coal, and the characteristics of the gas solid interactions (Clarkson & Bustin, 1999; Busch et al., 2004). The rate is commonly denoted as the difference between the total amount of CO_2 adsorbed at infinite time (M_∞) and total amount of CO_2 adsorbed at time 't' (M_t) divided by the M_∞ (Song et al., 2015). The expression is shown in Equation 3.1.

$$Adsorption\ rate = \left(\frac{M_\infty - M_t}{M_\infty}\right) \quad 3.1$$

The study conducted by Ramasamy et al., (2014) investigated the adsorption of CO_2 on different coal types and revealed a strong correlation between the adsorption capacity and coal properties. Moreover, existing literature indicates that the coal-CO_2 affinity is twice that of methane. Due to various factors such as the linear molecular structure of CO_2, its small molecular diameter, high adsorption affinity, large quadruple moment, and low activation energy leads to the desorption of methane from coal by carbon dioxide (Wojtacha-Rychter & Smoliński, 2017).

3.3 Adsorption equilibrium models

To understand the mechanism of adsorption of gases on solid surfaces, various models have been suggested in literature over the years based on the type of adsorption isotherm as illustrated in Figure 3.2. These models serve to establish the correlation between the amount of adsorbate molecules present on the adsorbent and the concentration of gas phase at equilibrium. To describe the CO_2 adsorption behavior on coal, inclusion of some of the isotherm models with two and three parameters are discussed here. Langmuir monolayer model, BET muti-layer model, and Dubinin's pore filling model are frequently utilized in literature and will be

further explained in the subsequent sections (Sakurovs et al., 2007; Gensterblum, 2013; Ayawei et al., 2017; Iftekhar et al., 2018).

3.3.1 Langmuir isotherm

In 1918, Irving Langmuir introduced the fundamental concept of monolayer adsorption. The Type I isotherm for microporous materials is commonly described using the classical theory, which is based upon the Langmuir equation as drawn in Figure 3.2 (Dutta et al., 2008). The mechanism of the model is presented in Figure 3.4-a. The Langmuir isotherm model, initially derived from kinetic investigations, is predicated on the premise that the adsorbent surface possesses a definite and energetically equivalent adsorption sites. Each site can accommodate a single molecule of a perfect gas during adsorption. These sites may engender either chemical or physical bonding, yet they must be strong enough to prevent the displacement of adsorbed molecules along the surface. This assumption distinguishes localized adsorption from non-localized adsorption, wherein adsorbed molecules retain mobility along the surface. Neglecting lateral interactions among the adsorbate molecules within the bulk phase, Langmuir considered the formation of a monolayer surface phase on the energetically homogenous surface of the adsorbent. (Dąbrowski, 2001). The Langmuir isotherm model, Equation 3.2, has been extensively utilized to quantify the adsorption of CH_4 and CO_2 on solids.

$$n_{ads} = \frac{n_{max} * P}{P_L + P} \qquad 3.2$$

n_{ads}: adsorbed moles, mol/g

n_{max}: maximum adsorption capacity, mol/g

P: pressure of gas (adsorbate), bars

P_L: Langmuir pressure where n_{max} is half (bars)

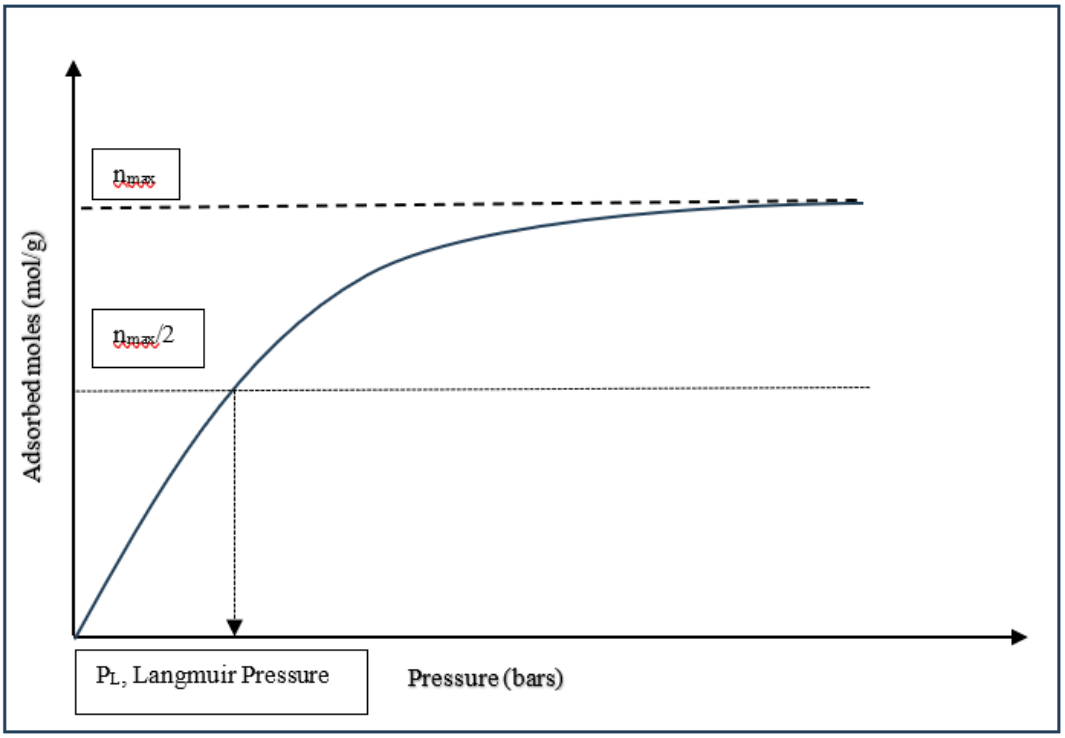

Figure 3.2. Langmuir type I isotherm (Modified from Keza et al., 2022).

The observation depicted in Figure 3.2 reveals that, under high-pressure conditions, the isotherm curve tends to level off. This phenomenon indicates the completion of available adsorption sites on the adsorbent, suggesting that the adsorbate has effectively occupied the monolayer capacity. At this point, the pressure is referred to as saturation pressure (P_s), and the amount of sorbed moles corresponding to the saturation pressure is denoted as maximum adsorbed moles (n_{max}). The pressure value at which the adsorbed mole's capacity equals half its maximum capacity is called the Langmuir pressure (P_L).

Langmuir made efforts to expand his theoretical framework in order to incorporate the presence of heterogeneity in solid adsorbents and the multilayer nature of adsorption. Consequently, the model was subsequently modified to consider lateral interactions between adsorbed molecules, their mobility, and the energetic surface heterogeneity of the solid adsorbent (Dąbrowski, 2001).

The Equation 3.2 can be expressed in terms of density instead of pressure for supercritical CO_2 (Meng et al., 2019).

$$n_{ads} = n_{max} * \frac{\rho_g}{\rho_L + \rho_g}$$

where ρ_g is the free gas phase density and ρ_L is the Langmuir density corresponding to half of n_{max}.

Modified Langmuir Model

To use the Langmuir model for excess adsorption, the above expression is modified with the inclusion of a correction factor (Meng et al., 2019).

$$n_{ex} = n_{max} * \left(1 - \frac{\rho_g}{\rho_a}\right) * \frac{\rho_g}{\rho_L + \rho_g} \quad 3.3$$

where ρ_a and ρ_g represent the densities of the adsorbed phase and the free gas phase, respectively.

The 'k' term is also introduced to the above Langmuir modified model, which is a correction factor to account for volumetric uncertainties and other factors such as swelling and compression that might affect the adsorption process. This correction factor helps refine the accuracy of the models and ensures a better fit between the experimental data and the theoretical predictions (Sakurovs et al., 2007).

$$n_{ex} = n_{max} * \left(1 - \frac{\rho_g}{\rho_a}\right) * \frac{\rho_g}{\rho_L + \rho_g} + \left(k * \rho_g\right) \quad 3.4$$

3.3.2 Brunauer, Emmett, and Teller (BET) model

During the early 1930s, it became apparent that the gas adsorption process on a solid adsorbent exceeds the formation of a monolayer, thereby enabling the formation of multiple layers under elevated pressure conditions. In order to investigate the

complex phenomenon of multilayer adsorption, Brunauer, Emmett, and Teller proposed the BET theory in 1938, which expands upon the principles of the Langmuir theory to account for the occurrence of multilayer adsorption as depicted in Figure 3.4-b (Brunauer et al., 1938). The multilayer formation process initiates at pressures significantly lower than the threshold necessary for achieving a complete monolayer. Consequently, it becomes challenging to ascertain the monolayer capacity based solely on experimental observations, rendering it impracticable. The BET theory is an extension of the assumptions put forth in the Langmuir model regarding the adsorption of monolayers. Based on the BET theory, it is postulated that every adsorbed species within a given layer serves as a potential site for adsorption in the subsequent layer. This phenomenon facilitates the formation of additional layers prior to the completion of the existing ones, as illustrated in Figure 3.3 (Azizian & Eris, 2021). Furthermore, it is proposed that the adsorption energy of the initial layer, which arises from the interaction between the adsorbate and adsorbent, possesses a distinct numerical value, while the subsequent layers exhibit equivalent adsorption energy. In addition, according to the theory, the migration of adsorbed species across distinct layers is prohibited, thereby restricting adsorption and desorption interactions exclusively to the gas phase and the adsorbed layers (Brunauer et al., 1938).

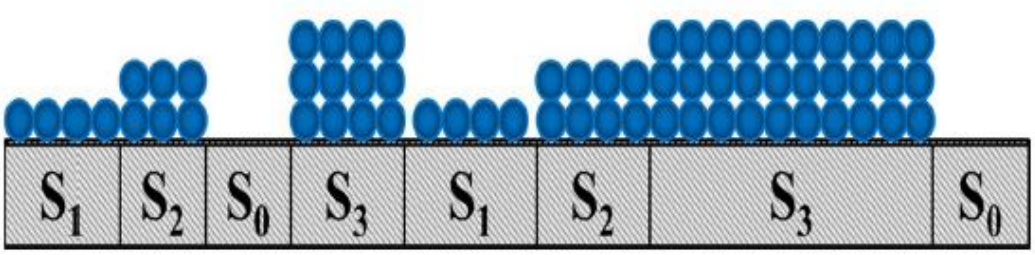

Figure 3.3. Schematic of BET multilayer adsorption (Azizian & Eris, 2021).

The applicability of the BET isotherm is limited to a narrow range of P/P_o values, specifically within the range of 0.05 to 0.35. The BET model, Equation 3.5, presents an expanded version of the Langmuir model that takes into consideration the intricacies associated with multilayer adsorption phenomena. This enhanced model

allows for a more precise examination of gas-solid interactions and facilitates the determination of surface area (Azizian & Eris, 2021).

$$\frac{x}{\left(\frac{P}{P_o}\right)(1-x)} = \frac{x_m}{C(1-x_m)} + \frac{(1-x_m)^2}{Cx_m} \quad 3.5$$

where, x: Amount of adsorbate adsorbed on the surface at relative pressure (P_o), mol/g.

x_m: Monolayer adsorption capacity (the maximum adsorption capacity at a monolayer coverage), mol/g.

C: Constant related to the energy of adsorption.

The linearized form of the BET equation is obtained by manipulating the original BET equation to a linear equation form:

$$\frac{1}{x\left(\frac{P}{P_o}\right)} = \frac{1}{x_m C} + \frac{(1-x_m)}{Cx_m}\left(\frac{P}{P_o}\right) \quad 3.6$$

3.3.3 D-R model: Theory of volume filling micropores (TVFM)

The D-R isotherm model is a widely employed theoretical framework in adsorption, which was introduced by Dubinin and Radushkevich in 1947, to describe the gas adsorption on microporous sorbents with heterogenous surfaces. The model is based on the theory of volume filling of micropores (TVFM), which originates from Polanyi's potential theory of adsorption. The utilization of this semi-empirical model is employed to elucidate the adsorption mechanism involving a Gaussian energy distribution onto heterogeneous surfaces, specifically on sorbents characterized by a highly developed porous structure encompassing micropores of diverse shapes and widths, such as coal. The D-R isotherm depends on a pore-filling mechanism, Figure 3.4-c, that involves Van der Waal's forces, rendering it suitable for physical adsorption phenomena.

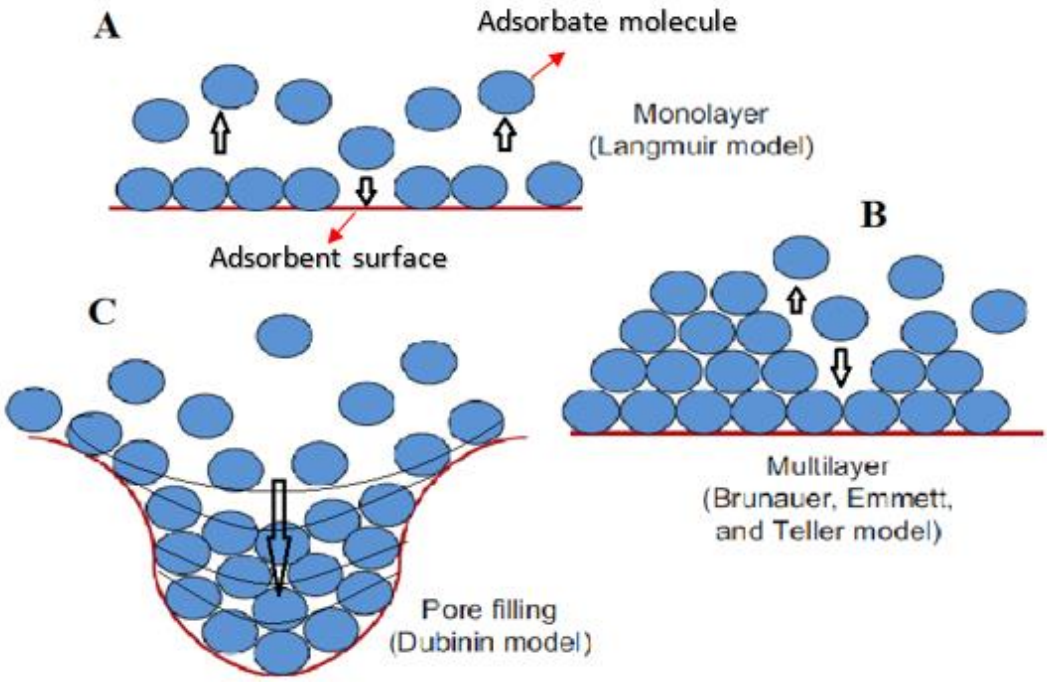

Figure 3.4. Adsorption mechanisms proposed by Langmuir, BET, and Dubinin model (Modified from Flores, (2014)).

The D-R isotherm is frequently utilized in distinguishing between physical and chemical adsorption of metal ions, particularly within the intermediate ranges of adsorbate concentrations. The D-R isotherm is notable for its temperature dependency, making it a valuable tool for analyzing adsorption data across various temperatures (Dąbrowski, 2001). Van der Waal's forces primarily govern this process and exhibit a multilayer nature. The conventional D-R model is expressed in Equation 3.7, derived by energy balance when adsorbate fills in the micropores of the adsorbent. It is important to acknowledge that the conventional D-R model possesses certain limitations and has been validated under low pressure conditions, wherein the volume of the adsorbed phase is negligible (Song et al., 2015). The validity of the conventional D-R model is limited to cases where the pressure of the gas is below the saturation pressure ($P<P_o$). To apply D-R model for wide range of pressure, for gases in supercritical state, D-R model has been modified with the inclusion of adsorbed phase density (ρ_a) instead of P_o. The term ($1-\rho_g/\rho_a$) in Equation 3.9 serves to account for the volume occupied by the adsorbed phase on the surface

of the sample (Sakurovs et al., 2007; Gensterblum, 2013). The modified model has the potential to be utilized in high-pressure adsorption experiments, specifically those involving supercritical CO_2. This can be achieved by substituting the P_o with the adsorbed phase density (ρ_a), and P with the free gas density (ρ_g), Equation 3.8.

$$n_{ads} = n_{max} * e^{-\left\{\left(\frac{R*T}{\beta*E_o}\right)^n * \left[\ln\left(\frac{P_o}{P}\right)\right]^n\right\}} \quad 3.7$$

n_{ads}: adsorbed amount, mol/g

n_{max}: max adsorbed amount in micropores. mol/g

R: gas constant = cc.bar.K^{-1}.mol^{-1}

T: temperature, K

β: affinity coefficient

E_o: heat of adsorption, J/mol

P_o: saturated vapor pressure, bars

n: heterogeneity parameter, restricted to n=2 for D-R isotherm

$$n_{ads} = n_{max} * e^{-D*\ln\left(\frac{\rho_a}{\rho_g}\right)^2} \quad 3.8$$

The 'D' parameter, which denoted as $D = (\frac{R*T}{\beta*E_o})^2$, is associated with the coal's affinity for carbon dioxide (CO_2). The affinity coefficient between CO_2 and coal, denoted as 'β', is determined to be 0.35 for CO_2 (Day et al., 2008). Meanwhile, E_o represents the characteristic heat of adsorption (Meng et al., 2019).

Sakurovs et al. (2007) proposed modified D-R model to be used with excess adsorption which is expressed in Equation 3.9. Larsen (2004) found that coal can both adsorb gas onto its surface and absorb gas internally. The sorption mechanisms exhibited by coal can be effectively described by DR equation. With this approach, the adsorption phenomenon is represented by DR model, while the absorption process is accounted for by a term that is directly proportional to the gas density, in

accordance with Henry's law constant, k. The term "k" encompasses void volume errors and volume change due to compression or swelling. After the adjustments to the previous model, D-R modified +k is expressed in Equation 3.10, which is applicable for supercritical CO_2 involving all the required parameters (Larsen, 2004; Ozdemir et al., 2004; Sakurovs et al., 2007).

$$n_{ex} = n_{max}\left(1 - \frac{\rho_g}{\rho_a}\right) e^{\left\{-D\left[\ln\left(\frac{\rho_a}{\rho_g}\right)\right]^2\right\}} \quad 3.9$$

$$n_{ex} = n_{max}\left(1 - \frac{\rho_g}{\rho_a}\right) e^{\left\{-D\left[\ln\left(\frac{\rho_a}{\rho_g}\right)\right]^2\right\}} + k\rho_g \quad 3.10$$

3.4 Excess adsorption

Excess adsorption holds significant importance in the gas-solid adsorption phenomenon as it pertains to the adsorption of molecules that surpass the coverage of a monolayer on the surface of a solid adsorbent. In the realm of CO_2 adsorption on coal, excess adsorption plays a vital role in comprehending the intricate dynamics between CO_2 molecules and the surface of coal. The concept of excess adsorption (n_{ex}) was first proposed by Gibbs in the late 19th century, wherein it refers to the amount of adsorbate that is adsorbed when the volume of the adsorbed phase (V_a) is neglected, shown in Figure 3.6 (Cao & Zhang, 2018).

Certainly, the terminology pertaining to "excess adsorption" in the context of adsorption studies, while somewhat paradoxical in its naming, is indeed a widely recognized and accepted term within the scientific community. In the adsorption studies, "excess adsorption" refers to the quantity of adsorbate molecules that are effectively retained on the surface of the solid adsorbent beyond what would be expected based solely on a monolayer coverage or a simple, uniform surface

adsorption. It essentially accounts for the surplus adsorbate molecules that are accommodated in the porous structure of the adsorbent, forming multilayer adsorption. While its nomenclature might initially appear as a misnomer or counterintuitive, "excess adsorption" has become a widely accepted word in the literature. It signifies a well-defined and recognized concept that enables scientists and researchers to quantitatively describe the behavior of adsorbates on porous materials.

The adsorbed amount measured directly from the experiments is referred to as Gibbs excess adsorption, denoted by n_{ex}, while the actual amount adsorbed on the coal surface is termed absolute adsorbed amount, denoted by n_{abs}. Under low pressure conditions, a resemblance is observed between these two values. However, under elevated pressure conditions involving the supercritical state of CO_2, a notable difference emerges (Meng et al., 2019). The observed difference between adsorbed phase density (ρ_{ads}) on the surface of coal and the free gas density (ρ_g) present in the cleats or pores of the coal matrix is the major cause of this difference.

Findings from many studies demonstrate a decline in the density of the adsorbed phase as the distance from the solid surface increases, as depicted in Figure 3.5. Area A shows the excess adsorption in the figure, which is the adsorbed phase, which has a higher density than the free gas phase. The absolute adsorption is represented by the sum of area A and area B in Figure 3.5 (Murata et al., 2001; Rouquerol et al., 2016).

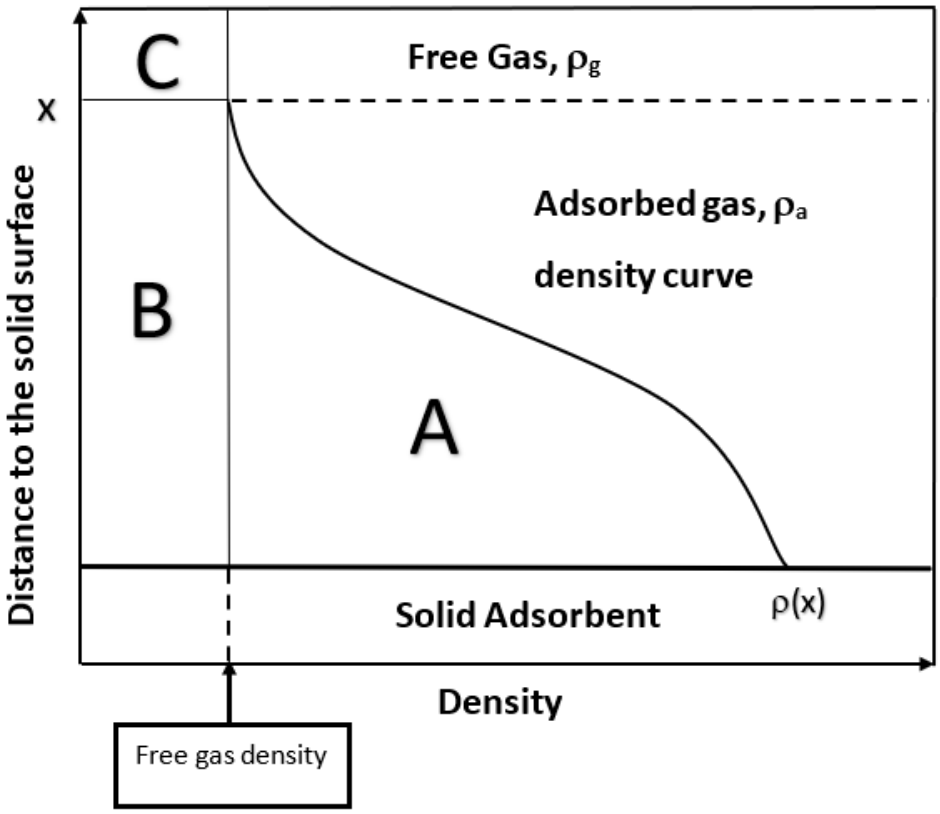

Figure3.5. Difference in adsorbed phase and free gas phase though Gibbs excess model (Modified from Meng et al., (2019)).

In some studies, however, the accuracy of the density function depicted in Figure 3.6 cannot be definitively ascertained, as they have indicated the possibility of higher or lower densities in the interfacial region compared to the density of the free gas (Király & Dékány, 1990; Gumma, 2003).

Gibbs excess adsorption is expressed in Equation 3.11.

$$\Gamma_{ex} = \int_0^{\infty} \left(\rho(x) - \rho_g\right) dx \qquad 3.11$$

The Equation $n_{abs} = n_t - \rho V_{void}$ is applicable to rigid solids. In this equation, ρ represents the molar density of the gas in the free space, n_t denotes the total moles of the adsorbate transferred into the sample cell, and V_{void} represents the void volume in the sample cell.

The Gibbs excess adsorption equation models have been extensively studied and documented in the literature (Meng et al., 2019).

$$n_{ex} = n_{abs} - \rho_g V_a$$

The variable V_a represents the volume of the adsorbed phase. The equation provided is expressed as:

$$n_{ex} = n_{abs} - \rho_g \left(- \frac{n_{abs}}{\rho_a} \right) \quad 3.12$$

Where ρ_a represents the density of the adsorbed phase, which needs to be determined in order to examine the above equation.

Various methodologies exist for determining the adsorbed density; however, no universally accepted standard has been established. Most of the methodologies are inferred from previous literature (Humayun & Tomasko, 2000; Sakurovs et al., 2007).

The present study involved the determination of the adsorbed density (ρ_a) utilizing the graphical approach, as detailed in Appendix D. The approach utilized in this study is founded upon Equation 3.12. It can be observed from the equation that the excess number of moles (n_{ex}) will be zero as the density of the free gas phase increases and eventually reach the density of the adsorbed phase. Hence, through the graphical representation of the relationship between density and the excess number of adsorbed moles, it is possible to estimate the density of the adsorbed phase by examining the point of intersection of the linear segment of the density profile where the excess moles reach zero (Song et al., 2015; Keza et al., 2022). The adsorbed density is subsequently employed as the initial point for optimizing adsorption modelling.

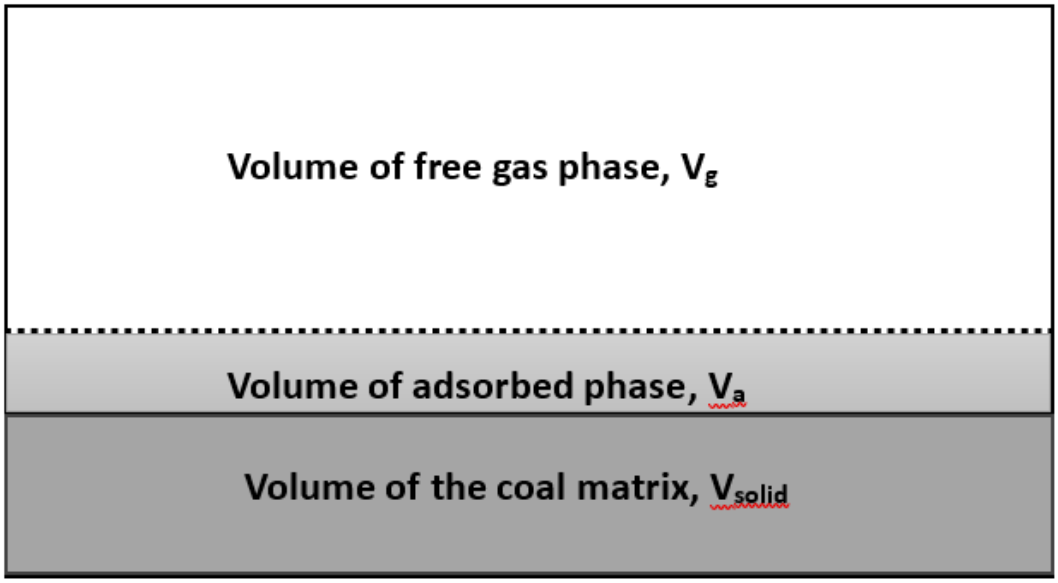

Figure 3.6. Adsorption of gas in sample cell (Modified from Meng et al., (2019)).

CHAPTER 4

EXPERIMENTAL METHODOLOGY

The CO_2 adsorption capacity of lignite coal samples from three different basins in Turkey were measured using the volumetric method, also known as the manometric method. This method is prefered over others such as gravimetric method due to its higher accuracy, low cost and practicality (Wang et al, 2021; Karimi et al, 2021).

The schematic of the apparatus is shown in the Figure 4.1. The apparatus consists of 2 independent chambers referred as reference cell and a sample cell connected with a valve. The chamber volumes, referred to as void volume in this study, were determined by Helium (He) gas expansion method, with pressures up to 80 bars at constant temperature of 313.15K. The volume of reference and sample cells are found to be 71.75 cc and 73.76 cc respectively. In a similar manner, to observe the adsorption phenomenon, CO_2 gas is introduced into the reference cell and then allowed to expand into the sample cell containing the coal sample. The number of moles of the gas that have been adsorbed onto the surface of the sample is calculated by measuring the drop in pressure and applying the real gas equation of state.

In order to facilitate comprehensive investigation of the adsorption phenomenon, a compression setup has been meticulously designed in conjunction with the experimental adsorption setup. This additional setup serves the crucial purpose of elevating the pressure to the desired level, which cannot be achieved using the standard CO_2 gas cylinder, which only allows for pressure up to 40 bars. The inclusion of the compression setup enables the pressure to be increased up to 80 bars, thus allowing for the observation of the behavior of supercritical CO_2 in the adsorption process. The intricate details of the compression method utilized in this study are expounded upon in the subsequent section. It is thus imperative to have

both the adsorption and compression setups in place to achieve an accurate and comprehensive analysis of the adsorption phenomenon.

4.1 Experimental setup

The experimental setup utilized in this study consists of a water bath that operates at a constant temperature of 313.15K, a high-pressure reference cell and a sample cell with volumes of 71.75 cc and 73.76 cc, respectively. The gas for the experiment is provided by the He/CO_2 tanks. The schematic of the setup is illustrated in Figure 4.1, and Figure 4.2 displays a photograph of the actual volumetric apparatus used in this study. The experiments were conducted using reference and sample cells made of brass and high-quality stainless steel (SS) tube fittings, as they can withstand pressures up to 250 bars. The components used in the experiments are listed in detail in Table 4.1.

It should be noted that the experimental setup design used in this study differs from the one utilized by Mr. C.B.Keza in his work on CO_2 adsorption on coal samples by the inclusion of a mechanical compression system to achieve higher CO_2 pressures (Keza, 2021). This design was chosen due to its demonstrated effectiveness and the need for consistency in experimental methodology as employed in several research papers on CO_2 adsorption on coals (Ozdemir et al, 2004; Ozdemir, 2017; Meng et al, 2019).

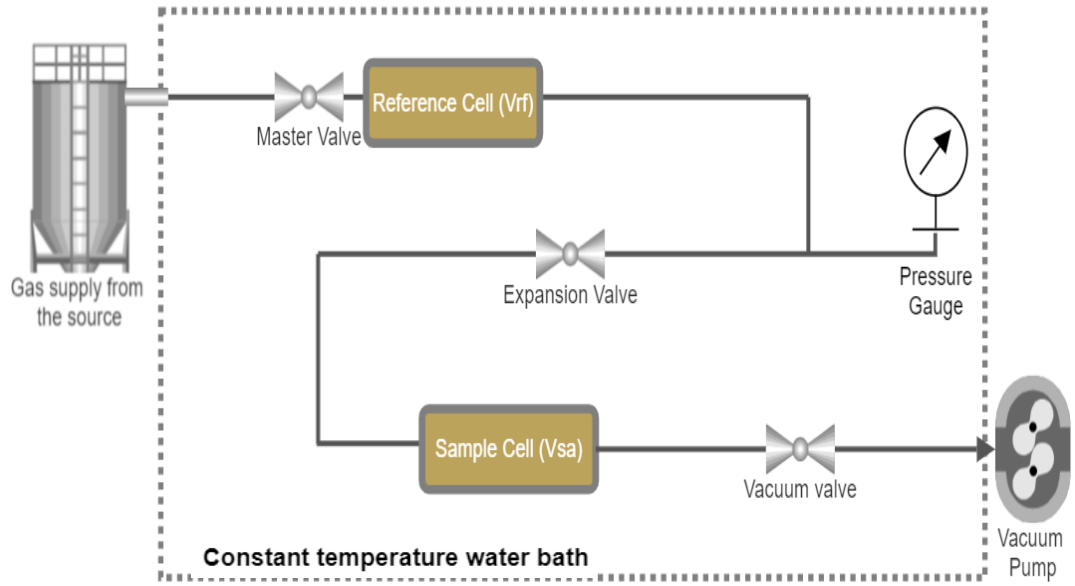

Figure 4.1. Schematic of volumetric setup

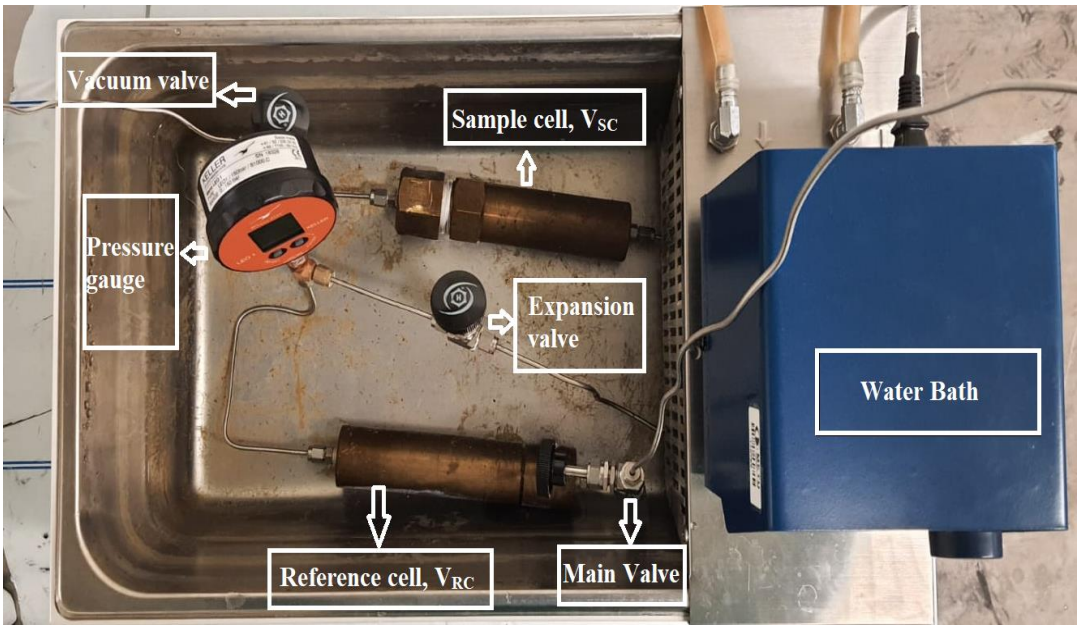

Figure 4.2. Experimental volumetric setup

Table 4.1. Components used for the experiments.

Components	Description
Water Bath	Water Circulation Bath (WCB) capacity of 6L, Temperature range: +5°C-100°C ± 0.1°C accuracy, WiseCircu® 22. Operated at 40°C for experiment.
Gas Cylinders (He and CO_2)	Helium Compressed from Praxair-(CAS no)7440-59-7, Purity: 99.5-100%. Carbon dioxide from Linde-(CAS no) 134-38-9, Purity: 99.9%.
Hand Hydraulic Pump	Enerpac, P142, Max 700 bars rating
Pressure Regulator	Kasweld Pressure Regulator measure up to 315bars.
Pressure Transducer (Digital manometer)	Keller AG Swiss Company, Mano LEO 1, Range: 0-150 bars, 3V battery (CR 2430), IP65 protection, Temperature rating up to 50°C.
Piston Cylinder	Iron piston cylinder of capacity 600cc.
Tubbing and Fittings	Stainless steel SS 1/8” and 1/16” tubing from Swagelok.
Valves	All the valves used are from Hamlet company. 2 two-way valves 1-AA H-300U-SS-L-R 1/8-RS type. 2 two-way valves SP-2 H-300-SS-L-L-1/8 type. 1 two-way valve SW-4 H-300-SS-L-R-1/8M. 1 three-way valve H-6800-SS-L-1/8-RCST.
Reference & Sample Cells	Brass chambers having approx. volume of 71.75 cc and 73.76 cc, handle up to 300bars.
Vacuum Pump	Hanning Elektro-werke, Type: E5zA2B-053, 220-240V.
Synthetic Oil	Mobil oil 5w-20.

4.1.1 Experimental setup for compressing CO_2 gas

To accurately analyze the adsorption behavior of supercritical CO_2, it is essential that the gas is in its supercritical state, which is achieved at pressures above 73.9 bars and temperatures above 304.21 K, as illustrated in Figure 4.3. However, the maximum pressure of the CO_2 tank provided by the vendor was only 45 bars, which necessitated the design of a specialized compression setup, as depicted in Figure 4.4. The specifications and ratings of the components used are provided in Table 4.2.

The compression setup consists of a hydraulic hand pump with a maximum rating of 700 bars, which is connected to a piston cylinder with a volume of 600cc and a 2-way valve. A T-connector is attached on top of the piston cylinder, with one side connected to an analog pressure gauge that accurately monitors the pressure buildup in the cylinder. The other side of the T-connector joins the compression setup to the main adsorption setup i.e., reference cell via a main valve. The inlet of the piston cylinder is joined with the main CO_2 tank, which initially provides pressure up to 45 bars. The hydraulic hand pump then uses synthetic oil in its reservoir having a capacity of 328cc to fill and compress the pressure in the piston cylinder up to 90 bars.

To estimate the required pressure for compressed CO_2, the real gas equation is used by applying the z-factors obtained from NIST database at room temperature (Linstrom, 1997). The compression of CO_2 takes place in stages, as incremental pressures are required for the adsorption experiments. In each stage, the gas is compressed to 100 bars until it reaches its supercritical state in the piston cylinder, and then the main valve is gradually opened to achieve the desired incremental pressure for the experiment. The procedure for one stage of incremental pressure has been thoroughly explained in the steps below:

1- The compression setup underwent a thorough leak test by passing CO_2 gas from the main cylinder through the system.

2- Any connections, valves, or gauges found to have leakage were repaired, tightened with Teflon, or replaced with new components.

3- The initial pressure in the piston cylinder was set to 45 bars using the CO_2 gas from the main tank.

4- 328 cc of synthetic oil is initially filled into the hydraulic hand pump reservoir, and then injected into the piston cylinder to build up pressure.

5- The hydraulic pump was operated to compress CO_2 gas in the piston cylinder up to 52.4 bars from initial 45 bars, until all the oil from the hydraulic pump tank was used.

6- The remaining volume left in the piston cylinder to compress the gas was 272 cc out of a total of 600 cc.

7- The hydraulic pump was refilled with 160 cc of synthetic oil to ensure that the remaining volume of compressed CO_2 gas in the piston cylinder would be at least 100 cc at the end.

8- The oil was then pumped into the piston cylinder again, compressing gas up to 100 bars.

9- The hydraulic pump was stopped once the targeted pressure was reached, and the main valve was gradually opened to take the required incremental pressure above 45 bars.

10- The synthetic oil was drained back into a beaker to refill the hand pump and steps 3-10 were repeated until all the incremental readings up to 80 bars are recorded for the adsorption experiments.

These steps were taken to ensure that the system was operating correctly and that the CO_2 gas was compressed incrementally to the desired pressure until it changes its state to supercritical for the adsorption experiments.

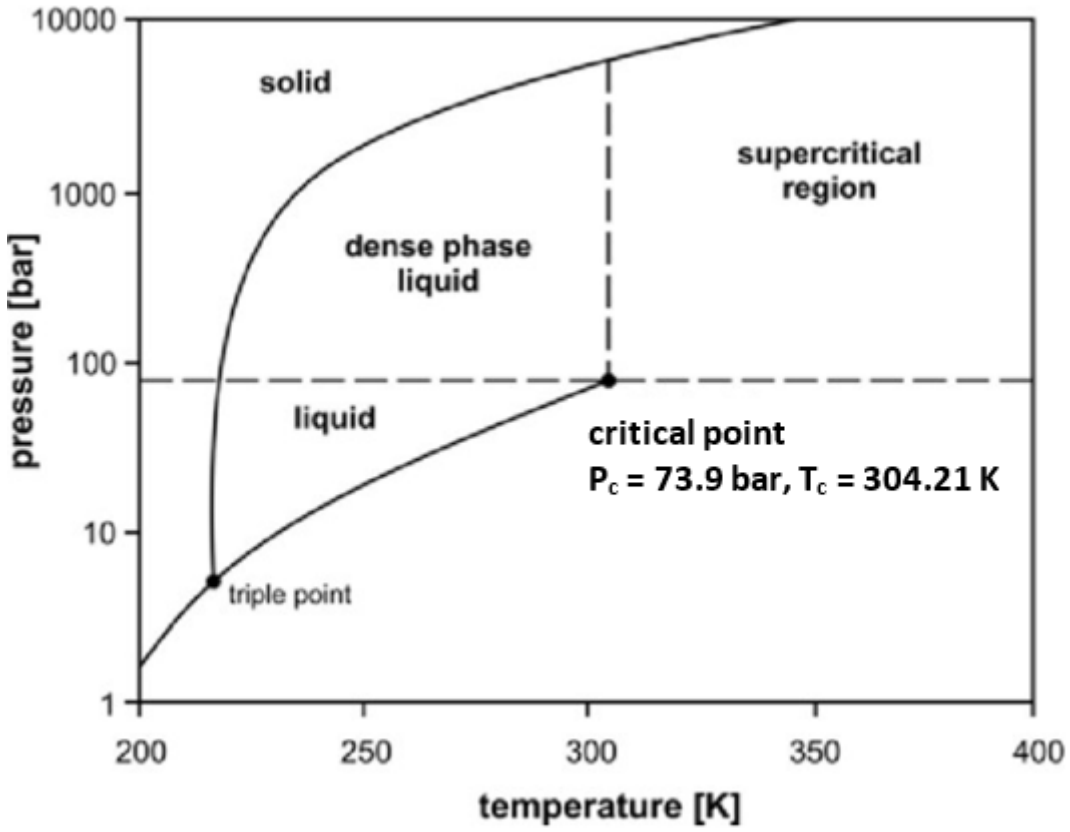

Figure 4.3. Phase diagram of CO_2 (Modified from Witkowski et al., (2014)).

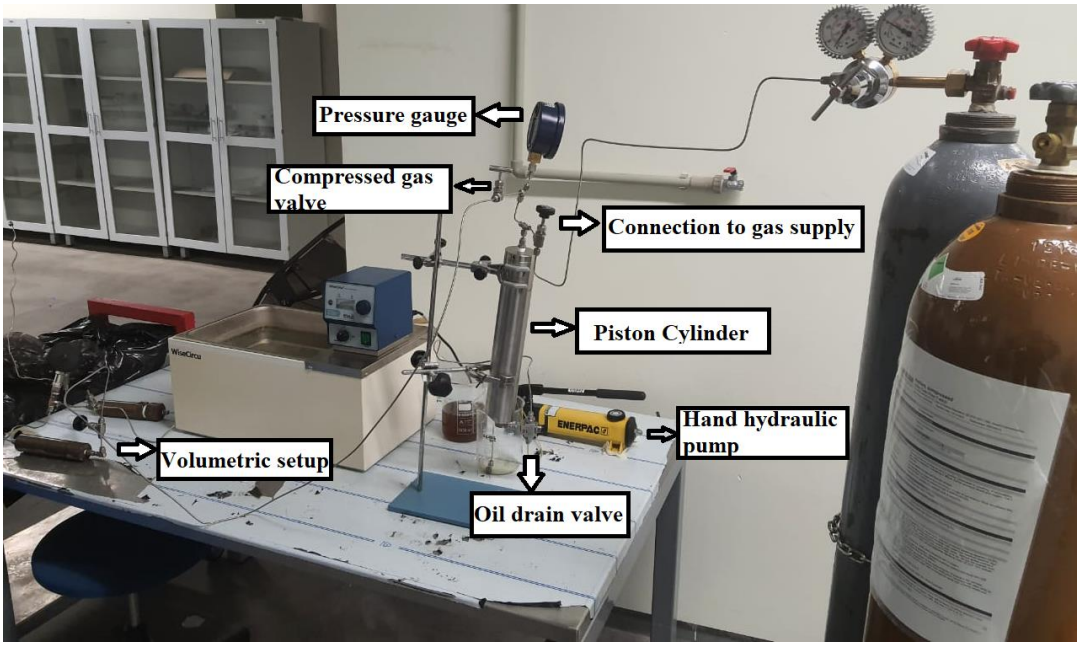

Figure 4.4. Compression setup attached to volumetric setup.

4.2 Coal sample storage and preparation

The Turkish Coal Enterprises (TKI) provided lignite samples from the Çankırı, Elazığ Sivrice, and Amasya Merzifon basins in Turkey shown in Figure 4.5. Locations of the samples from the basins in Turkey are depicted in Figure 4.6. The coal samples were originally in the form of chunks and were stored in the refrigerator to prevent any changes in their moisture and volatile matter content. This process was necessary since samples may degrade over time from exposure to heat, humidity, and other environmental factors. Additionally, as highlighted in prior studies (Schmidt, 1945; Yohe, 1958), storing the samples in a cool place is crucial for maintaining the accuracy and repeatability of adsorption experiments and results as each sample went through three times for adsorption experiments with variable weights.

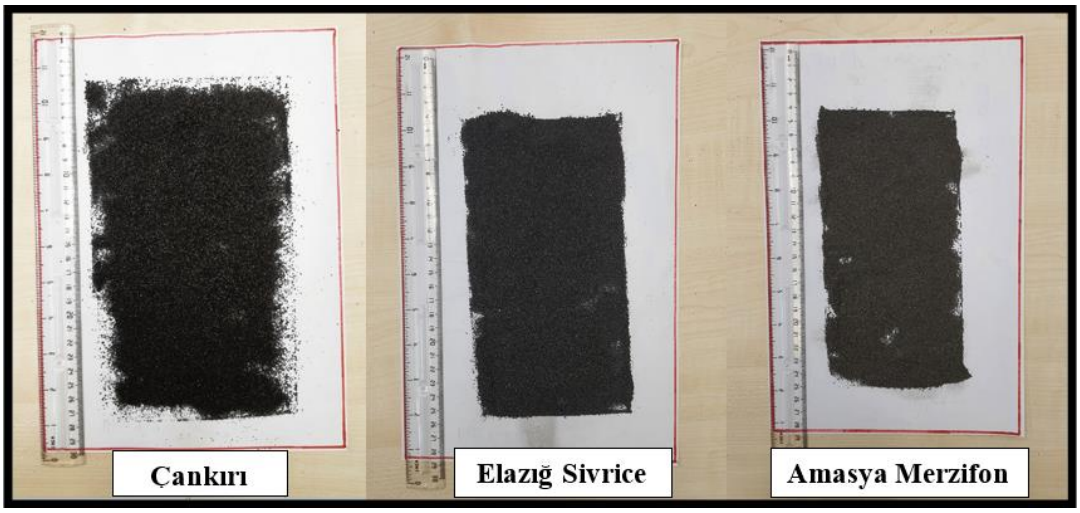

Figure 4.5. Coal samples used in experiments.

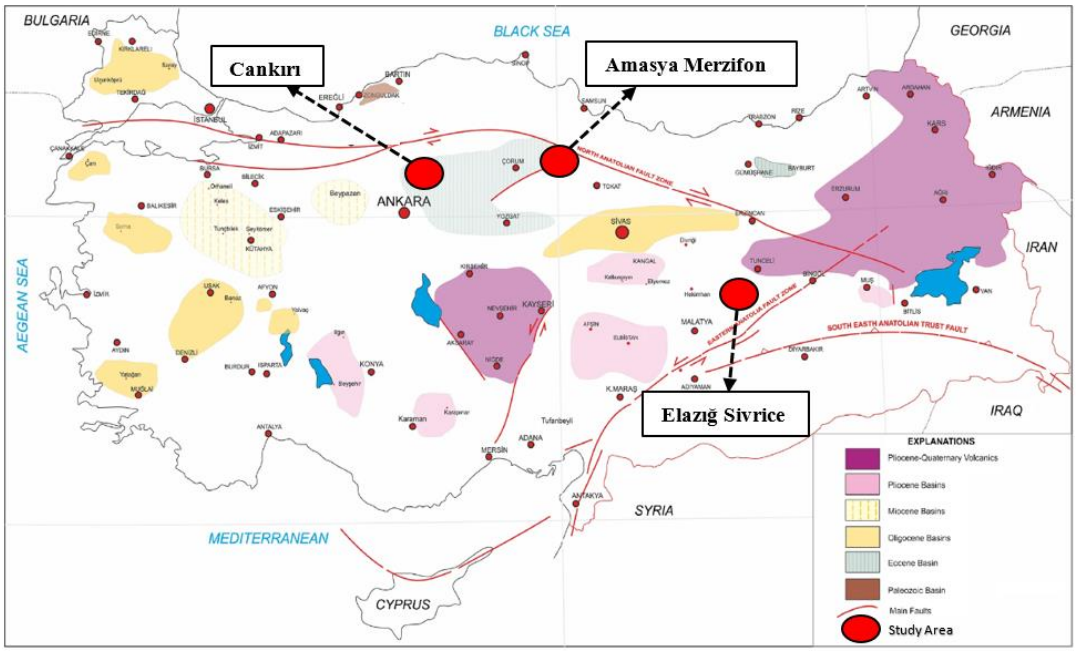

Figure 4.6. Locations of studied samples from Turkey (Modified from Toprak, (2009)).

Coal samples were crushed with an iron rod in a heavy metal cylinder, as depicted in Figure 4.7, to acquire a powdered form for faster diffusion time during adsorption experiments. After that, each sample was put through a variety of mesh sizes in a laboratory sieve test (ISO 3310-1), aiming to get the desired coal particle size. For this purpose, the mesh sizes 2.0 mm (10), 1.0 mm (18), 0.5 mm (35), 0.250 mm (60), and 0.125 mm (120) are used. Figures 4.8 shows the sieve shaker and mesh sizes with the numbers used for the sieve analysis. A coal sample with a particle size of 0.250 mm is used in the current study to examine the adsorption. Since coal can rapidly and irreversibly adsorb atmospheric oxygen (Schmidt, 1945), therefore, to prevent impact on the surface properties and its adsorption characteristics, each

crushed sample is individually dried at 60°C for four hours and then transferred to air-tight plastic bottles.

Figure 4.7. Iron rod and heavy metal cylinder for crushing samples

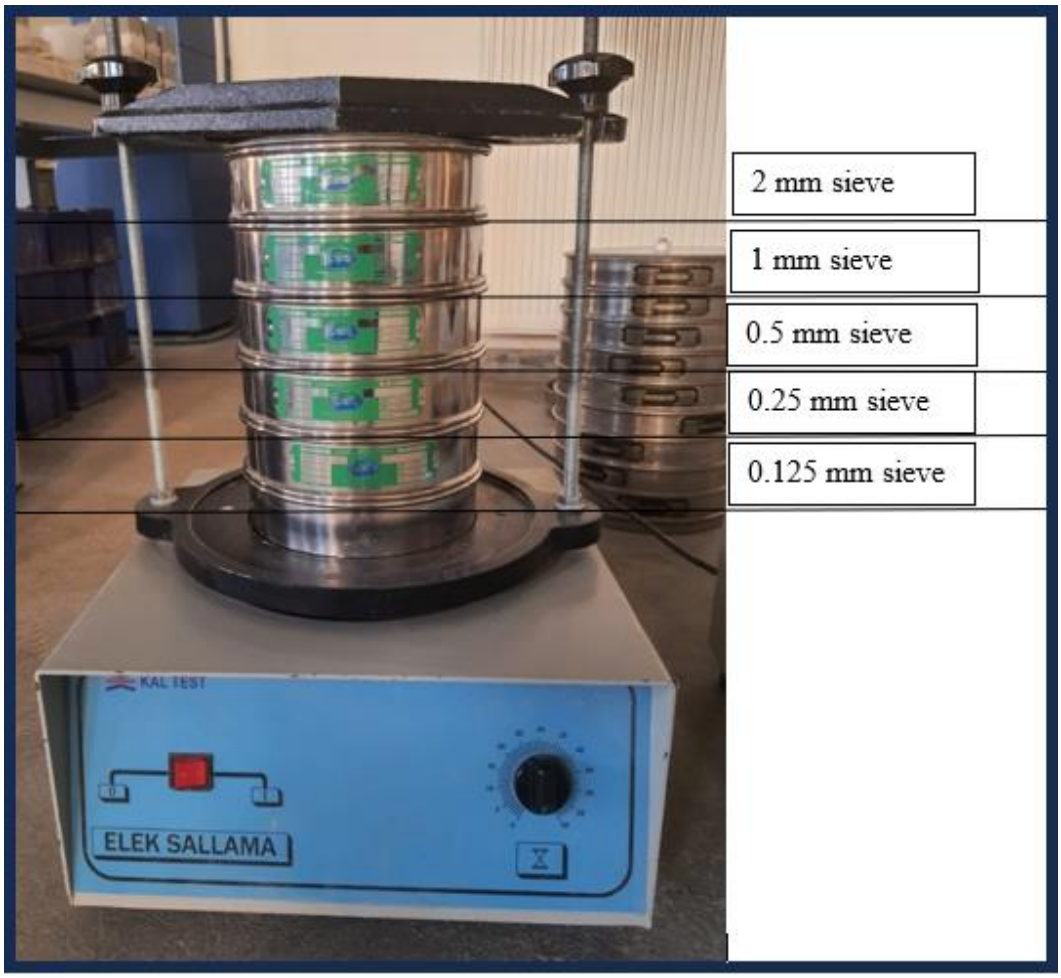

Figure 4.8. Sieve shaker and mesh sizes

Before transferring the coal samples into the adsorption cells, a specific amount of coal was weighed on a mass balance to account for the moisture loss, and it was then dried in situ using the oven under vacuum at 110°C for 36 hours, as recommended in the literature (Ozdemir, 2004; Meng et al., 2019). The samples were weighed again after drying, and the difference in weight is recorded as the moisture loss or shrinkage factor. This factor can significantly affect adsorption isotherms, and it is discussed in detail in the following sections.

TKI conducted a proximate analysis of the coal characteristics in accordance with the standards set by ASTM D 7582. The results of the proximate analysis are presented in Table 4.2 and include the moisture content (M), volatile matter content (VM), fixed carbon (FC), and huminite reflectance (HR). The Equation 4.1 proposed

by Rice (1993), which is defined by the volatile matter value, is employed to calculate the huminite reflectance (Rice, 1993).

$$R_o(\%) = -2.172 \times \log(VM_{daf}) + 5.092 \quad (4.1)$$

Table 4.2. Proximate analyses results of the coal samples.

Parameter	Sample		
	Çankırı	**Elazığ Sivrice**	**Amasya Merzifon**
Moisture (%)	11.20	9.18	4.77
VM (%)	34.68	34.75	30.35
Ash (%)	8.15	4.66	42.71
FC (%)	45.96	51.40	21.05
HR (%)	1.75	1.75	1.87

*HR (%) is calculated from the Equation 4.1 above
*All values are on a dry basis
*Determined by TKI laboratories according to ASTM D 7582.

4.3 Experimental procedure

All connections between the sample and reference cells are established after transferring the pulverized coal sample to the sample cell. The entire setup is then immersed in a water bath maintained at a constant temperature of 40°C. The Helium gas is then passed through the manometric setup for about 3 hours to check for leaks. In case any leak is detected by observing bubbles in the water, the joints are re-tightened by Teflon. Once the setup is confirmed to be free of leakage, a vacuum pump shown in Figure 4.9 is attached to the system to vent out all the trapped gas.

Figure 4.9. Vacuum pump

The helium gas expansion method is employed to determine the cell volumes and void volume for the sample cell, as He is an inert gas and considered as non-sorbing (Gensterblum, 2013). Once the void volume of the sample cell is determined, the gas is completely vented out using the vacuum pump. The main connection from the He cylinder is then switched to CO_2 cylinder to initiate the adsorption experiments. Pressure in the reference cell (P_{RC}), Pressure in the Sample cell (P_{SC}), and Equilibrium pressure (P_{Eq}) are monitored to calculate the adsorption using Gibbs' excess adsorption Equation 4.2 (Meng et al., 2019).

$$n_{ex} = n_{abs} - \rho_g V_a \qquad 4.2$$

Where n_{abs} are the absolute moles and $\rho_g V_a$ are the moles in adsorbed phase. The detailed experimental procedure is explained in the following steps and illustrated in Figure 4.10:

Step 1:

- Initially, all valves (master, expansion, and vacuum) are closed, and the pressure in the reference cell and sample cell are equal.
- The master valve is opened, and CO_2 is injected into the reference cell from the main cylinder while keeping the expansion valve closed. Once the desired pressure is reached in the reference cell, the master valve is closed.

Step 2:

- The pressure reading in reference cell (P_{RC}) is recorded after 2-3 minutes to allow the CO_2 pressure to stabilize with the temperature in the reference cell.
- The expansion valve is opened to allow CO_2 to flow into the sample cell. The pressure will immediately drop due to expansion.

Step 3:

- Adsorption starts as the pressure in the sample cell decreases, and the readings are recorded every minute for the first hour and then every fifteen minutes thereafter until it stays constant.

Step 4:

- Equilibrium pressure (P_{EQ}) is recorded once the pressure remains constant for 30 minutes.

The next injection takes place once the pressure remains constant and the expansion valve is closed. Since there will be gas in both RC and SC from the previous injection, the pressure increase will be incremental. This procedure also reflects possible field application.

1. The master valve is opened again, and the pressure is increased to the desired level in the reference cell.
2. The experiment will be repeated from step 1 to step 4 until the maximum pressure limit of CO_2 is reached from the main cylinder, which is 45 bars.
3. For the CO_2 pressure above 45 bars, the gas supply connection is switched from the CO_2 cylinder to the compressor setup while keeping the main valve closed.

4. Further pressure increase is achieved from the compressor setup in a manner similar to that mentioned from Step 1 to Step 6 until the desired pressure limit of 80 bars is reached in the volumetric setup.

After recording all the pressure readings at each interval, the gas supply is turned off from the main supply, and all the gas in the volumetric setup is vented out from the vent valve. The water bath is turned off, and the coal sample is removed from the sample cell and dried in a vacuum oven at 110°C for an hour. The setup is ready for the next sample to be loaded following the same procedure.

Each coal sample was experimented with three times. During each trial, no fewer than eight equilibrium pressure (P_{EQ}) readings obtained. Each P_{EQ} reading demanded careful monitoring over an extended period, often spanning two hours, until a consistent (stabilized pressure) reading was maintained for at least 30 minutes. In total, each comprehensive experiment required a time investment of approximately 10 to 12 hours. In cases where the P_{EQ} reading exhibited a continuous decline at a consistent rate after the initial 2-hour mark, a potential setup leakage was suspected. Under such circumstances, the entire experiment was reinitiated following the rectification of any identified leaks.

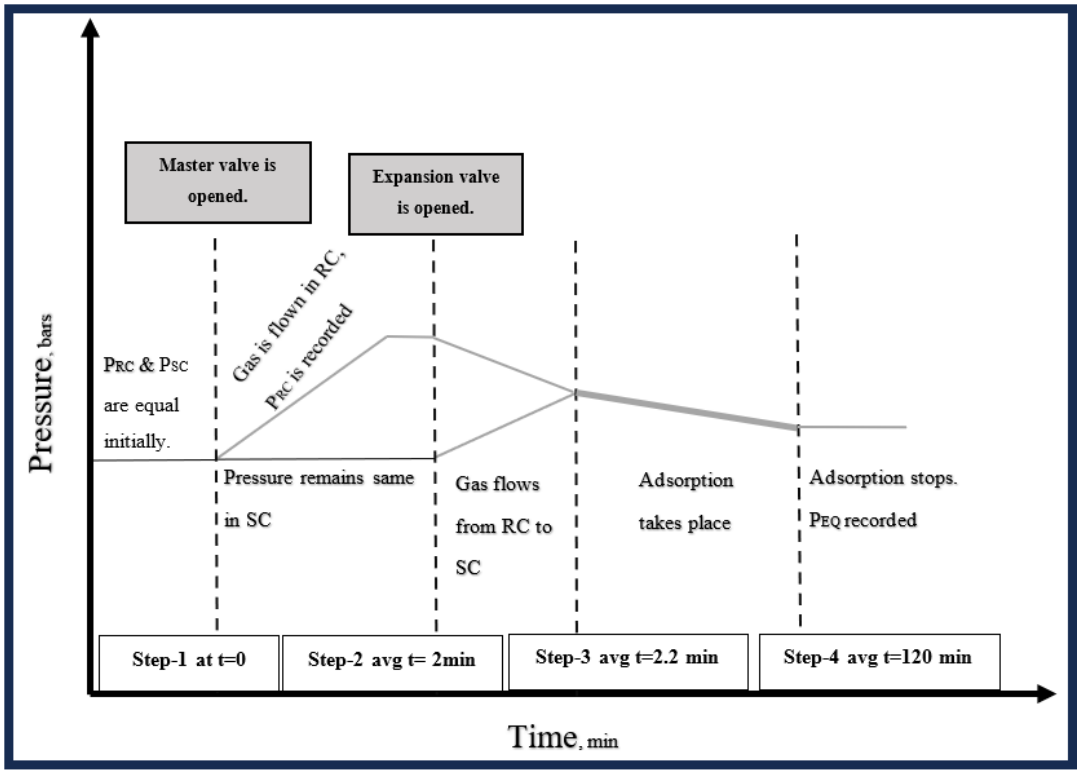

Figure 4.10. CO_2 adsorption process graphical representation in a volumetric setup (Modified from Keza et al., 2022)

(RC: reference cell; SC: sample cell; P_{EQ}: Pressure in equilibrium)

4.3.1 Void volume estimation

The helium displacement method is employed to find out the volumes for the Reference cell (V_{RC}), Sample cell (V_{SC}), and Void volume (V_{Void}) (Ozdemir, 2017). The system's total volume includes the tubing line volumes, V_{RC}, V_{SC}, V_{Void}, and matrix pore volume. Void volume refers to the empty space which is left unoccupied by the coal sample in the sample cell. The reason helium gas is used as a reference gas is because it is inert in nature and considered non-sorbing. Helium is commonly used to determine cell volumes due to its small molecular size of 140 pm which helps the gas molecules penetrate the coal pores easily (Gensterblum, 2013). At the same

time, it is commonly assumed that the same pore volume is accessed by helium as CO_2 which has a molecular size of 232 pm (Sakurovs et al., 2009).

The volumes of reference and sample cells are estimated initially using the same method. V_{RC} and V_{SC} will stay constant throughout the experiment. Consequently, the void volume is calculated by injecting the known quantities of helium each time the coal sample is loaded into the sample cell. The He gas is injected sequentially into the system without venting it out. The conservation of mass principle is applied using the real gas equation to derive the Equation 4.3 for V_{Void} provided in Appendix-A.

$$V_{Void} = \left(\frac{\frac{P_n}{Z_n} - \frac{P_{Eq(n)}}{Z_{Eq(n)}}}{\frac{P_{Eq(n)}}{Z_{Eq(n)}} - \frac{P_{Eq(n-1)}}{Z_{Eq(n-1)}}} * V_{RC} \right) \qquad 4.3$$

In the above equation, P_n denotes the pressure in reference cell at n^{th} injection, Z_n is the compressibility constant at Pressure P_n, $P_{Eq(n)}$ is the equilibrium pressure at the n^{th} injection, $Z_{Eq(n)}$ is the compressibility constant at Pressure $P_{Eq(n)}$, $P_{Eq(n-1)}$ refers to the equilibrium pressure of the previous step where $Z_{Eq(n-1)}$ is compressibility constant at $P_{Eq(n-1)}$.

Once the coal is placed in the sample cell, incremental injections of helium gas have been made to the reference cell, and the gas is allowed to expand in the sample cell. Both the pressures in the reference cell and the equilibrium are observed to estimate the void volume. At least eight sequential injections are recorded at pressures up to 80 bars without venting the gas from the previous injection. The reason for the several injections is to reduce the error and achieve consistency in the void volume. The V_{Void} at each pressure interval is recorded and the average is taken for the best estimate. The compressibility factor for He gas is calculated using the Equation 4.4, which is based on experimental data from National Bureau of Standards Technical Note 631 for helium (Sudibandriyo et al., 2003; Keza, 2021). This equation takes

into account the temperature (T) in kelvin (K) and the pressure (P) in bars to determine the compressibility factor.

$$Z_{He} = 1 + \frac{1471 * 10^{-6} - 4779 * 10^{-9} * T + 492 * 10^{11} * T^2}{P} \qquad 4.4$$

4.3.2 CO_2 adsorption measurement

The determination CO_2 adsorption followed a similar method as void volume estimation however the gas injected here is CO_2. The reference cell was first pressurized with CO_2. A few minutes were given to achieve a thermal equilibrium at 313.15 K. Once the temperature and pressure readings were stable, an expansion valve was opened to transfer the gas into the sample cell. A considerable amount of time was given to the gas at each pressure interval to reach equilibrium and once the pressure stayed constant for more than 30 minutes, the equilibrium reading was recorded. After the first reading, the reference cell was injected with additional CO_2 and the process was repeated. A single adsorption analysis on a coal sample consists of 8 or more incremental sequential pressure steps where pressure and temperature were monitored continuously in both the cells to verify thermal and kinetic equilibration. The total time for each experiment took approximately 18-20 hours.

The Gibbs' excess adsorption equation, which is universally applicable and valid under super critical conditions, is employed to calculate the adsorbed gas on the coal samples (Goodman et al., 2004). Equation 4.5 is derived using the real gas law which accounts for gas compressibility Z factor, determined from NIST database as provided in detail in Appendix-E (Linstrom, 1997). Consequently, excess adsorbed amount (n_{ex}) is calculated stepwise at every pressure injection using Equation 4.5 below. Derivation of the equation is explained in Appendix-C.

$$\Delta n_{ex} = \left(\frac{V_{RC}}{R * T}\right) * \left(\frac{P_n}{Z_n} - \frac{P_{Eq(n)}}{Z_{Eq(n)}}\right) - \left(\frac{P_{Eq(n)}}{Z_{Eq(n)}} - \frac{P_{Eq(n-1)}}{Z_{Eq(n-1)}}\right) * \left(\frac{V_{Void}}{R * T}\right) \qquad 4.5$$

Where P_n is the injection pressure before the gas expansion and Z_n is compressibility factor at P_n. $P_{Eq(n)}$ is the equilibrium pressure after the gas expansion and $Z_{Eq(n)}$ is compressibility factor at $P_{Eq(n)}$. $P_{Eq(n-1)}$ is the equilibrium pressure of the previous injection and $Z_{Eq(n-1)}$ is compressibility factor at $P_{Eq(n-1)}$). R is the universal gas constant and T is temperature in Kelvin.

The above Equation 4.5 is for single injection pressure and therefore, to estimate the cumulative excess adsorption (n^{ex}) at the end of the last incremental pressure j^{th} step is determined from Equation 4.6.

$$\Delta n_{ex} = \Delta n^{ex}{}_1 + \Delta n^{ex}{}_2 + \Delta n^{ex}{}_3 + \Delta n^{ex}{}_4 + \cdots + \Delta n^{ex}{}_j \qquad 4.6$$

Once we obtained the cumulative excess adsorption by repeating the steps at sequentially higher pressures, the adsorption isotherms (experimental) are plotted. The quantity of gas adsorbed is typically expressed as an intensive quantity (mmol/g-coal) by dividing the total moles adsorbed (n_{ex}) by the mass of the adsorbent (coal) present in the sample cell, thus accounting for adsorption per unit mass of the adsorbent (Sudibandriyo et al., 2003).

4.3.3 Methodology Overview: Excess to Absolute Adsorption Calculation and Model Fitting

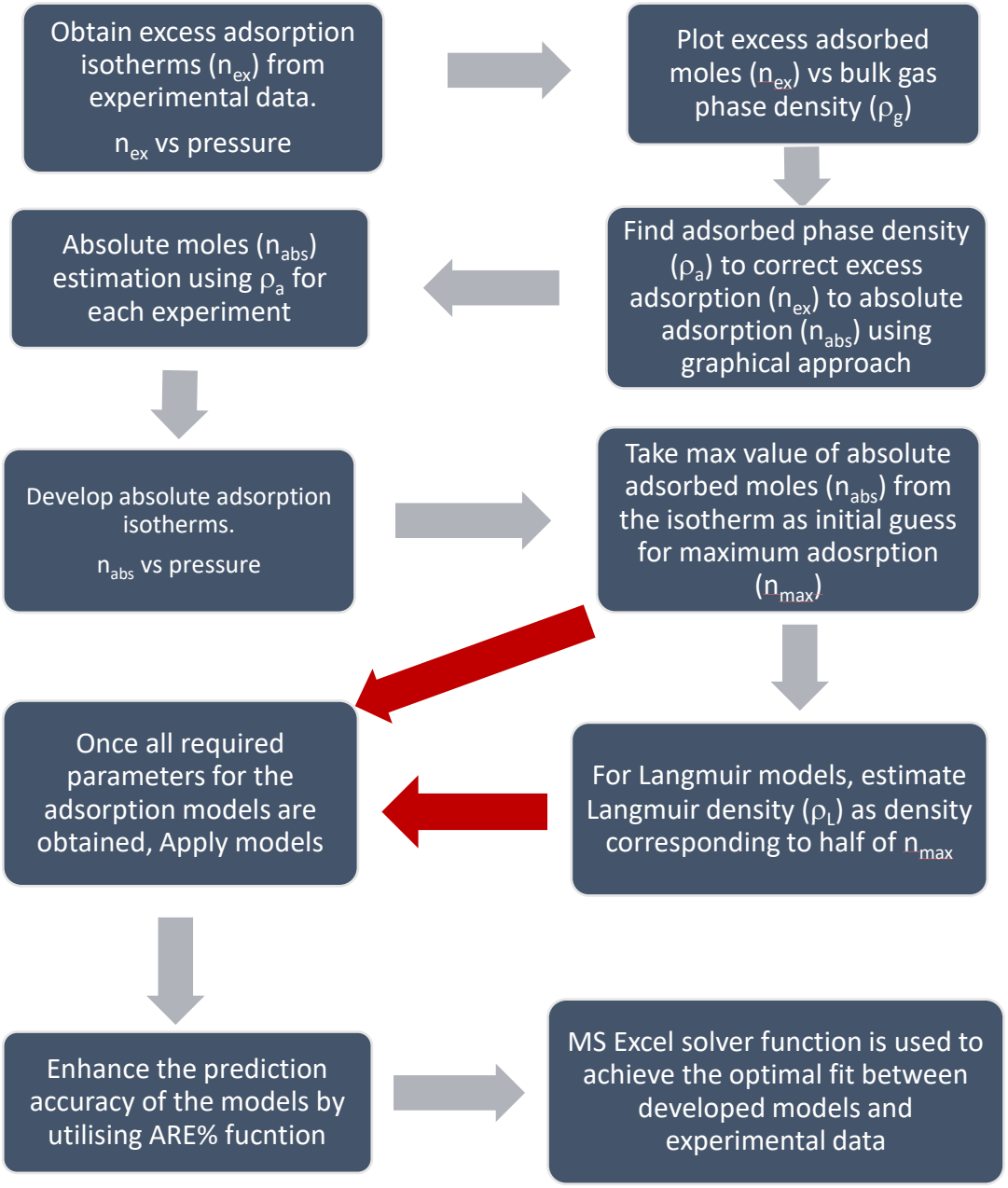

CHAPTER 5

RESULTS AND DISCUSSION

5.1 Adsorption behavior of supercritical CO_2

As mentioned in the section of adsorption theory, the adsorption amount derived directly from experimental tests is referred to as the Gibbs excess adsorption amount, denoted by the excess number of moles (n_{ex}). It is the total amount of gas estimated to be adsorbed when the volume of adsorbed phase, V_{ads}, is neglected. It does not represent the actual adsorption, represented by the absolute amount of gas adsorbed (n_{abs}) (Chen et al., 2016; Ozdemir, 2017; Meng et al., 2019).

Figure 5.1 illustrates the excess adsorption isotherm of Çankırı coal sample for three experimental trials. Each adsorption experiment is depicted in a distinct polynomial line based on the mass of coal sample and the number of excess moles adsorbed (n_{ex}). However, the adsorption behavior is consistent across each experiment. The lines represent the best possible fit of the data for the excess adsorption isotherm to Equation 4.5. Excess adsorption gradually increases as pressure rises until it reaches a maximum value. Subsequently, the excess adsorption amount begins to decrease as pressure increases further. This occurs because as the pressure rises, more CO_2 molecules are available to interact with the coal surface, increasing the excess adsorption amount. However, as the pressure continues to rise, a point is attained (near a critical value) where the available adsorption site on the coal surface becomes saturated with CO_2. At this stage, the excess adsorption amount reaches its maximum, indicating that the layer of adsorbed CO_2 effectively covers the coal particles. The pressure increase beyond this point does not substantially contribute to additional coal surface adsorption. Instead, the excess adsorption amount began to decline.

There are two major factors contributing to the decline. First, the decrease in excess adsorption is attributable to the increased free gas density (ρ_g) of CO_2 molecules in the sample cell, which reduces the amount of free space available for additional CO_2 molecules to adsorb onto the coal surface. Another reason for the decline is the effect of adsorbed phase volume which is not accounted for in the volumetric calculations.

In the volumetric experiments, the determination of number of moles in the sample cell relies on multiplying the equilibrium pressure with the void volume, as shown in Equation 4.5. This calculation assumes a constant void volume throughout the adsorption process. However, in reality, as CO_2 molecules are adsorbed onto the coal surface, they occupy space within the initially available void volume, which was intended for gas phase molecules. Consequently, as pressure increases and more CO_2 molecules are adsorbed, the adsorbed phase volume becomes more significant, while the remaining void volume for additional gas phase molecules diminishes, leading to a reduction in the excess adsorption amount (n_{ex}).

The omission of the adsorbed phase volume in the volumetric calculation results in an overestimation of the available void volume and, consequently, the number of moles in free gas phase. As a result, the number of moles in the adsorbed phase is underestimated. However, by determining the adsorbed phase density (ρ_{ads}) (see Appendix-D), it becomes possible to account for the additional volume occupied by the adsorbed molecules. Once ρ_{ads} is obtained, the number of moles in adsorbed phase, referred to as absolute adsorbed moles (n_{abs}), can be obtained using Equation 5.1. This approach allows for the development of absolute adsorption isotherms, facilitating a better understanding of the adsorption behavior.

$$n_{abs} = n_{ads} = \frac{\rho_{ads}}{\rho_{ads} - \rho_g} * n_{ex} \qquad 5.1$$

The absolute adsorption isotherms for Çankırı coal samples of three different weights are depicted by the distinct polynomial lines in Figure 5.2. These isotherms demonstrate a consistent increase in the absolute adsorption amount (n_{abs}) with increasing pressure. Initially, the rate of increase is high, but it eventually reaches a

point where n_{abs} stabilizes. Moreover, both the adsorbed density (ρ_{ads}) and free gas density (ρ_g) are observed to increase with pressure in Figure 5.1 and Figure 5.2, but ρ_{ads} tend to exhibit a faster increase towards a maximum value.

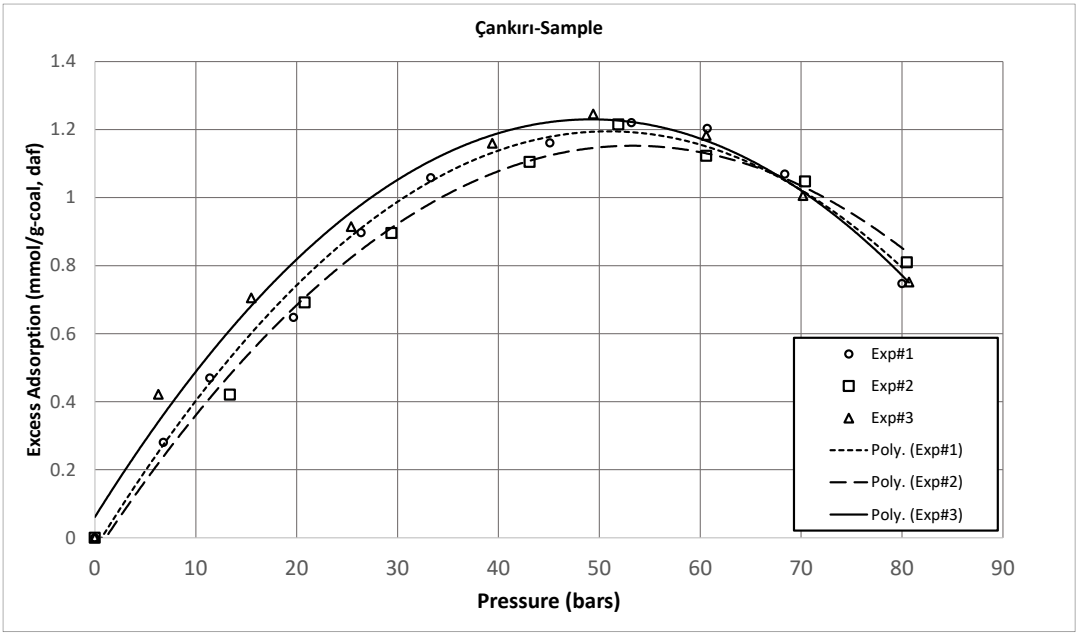

Figure 5.1. Excess adsorption isotherm for Çankırı coal sample

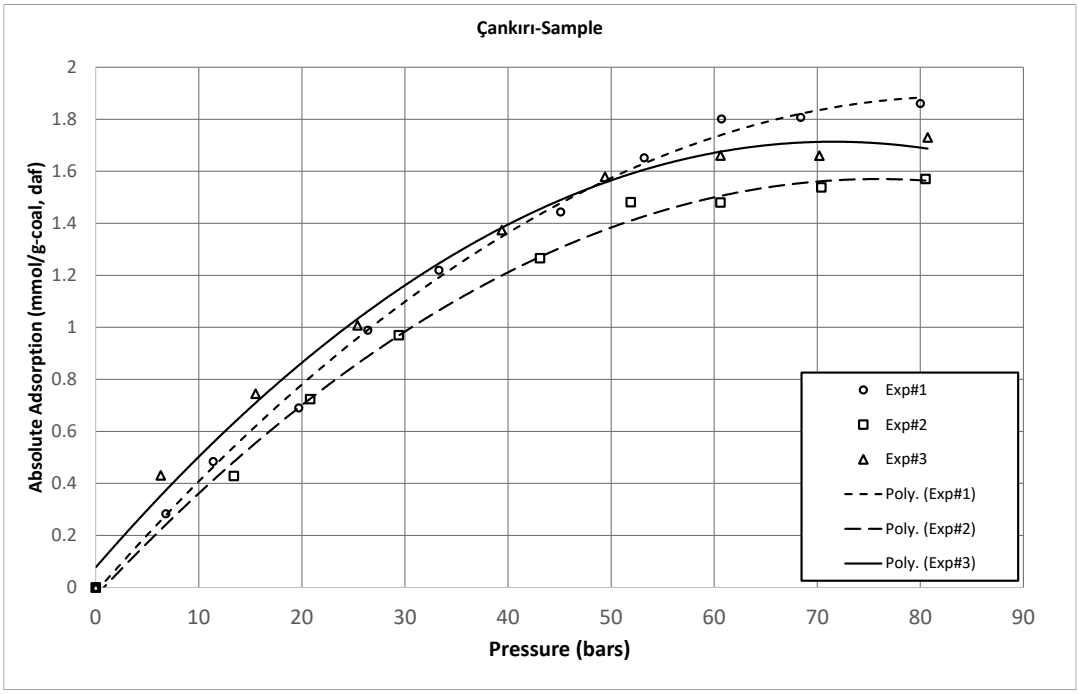

Figure 5.2. Absolute adsorption isotherm for Çankırı coal sample

5.1.1 Adsorption kinetics and equilibrium time for adsorption

The kinetics of CO_2 adsorption is a critical aspect in understanding the dynamic nature of CO_2 molecules interacting with the coal surface. Examining adsorption kinetics yields significant insights into the rate at which CO_2 molecules are adsorbed onto the coal surface (Ozdemir, 2017). The rate is commonly denoted as the difference between the total amount of CO_2 adsorbed at infinite time (M_∞) and total amount of CO_2 adsorbed at time 't' (M_t) divided by the M_∞ (Song et al., 2015).

To examine the adsorption kinetics in this study, Çankırı coal sample is loaded to the sample cell and CO_2 gas is injected systematically at three different pressures, 6.8, 26.4, and 45.1 bars. Each time the gas is vented out from the system before injecting the succeeding pressure. Equilibrium pressure (P_{Eq}) was monitored simultaneously with time. Figure 5.3 shows three different pressures at constant temperature of 313.15K. The figure demonstrates the adsorption rate, quantified by the expression $(M_\infty-M_t)/(M_\infty)$. Upon analysis of the graph, there is a consistent decline in the kinetics data over time. Notably, the duration needed to achieve equilibrium at a

pressure of 45.1 bars is comparatively shorter than that required at a pressure of 6.8 bars. This indicates that the adsorption rate increases with increasing pressures, particularly at lower pressure levels (Song et al., 2015).

The experimental data and observations have shown that the kinetics of CO_2 adsorption on coal exhibits the time-dependent characteristics, with an initially high adsorption rate that gradually decreases until reaching a state of equilibrium. The decrease in the rate of adsorption can be attributed to various factors, including the limited availability of the adsorption sites, diffusion limitations, and molecular interactions between CO_2 and the surface of coal. In addition, the adsorption kinetics of CO_2 can be influenced by pressure (Ozdemir, 2017). At reduced pressures, the adsorption rate generally increases with increasing pressure due to higher driving force that facilitates CO_2 molecules interaction with the coal surface. Nevertheless, under elevated pressures, there may be fluctuations in the initial adsorption stage caused by temperature variations with the adsorption cell (SC) after the injection of high-pressure CO_2.

The studies conducted by Charrière et al. (2010), which highlight similar trends in the adsorption kinetics of CO_2 at various pressures and temperatures, support the aforementioned observations. A thorough examination of pertinent research can help understand the behavior of CO_2 adsorption on coal. A better understanding can be utilized to optimize the process of adsorption for the purpose of CCS in various applications. Additional research is required to explore complex mechanisms and parameters that govern the kinetics of CO_2 adsorption.

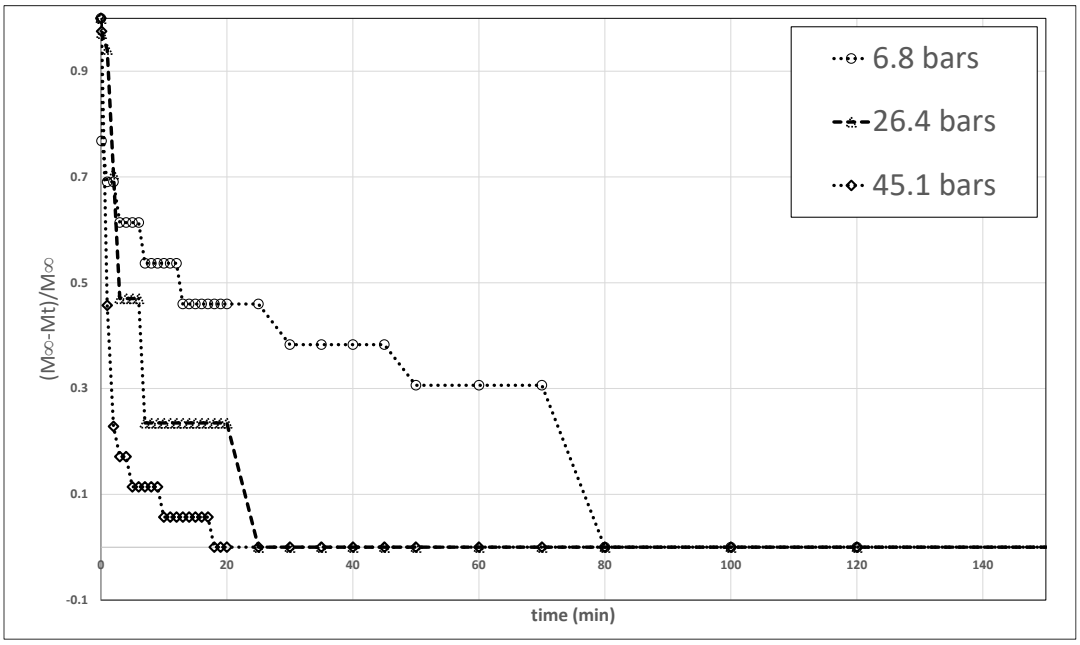

Figure 5.3. Experimental adsorption kinetics for CO_2 on dry Çankırı coal at 313.15K

5.2 Interpretation of adsorption isotherms using models

There are several adsorption models proposed in the literature to predict the behavior of the CO_2 in coal seams and to fit the experimental data such as Langmuir monolayer model, BET multi-layer model, and Dubinin's pore filling model as explained in section 3.3. In this study we have employed Langmuir modified, Langmuir modified +k, D-R modified, and D-R modified +k models to best fit the adsorption data of three Turkish coals as summarized in Table 5.1 below. These optimal models are selected based on a comprehensive analysis of the available parameters, their well-established reputation in the field of adsorption studies in literature, and their ability to capture the intricate adsorption phenomenon exhibited by the coal samples (Sakurovs et al., 2007; Dutta et al., 2008; Song et al., 2015; Meng et al., 2019; Liu et al., 2019; Guodai et al., 2021).

Table 5.1. Adsorption models (Meng et al., 2019).

Models	Equation
Modified Langmuir	$n_{ex} = n_{max} * \left(1 - \frac{\rho_g}{\rho_a}\right) * \frac{\rho_g}{\rho_L + \rho_g}$
Modified Langmuir + k	$n_{ex} = n_{max} * \left(1 - \frac{\rho_g}{\rho_a}\right) \frac{\rho_g}{\rho_L + \rho_g} + k\rho_g$
Modified D-R	$n_{ex} = n_{max} \left(1 - \frac{\rho_g}{\rho_a}\right) e^{\left\{-D\left[\ln\left(\frac{\rho_a}{\rho_g}\right)\right]^2\right\}}$
Modified D-R + k	$n_{ex} = n_{max} \left(1 - \frac{\rho_g}{\rho_a}\right) e^{\left\{-D\left[\ln\left(\frac{\rho_a}{\rho_g}\right)\right]^2\right\}} + k\rho_g$

In addition to applying the above-mentioned models, Average Relative Error (ARE) function, Equation 5.2, is utilized as a metric to evaluate the performance and to improve the prediction accuracy of each of these models in fitting the experimental data (Kumar et al., 2008; Song et al., 2015; Ayawei et al., 2017). Once the modeled isotherms are developed, The Microsoft Excel Solver tool is utilized as a powerful computational tool to optimize the fit between the developed models and the experimental data. The results of the best fit from the actual adsorption data were plotted against the predicted isotherms as indicated in Figure 5.4 to 5.9. The selection of the model yielding the minimum sum of errors serves as a robust indicator of its superior performance and suitability in describing the CO_2 adsorption behavior of the coal samples (Guodai et al., 2021).

$$ARE = \frac{100}{N} \sum_{i=1}^{N} \left| \frac{n_{ex} - n_{mod}}{n_{ex}} \right|_i \qquad 5.2$$

Where n_{ex} and n_{mod} is the amount of excess adsorption obtained from experimental results and models, and N is the total number of data points for each sample.

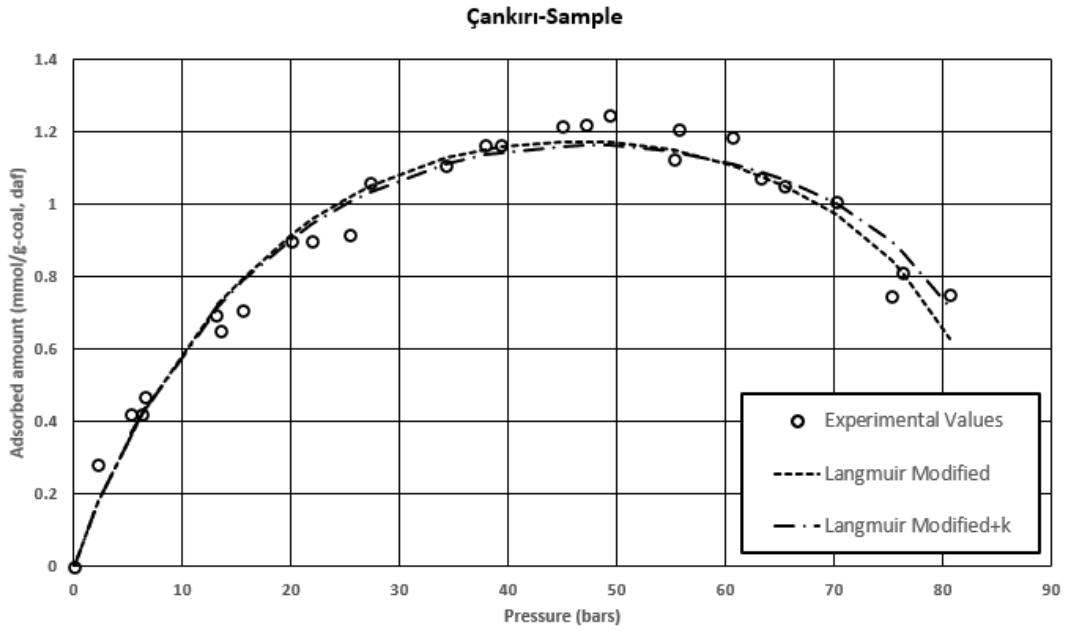

Figure 5.4. CO_2 adsorption data of Çankırı coal showing the Langmuir model fit.

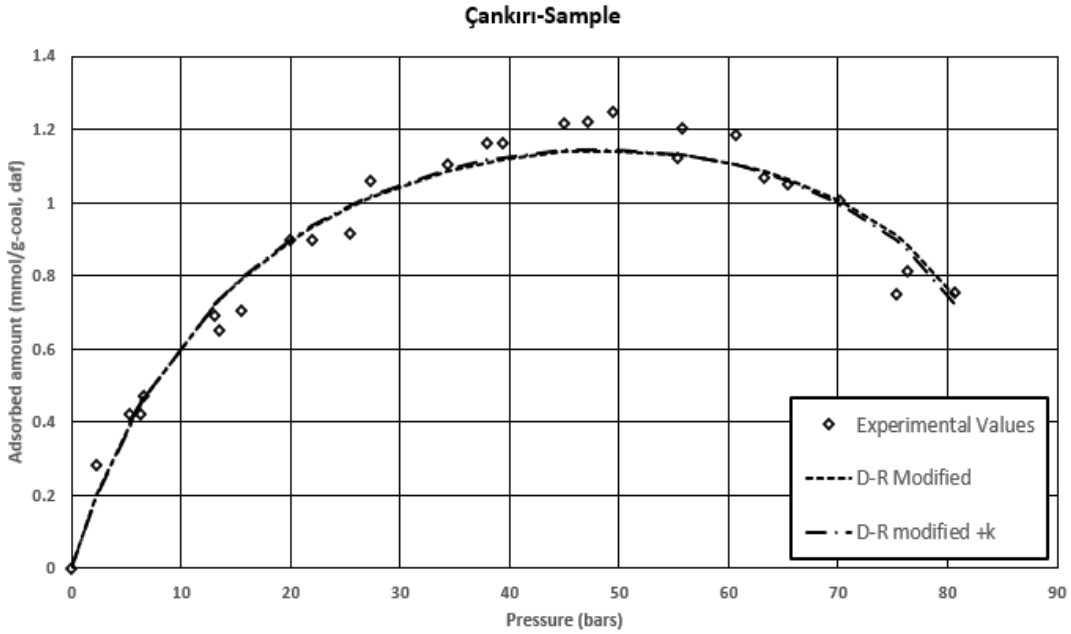

Figure 5.5. CO_2 adsorption data of Çankırı coal showing the D-R model fit.

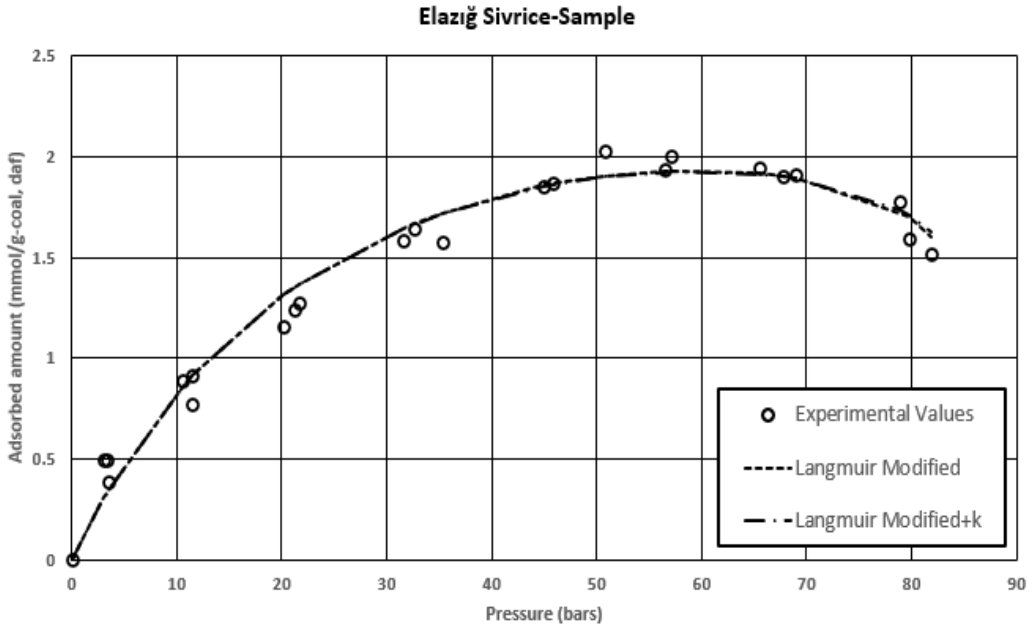

Figure 5.6. CO_2 adsorption data of Elazığ Sivrice coal showing the Langmuir model fit.

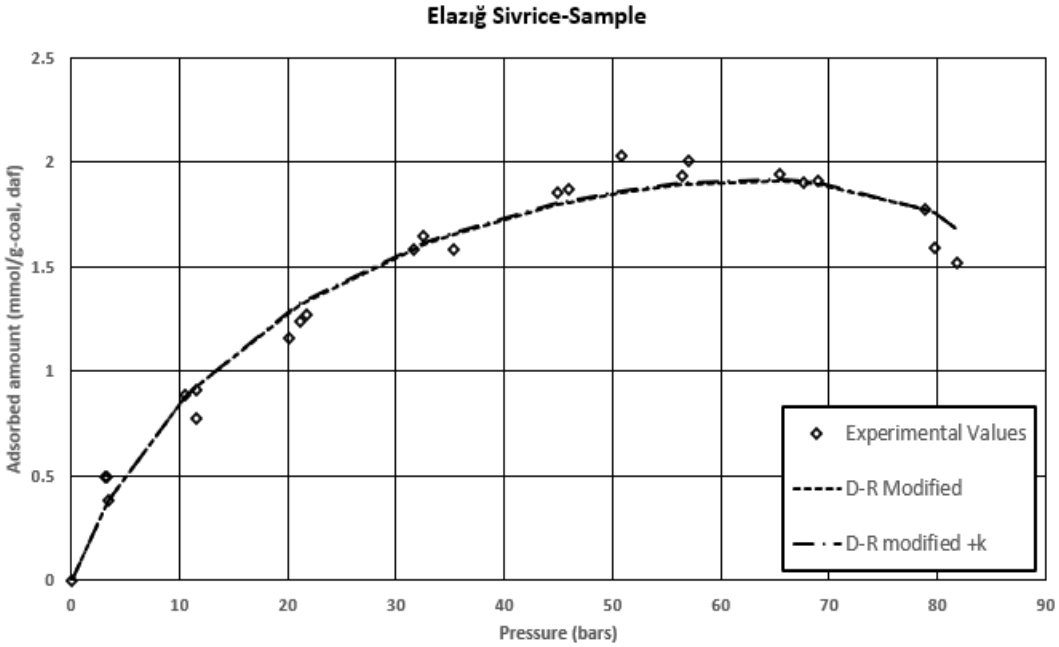

Figure 5.7. CO_2 adsorption data of Elazığ Sivrice coal showing the D-R model fit.

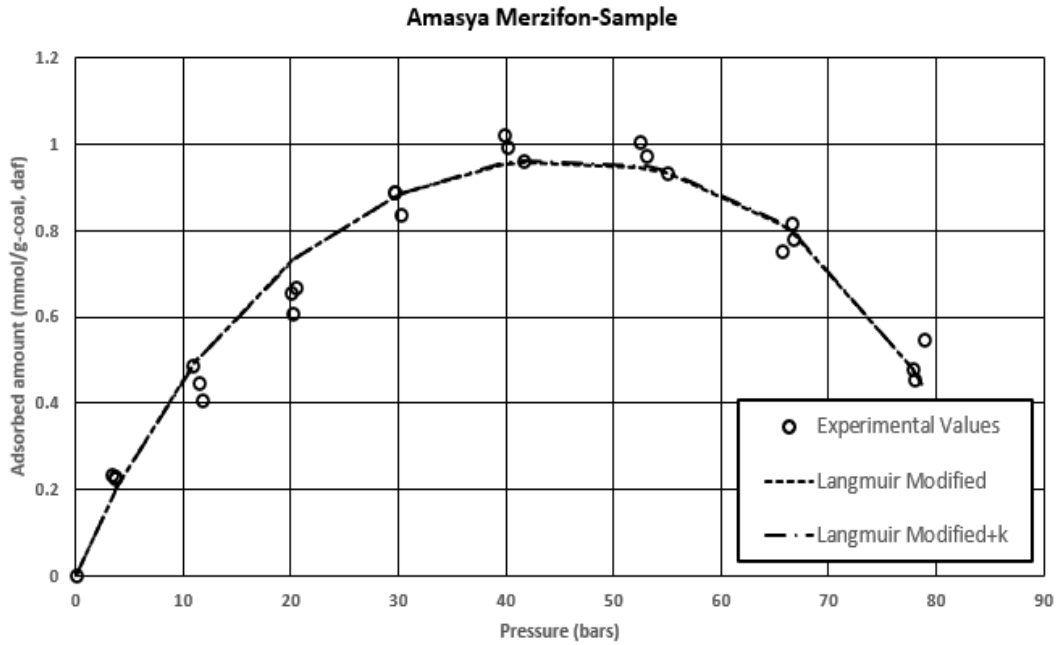

Figure 5.8. CO_2 adsorption data of Amasya Merzifon coal showing the Langmuir model fit.

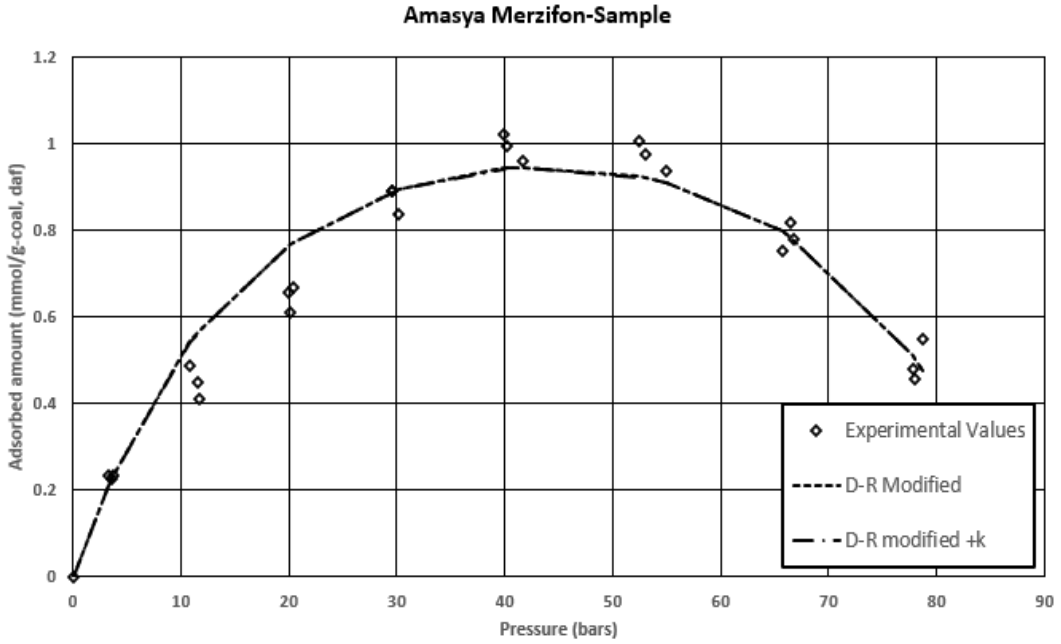

Figure 5.9. CO_2 adsorption data of Amasya Merzifon coal showing the D-R model fit.

The results of the fitted parameters for the Langmuir modified and D-R modified models are presented in Table 5.2 to 5.4. All four models are able to accurately describe the CO_2 adsorption behavior as all isotherms above fit the experimental data, but the D-R modified model performs better than the Langmuir model, as indicated by the lower ARE percentages.

The D-R model takes into consideration the energy distribution of adsorption sites and heterogeneity of the coal surface, both of which are essential for accurately describing the adsorption behavior. The better fit of the D-R model compared to the Langmuir model implies that the adsorption mechanism of gases in coal is predominantly governed by the pore-filling mechanism rather than monolayer coverage (Sakurovs et al., 2007). The higher ARE% observed for Langmuir models may be a result of their inability to account for intricate adsorption phenomenon observed in coal samples. The Langmuir model assumes monolayer adsorption on homogenous surfaces, which may not accurately represent the actual adsorption process involving multiple layers and heterogenous surfaces.

In addition, the 'k' term in the Langmuir modified +k and D-R modified +k equations accounts for the volumetric change, which includes swelling and contraction. In this study, we observed a slight shrinkage upon moisture loss by reduction in weight and swelling upon CO_2 adsorption by increase in weight of coal sample, but the 'k' term is negligible relative to other parameters and has no major influence on overall adsorption capacity. There could be several reasons for this, including the inherent characteristics and composition of coal samples, as they are all low rank Lignite coals, with nearly identical chemical properties (Liu et al., 2019). The operating conditions of the adsorption experiments, such as pressure range, may not be conducive to inducing substantial volume changes in the coal samples. This also corroborates with the findings of other studies, in which several researchers observed significant variations in the 'k' term on high pressures up to 200bars, whereas the

highest pressure observed in this study was 83 bars (Sakurovs et al., 2007; Dutta et al., 2008).

Table 5.2. Optimal fitting parameters for Çankırı coal

Çankırı Coal					
	n_{max} (mmol/g)	**ρ_L (mol/cc)**	**ρ_a (mol/cc)**	**k (cc/mol)**	**ARE (%)**
Langmuir Modified	2.23	0.0010	0.0097	-	6.58
Langmuir Modified +k	2.09	0.00096	0.011	0.06	6.55
	n_{max} (mmol/g)	**ρ_a (mol/cc)**	**D**	**k (cc/mol)**	**ARE (%)**
D-R Modified	1.81	0.011	0.09	-	6.42
D-R Modified+k	1.83	0.011	0.09	0.04	6.42

Table 5.3. Optimal fitting parameters for Elazığ Sivrice coal

Elazığ Sivrice Coal					
	n_{max} (mmol/g)	**ρ_L (mol/cc)**	**ρ_a (mol/cc)**	**k (cc/mol)**	**ARE (%)**
Langmuir Modified	3.27	0.0012	0.016	-	7.68
Langmuir Modified +k	3.22	0.0011	0.017	0.15	7.67
	n_{max} (mmol/g)	**ρ_a (mol/cc)**	**D**	**k (cc/mol)**	**ARE (%)**
D-R Modified	2.98	0.018	0.086	-	6.66
D-R Modified	2.99	0.012	0.087	0.15	6.65

Table 5.4. Optimal fitting parameters for Amasya Merzifon coal

Amasya Merzifon Coal					
	n_{max} (mmol/g)	ρ_L (mol/cc)	ρ_a (mol/cc)	k (cc/mol)	ARE (%)
Langmuir Modified	1.60	0.00085	0.009	-	9.98
Langmuir Modified +k	1.60	0.00085	0.009	0.07	9.98
	n_{max} (mmol/g)	ρ_a (mol/cc)	D	k (cc/mol)	ARE (%)
D-R Modified	1.57	0.0087	0.11	-	9.35
D-R Modified	1.56	0.0088	0.11	0.07	9.35

5.3 Effect of coal characteristics and volumetric changes on adsorption

The proximate analysis results shown in Table 5.5 of Çankırı, Elazığ Sivrice, and Amasya Merzifon coal samples, yielded valuable insights on the CO_2 adsorption capacity of coal (n_{max}). Previous studies have indicated that various factors, such as coal rank, coal type, and physiochemical properties, including proximate analysis and moisture content, can influence coal adsorption characteristics (Faiz et al., 2007; Pini et al., 2011; Kim et al., 2011).

Coals with a higher percentage of Fixed Carbon (FC%) have been shown to exhibit higher adsorption capacity. Research indicates that an increase in coal's FC content leads to higher specific surface area and pore volume, accompanied by smaller, more uniformly arranged coal particles. This enhanced surface area and pore structure provide greater space for gas adsorption, thereby increasing CO_2 adsorption capacity of coal (Cheng et al., 2017). In our research, a positive correlation is observed between the FC and n_{max} for these coal samples (Figure 5.10). Among the samples, Elazığ Sivrice displayed the highest FC (51.40%), followed by Çankırı (45.96%),

while Amasya Merzifon had a substantially lower FC (21.05%). This trend was consistent with the observed n_{max}, where Elazığ Sivrice showed the highest adsorption capacity (2.99 mmol/g-coal), followed by Çankırı (1.83 mmol/g-coal), while Amasya Merzifon had relatively lower n_{max} (1.56 mmol/g-coal).

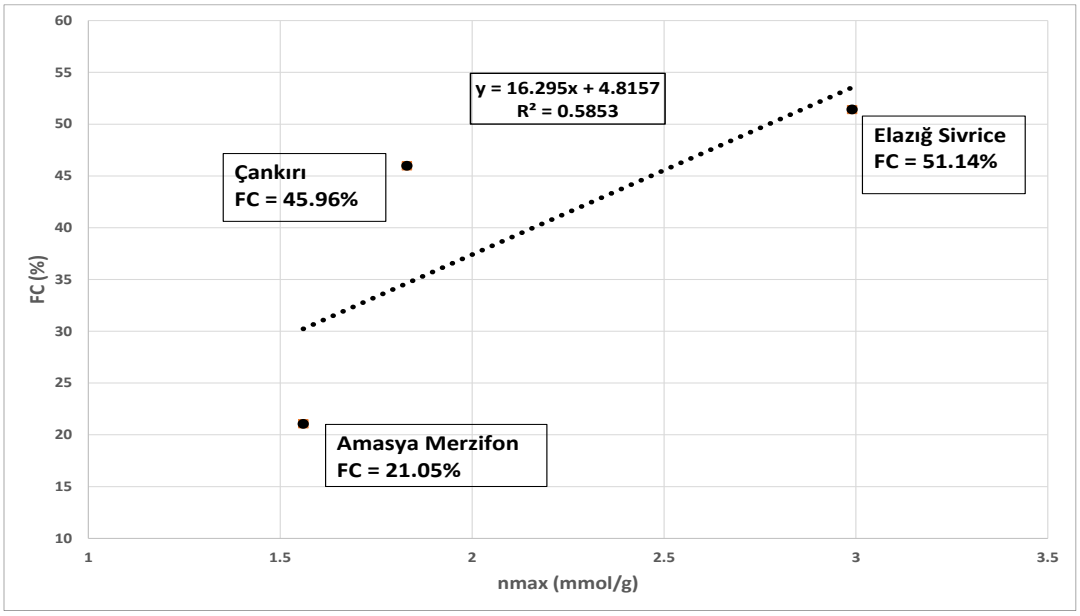

Figure 5.10. Correlation between FC% and n_{max}

In low-rank coals, such as lignite and subbituminous coal, the Huminite Reflectance (HR%) is employed as a measure of thermal maturity (Thomas, 2013). Analyzing the HR% values of the coal samples, calculated from Equation 4.1 (Rice, 1993), reveals that Amasya Merzifon possesses the maximum level of maturity. Prior studies have highlighted the significance of organic matter content for gas adsorption on coal, with huminite specifically influencing the CO_2 adsorption due to its associated micropore connections (Mangi et al., 2022; Tambaria et al., 2023). This experimental result in Table 5.5 is consistent with those findings, where a correlation is observed between huminite content and CO_2 adsorption capacity. Notably, despite Amasya Merzifon having the lowest FC%, it has a reasonable adsorption capacity due to a slightly higher HR%. Çankırı and Elazığ Sivrice both had HR values of 1.75%, while Amasya Merzifon had a marginally higher value of 1.87%.

A higher moisture content in coal can also have adverse effects on its adsorption capacity. Dry coal is widely characterized as a 'non-wet' material, primarily due to its inherent hydrophobic nature. This property means that coal typically resists the absorption or penetration of water on its surface. However, it is imperative to recognize that coal may retain moisture, despite its non-wet nature. This moisture content may arise from various sources, including exposure to humid atmospheric conditions during storage and transportation or from the original geological formation process (Shojai Kaveh et al., 2012).

Moisture occupies the adsorption sites on the surface of coal, limiting the availability of active sites for CO_2 adsorption (Gensterblum, 2013). Additionally, moisture forms a film around the coal particles, reducing the effective area and impeding gas adsorption (Ozdemir, 2004; Zhao et al., 2018). According to the data presented in Table 5.5, Çankırı coal exhibits the highest moisture content (11.20%) followed by Elazığ Sivrice (9.18%), while Amasya Merzifon sample demonstrates a relatively lower moisture content of 4.77%. As explained in the preceding chapter, all the coal samples underwent a drying process before the adsorption experiments to mitigate the effect of moisture content (Tambaria et al., 2023). As shown in Figure 5.11, There is visible mass difference between the as-received and the dried coal samples. Çankırı sample, which had the highest initial moisture content, also demonstrated the maximum amount of shrinkage of around 9% following the drying process. Similarly, Elazığ Sivrice coal, which had a higher moisture % than Amasya Merzifon coal, exhibited a higher degree of shrinkage of around 6%. The findings presented in this study provide empirical support for the theoretical framework established in prior studies (Deevi & Suuberg, 1987; Ozdemir et al., 2004; Tambaria et al., 2023). Nevertheless, it is important to acknowledge that shrinkage does not have a direct correlation with the CO_2 adsorption capacity. Instead, it functions as an indicator of the reduction in mass of the sample caused by the loss of moisture during the drying procedure.

Table 5.5. Comparison of coal characteristics and CO_2 adsorption capacity

Samples	n_{max} (mmol/g-coal)	Fixed Carbon FC (%)	Moisture (%)	Huminite Reflectance *HR (%)
Çankırı	1.83	45.96	11.20	1.75
Elazığ Sivrice	2.99	51.40	9.18	1.75
Amasya Merzifon	1.56	21.05	4.77	1.87

*HR (%) is calculated from the Equation 4.1
*All values are on a dry basis

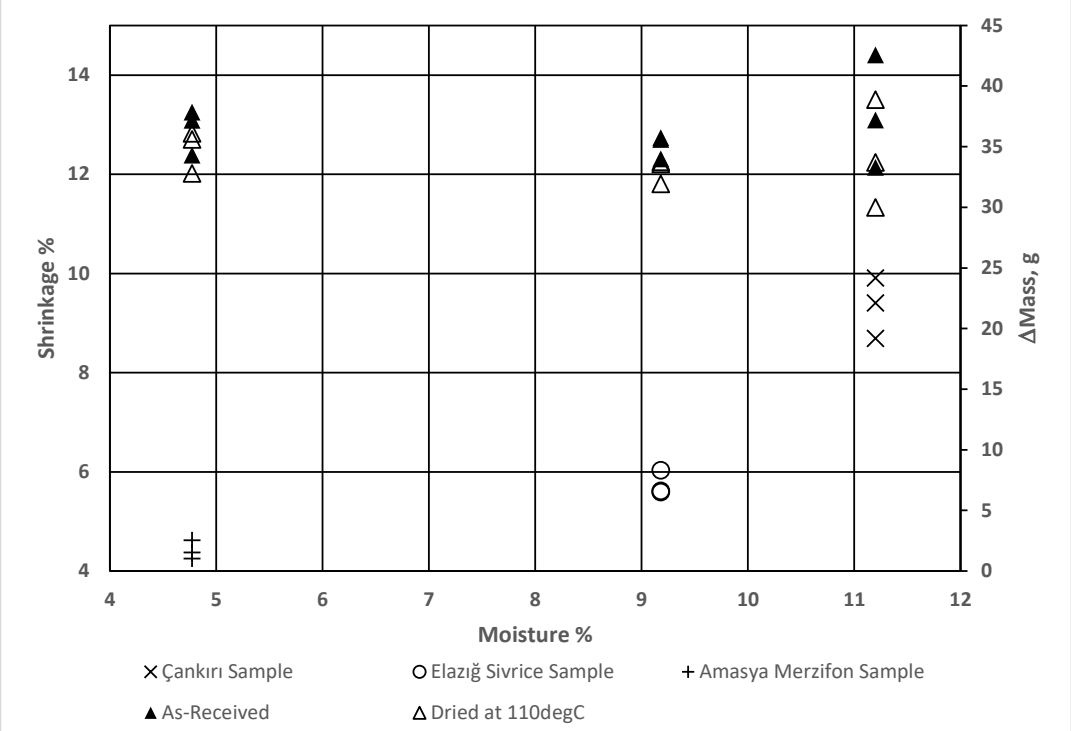

Figure 5.11. Comparison of mass change and percent shrinkage of the coal samples upon drying.

5.4 Combined excess (n_{ex}) and absoulte (n_{abs}) adsorption isotherms

To ensure enhanced precision, a series of CO_2 adsorption experiments were conducted on three distinct coal samples, namely Çankırı, Elazığ Sivrice, and Amasya Merzifon, with each sample being subjected to three repetitions. The measurements of excess adsorption were taken at various equilibrium pressures, and the resulting data were aggregated, and presented in Figure 5.12, as depicted below. Subsequently, Absolute adsorption isotherms were developed for each coal sample after each experimental run, and these results are displayed in Figure 5.13. The graph illustrates the highest level of adsorption exhibited by the Elazığ Sivrice sample, followed by Çankırı and Amasya Merzifon samples. Notably, the isotherm for Amasya Merzifon demonstrates a prominent peak at approximately 55 bars, further highlighting its unique adsorption behavior.

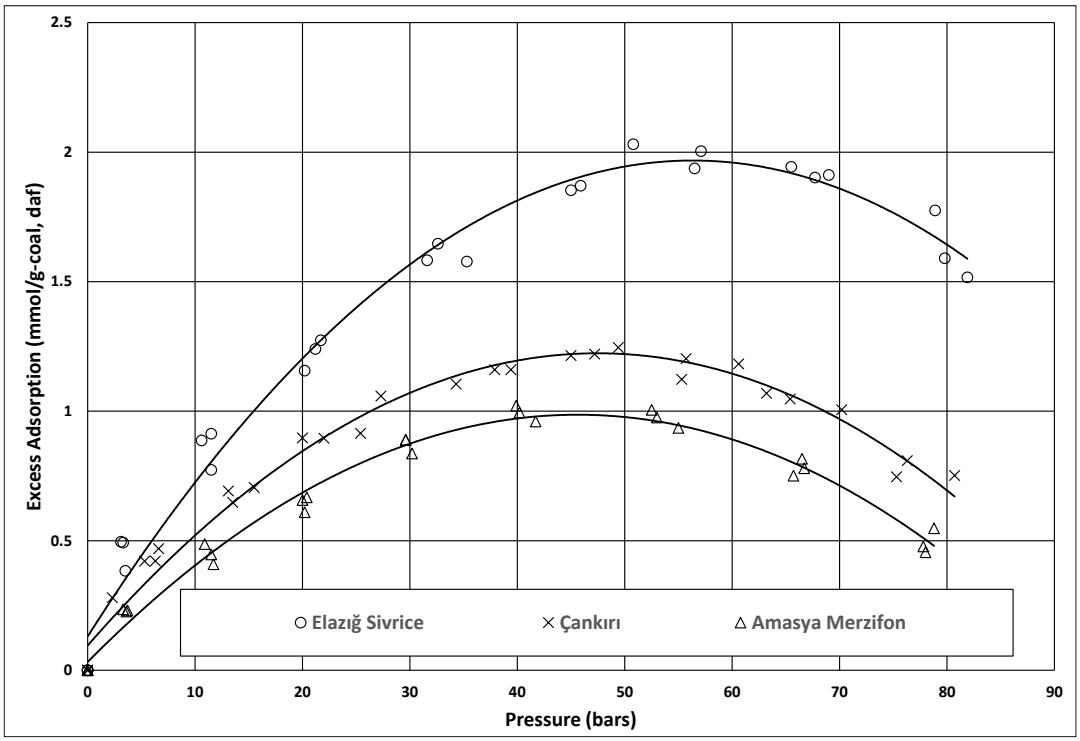

Figure 5.12. Combined excess adsorption isotherms of all the coal samples.

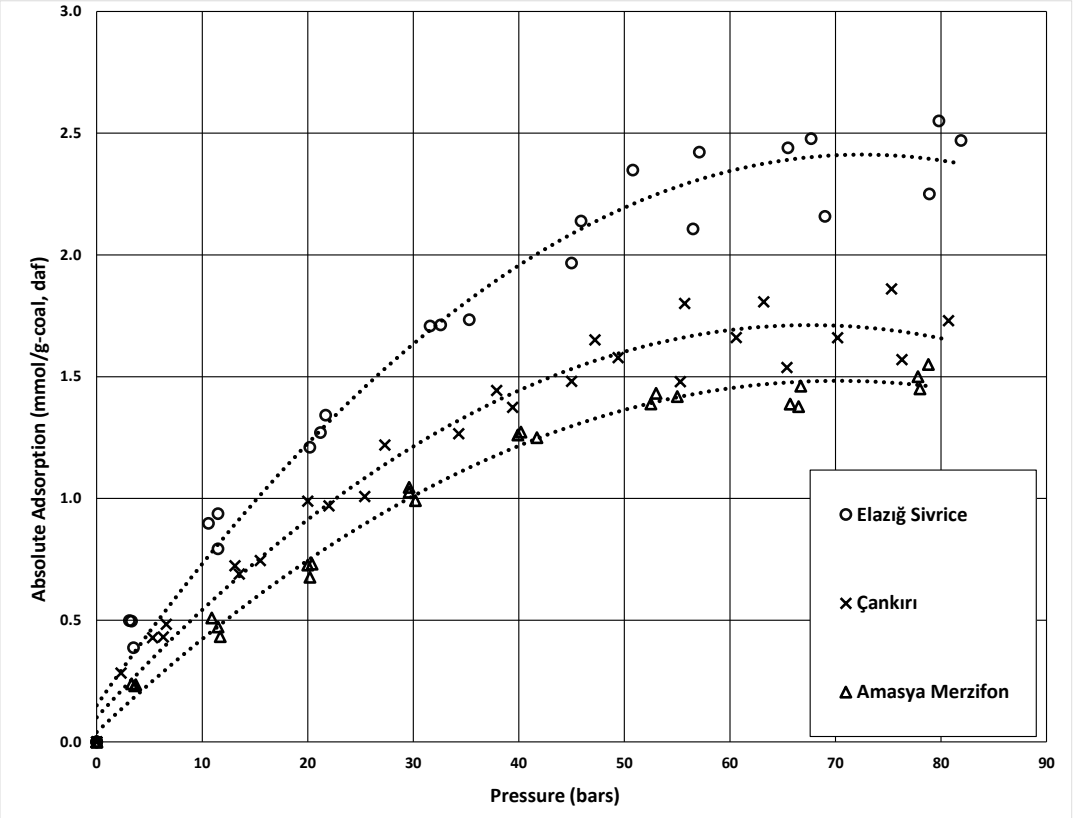

Figure 5.13. Combined absolute adsorptions for all the coal samples.

5.5 Storage capacity of CO_2 in studied basins

The assessment of storage capacity for CO_2 in coal seams is a critical aspect for evaluating the viability of Carbon Capture and Storage (CCS) as means to mitigating greenhouse gas emissions. In order to estimate the storage capacity, several methodologies are utilized in literature, encompassing geological surveys, laboratory experiments, and computational modelling (Bachu et al., 2007; Nah, 2010). This study has employed the theoretical formula, Equation 5.3, for storage capacity (S.C).

$$Storage\ capacity = adsorbed\ gas + free\ gas$$

$$S.C = [V_{coal} * \rho_{coal} * (1 - \emptyset) * n_{max} * (1 - a - m)] + [V_{coal} * \emptyset * \frac{S_g}{B_g}] \quad 5.3$$

Where V_{coal} is the volume of the coal seam (m^3), ρ_{coal} is the density of coal (g/cc), Ø is the cleat porosity, n_{max} is the maximum adsorption of CO_2 on coal estimated from the D-R model (mmol/g), 'a' & 'm' are the ash and moisture content (%), S_g is the gas saturation, taken as 10% and B_g is the formation volume factor for the gas phase (Ozdemir, 2004).

Accurately determining the storage capacity of a coal seam requires comprehensive information derived from both laboratory experiments and field data. However, due to limited access to these resources, assumed values for the parameters used in the literature have been adopted. For instance, Seidle (2011) estimated the cleat or fracture porosity of low-rank coals as 1%, while Nelson et al. (2000) reported an effective porosity range of 0.6% to 1.2% for such coals. In this study, a porosity value of 1% has been assumed for the coal seams (Weniger et al., 2016). The density of coal (ρ_{coal}) is estimated using Equation 7.5, suggested by Seidle (2011). The organic density (ρ_o) and ash density (ρ_a) are considered as 1.25 g/cc and 2.55 g/cc, respectively, while the density of water (ρ_w) is assumed to be 1g/cc. In this equation '*a'* and '*w'* parameters are the ash % and moisture %. The coal density values used here have also been corroborated by other relevant literature sources (Gül & Küçükkarasu, 2020).

$$\rho_{coal} = \frac{1}{\frac{1-a-w}{\rho_o} + \frac{a}{\rho_a} + \frac{w}{\rho_w}} \tag{5.4}$$

The formation volume factor for gas (B_g) is calculated from Equation 7.6 (Guo & Ghalambor, 2005). The formula incorporates various factors, including the standard pressure (P_{SC}) of 1.013 bars, the standard temperature (T_{SC}) of 293.15 K, and the compressibility factor at standard conditions (Z_{SC}). In this study, the pressure at reservoir conditions (P) and the reservoir temperature (T) are considered, with a reservoir temperature of 313.15 K selected for this investigation.

$$B_g = \frac{V}{V_{SC}} = \frac{P_{SC}}{P} * \frac{T}{T_{SC}} * \frac{Z}{Z_{SC}} \tag{5.5}$$

The estimated reserves of coal seams reported until 2019, along with the maximum calculated CO_2 storage potential of corresponding coal basins, are presented in Table 5.6. Figure 5.14 shows a graphical representation of the projected storage capacity of CO_2 in million tons, based on theoretical estimations, across various pressure levels, ranging up to 80 bars. It is worth noting that Elazığ Sivrice, in spite of having lower reserves in comparison to Çankırı, exhibits the highest storage capacity due to its maximum adsorption capacity. In contrast, Amasya Merzifon has the least number of reserves, thereby indicating the lowest storage capacity.

For a comprehensive assessment of CO_2 storage capacity in terms of years, it is imperative to consider the emissions of CO_2 stemming from a 100 MW coal power plant. The widely accepted industry average for CO_2 emissions from coal power plants, as substantiated by existing literature, stands at approximately 1 kg per kilowatt-hour (kWh) of electricity generated (Mittal, 2012; EIA, 2021). In line with this, accounting for the operational efficiency of the power plant, estimated at 70%, we derive the annual energy output as follows:

Energy (kWh/year) = (100 * 1000) * (365 * 24 * 0.7)

Energy = $6.13 * 10^8$ kWh/year

Consequently, it can be inferred that such a power plant would release an annual volume of 0.613 Mt of CO_2. These emissions serve as a basis for evaluating the CO_2 storage potential in the studied basins, presented in Table 5.6. Notably, Elazığ Sivrice emerges as the most promising candidate for long-term CO_2 storage, with a capacity exceeding a decade. Following closely, Çankırı exhibits an estimated storage potential of 8 years, while Amasya Merzifon indicates a capacity to retain CO_2 for a duration of 2 years.

Nevertheless, it is important to recognize that specific parameters utilized in the assessment of CO_2 storage capacity are obtained from existing scholarly sources, and the resulting outcomes are only approximate estimations owing to the limited availability of up-to-date data. The actual emissions and energy production values

may vary among other plants, and the calculation is based on the assumptions made for this study.

Table 5.6. Approximated CO_2 storage capacity in coal seams

Coal Basin	Estimated Reserves (Mt) (MTA, 2021)	Estimated Storage of CO_2 (Mt)	Specific Storage ($ktCO_2$/Mt-coal)	Storage Potential (years)
Elazığ Sivrice	88	6.28	41.8	10
Çankırı	123	5.15	71.4	8
Amasya Merzifon	24.8	1.08	43.5	2

*Reserves estimates for the coal seams are taken from (MTA, 2021)

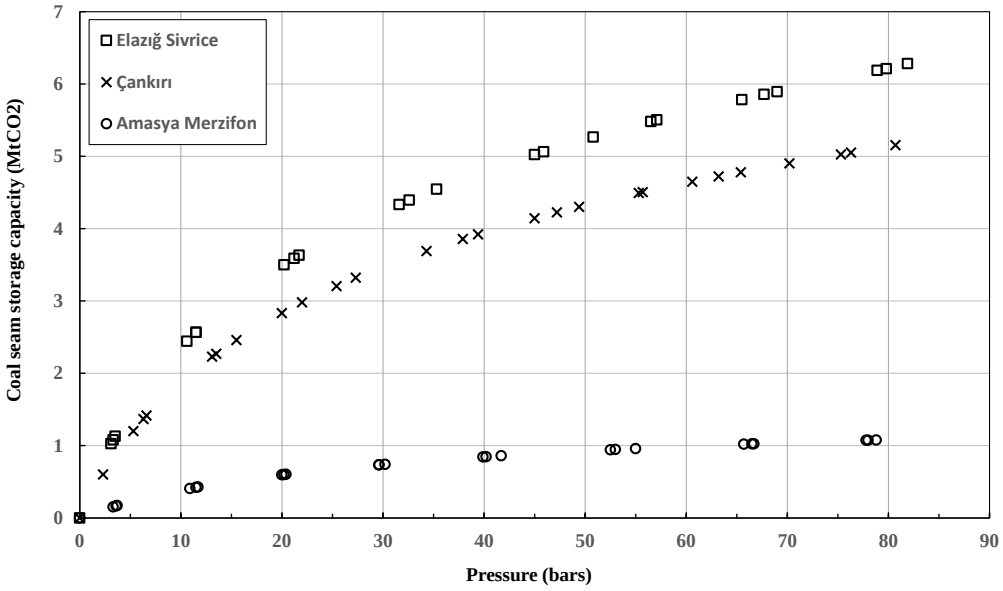

Figure 5.14. Storage capacity of the studied basins

CHAPTER 6

CONCLUSION

In this study, a series of experimental investigations of CO_2 adsorption were carried out on three Turkish lignite coal samples from Çankırı, Elazığ Sivrice, and Amasya Merzifon coal seams. A volumetric setup was modified with compression setup to measure the CO_2 adsorption on these coal samples at 313.15 K by incrementally injecting CO_2 in a sequential manner up to 85 bars. Compression setup was used to increase the CO_2 pressure to the required levels.

The research sheds light on the variations in CO_2 adsorption behavior across three different coals, emphasizing the influence of coal characteristics. Additionally, it highlights the kinetics of adsorption as pressure levels increase, enriching our understanding of this critical process. Moreover, by estimating the CO_2 storage capacity within the studied basins, based on emissions from a 100MW power plant, this research might contribute essential information for future carbon capture and storage endeavors.

- Four adsorption models, namely Langmuir modified, Langmuir modified +k, D-R modified, and D-R modified +k, were utilized to develop adsorption isotherms. All these models showed a high level of agreement with the experimental data, exhibiting an average relative error (ARE) that was well within the acceptable range of ± 9%.
- Among these adsorption models, it was found that the D-R modified model performs slightly better when applied to all coal samples, effectively capturing the complexities of the adsorption behavior. Additionally, this suggests that the pore-filling mechanism of CO_2 is starting to have an impact, although it is not yet the prevailing mechanism. This is supported by the fact

that the Langmuir modified model also provides a reasonable match, indicating that the adsorption is not too far from monolayer coverage.

- Following the analysis of the fit parameters within the D-R modified model, it is observed that the maximum CO_2 adsorption capacity (n_{max}) is determined to be 1.83 mmol/g for the Çankırı sample, 2.99 mmol/g for the Elazığ Sivrice sample, and 1.56 mmol/g for the Amasya Merzifon sample. It is important to note that all values are reported on a "daf" basis. These values are in accordance with the literature on the adsorption behavior of similar ranks of coal as well as aligning with the previous research carried out by Mr. C.B.Keza on Lignite coal samples (Keza, 2021).
- Coal characteristics also had an impact on the adsorption capacity n_{max}. From Table 5.5, a positive correlation between Fixed Carbon (FC)% and adsorption capacity is observed that reveals the significance of coal composition, with higher FC% translating to enhanced adsorption potential. The interaction of HR% and moisture content reveals the subtle yet influential role of these variables in modulating adsorption behavior. It is essential to acknowledge that these observations are drawn from the analysis of three specific coal samples. It is noteworthy that these results align with existing literature, which has previously indicated such correlations.
- A theoretical model was employed to assess the approximate estimation of storage capacity considering parameters like coal seam volume, density, cleat porosity, and adsorption properties. The study acknowledged the challenges associated with restricted data availability and addressed this issue by utilizing existing literature values to estimate the parameters. Elazığ Sivrice basin demonstrated promising storage potential of 6.28 Mt despite lower reserves, followed by Çankırı 5.15 Mt, while Amasya Merzifon showcased the lowest storage capacity of 1.08 Mt. Similarly, the predicted storage durations for Elazığ Sivrice, Çankırı, and Amasya Merzifon were 10 years, 8 years, and 2 years, respectively.

The research integrates adsorption experiments with models, leading to a thorough understanding of the CO_2 adsorption phenomenon on various Turkish lignite coals. The trends, correlations, and storage capacities that have been observed collectively add to the broader academic discussion on sustainable environmental practices and strategies for mitigating carbon emissions. By merging practical results with theoretical insights, the study underscores the importance of coal properties in influencing adsorption behaviors. This has practical implications for utilizing CO_2 adsorption in carbon capture and storage technology. In alignment with existing literature and prior research, this work simplifies complex concepts, contributing to the understanding of CO_2 adsorption on coal and supporting a more eco-conscious and sustainable path forward.

6.1 Recommendations

In the realm of real field applications, it is important to recognize that the coal samples utilized in laboratory experiments may not fully represent the complex and heterogeneous nature of coal seams found in natural geological formations. Real-world non-mineable coal seams often exhibit variations in porosity, compaction, and the presence of moisture or connate water. These variations can significantly influence the adsorption behavior of CO_2.

To address these aspects comprehensively, additional experiments involving core samples extracted directly from coal seams under in-situ conditions would be highly recommended. These experiments could provide insights into the impact of natural moisture content, porosity, and compaction on CO_2 adsorption.

Given the limited pressure range investigated in this study, it is recommended to conduct experiments at substantially higher pressures and temperatures to replicate the environmental conditions of various coal seams. This would lead to more precise and field-relevant results, hence improving the applicability of the findings for actual carbon capture and storage endeavors.

Additionally, when estimating storage capacities of coal basins, it is advisable to rely solely on non-minable coal reserve volumes, as minable reserves, typically located close to the surface without adequate confining strata, are not suitable for carbon capture and storage (CCS) initiatives. Hence, a more accurate estimation of storage capacity can be achieved through this approach.

In the pursuit of CCS projects, it is imperative to prioritize the integrity of cap-rock, which serves as a confining layer. In addition, it is essential to thoroughly evaluate the long-term interactions between CO_2 and coal. Comprehensive investigations into these aspects are essential for ensuring the safety and success of CCS initiatives.

REFERENCES

Al Hameli, F., Belhaj, H., & Al Dhuhoori, M. (2022). CO2 Sequestration Overview in Geological Formations: Trapping Mechanisms Matrix Assessment. Energies, 15(20), 7805. https://doi.org/10.3390/en15207805

Aminu, M. D., Nabavi, S. A., Rochelle, C. A., & Manovic, V. (2017). A review of developments in carbon dioxide storage. Applied Energy, 208, 1389–1419. https://doi.org/10.1016/j.apenergy.2017.09.015

Andersen, T. N. (1968). Physical Adsorption: The Solid-Gas Interface . E. Alison Flood, Ed. Dekker, New York, 1967. Vol. 1, xviii + 514 pp., illus. $21.75; vol. 2, xvi + 661 pp., illus. $27.50. Science, 159(3815), 85. https://doi.org/10.1126/science.159.3815.619.a

Ansaloni, L., Alcock, B., & Peters, T. A. (2020). Effects of CO2 on polymeric materials in the CO2 transport chain: A review. International Journal of Greenhouse Gas Control, 94, 102930. https://doi.org/10.1016/j.ijggc.2019.102930

ASTM. (2011). Test Method for Microscopical Determination of the Reflectance of Vitrinite Dispersed in Sedimentary Rocks. American Society for Testing and Materials. http://www.astm.org/cgi-bin/resolver.cgi?D7708-11

Ayawei, N., Ebelegi, A. N., & Wankasi, D. (2017). Modelling and Interpretation of Adsorption Isotherms. Journal of Chemistry, 2017, 1–11. https://doi.org/10.1155/2017/3039817

Azizian, S., & Eris, S. (2021). Adsorption isotherms and kinetics. In Interface Science and Technology (Vol. 33, pp. 445–509). Elsevier. https://linkinghub.elsevier.com/retrieve/pii/B9780128188057000114

Bachu, S., Bonijoly, D., Bradshaw, J., Burruss, R., Holloway, S., Christensen, N. P., & Mathiassen, O. M. (2007). CO2 storage capacity estimation: Methodology and gaps. International Journal of Greenhouse Gas Control, 1(4), 430–443. https://doi.org/10.1016/S1750-5836(07)00086-2

Bratek, K., Bratek, W., Gerus-Piasecka, I., Jasieńko, S., & Wilk, P. (2002). Properties and structure of different rank anthracites. Fuel, 81(1), 97–108. https://doi.org/10.1016/S0016-2361(01)00120-X

Brunauer, S., Emmett, P. H., & Teller, E. (1938). Adsorption of Gases in Multimolecular Layers. Journal of the American Chemical Society, 60(2), 309–319. https://doi.org/10.1021/ja01269a023

Burnard, K. (2003). Special Issue on Clean Coal Technologies. Proceedings of the Institution of Mechanical Engineers, Part A: Journal of Power and Energy, 217(1), i–ii. https://doi.org/10.1177/095765090321700101

Busch, A., Gensterblum, Y., Krooss, B. M., & Littke, R. (2004). Methane and carbon dioxide adsorption–diffusion experiments on coal: Upscaling and modeling. International Journal of Coal Geology, 60(2–4), 151–168. https://doi.org/10.1016/j.coal.2004.05.002

Bustin, R. M., Cameron, A. R., Grieve, D. A., & Kalkreuth, W. D. (1985). Coal Petrology-its principles, methods, and applications.

Cao, L., & Zhang, Y. (2018). Interpretation of Gibbs surface excess model for gas adsorption on heterogeneous coal particle. Fuel, 214, 20–25. https://doi.org/10.1016/j.fuel.2017.10.109

Charrière, D., Pokryszka, Z., & Behra, P. (2010). Effect of pressure and temperature on diffusion of CO2 and CH4 into coal from the Lorraine basin (France). International Journal of Coal Geology, 81(4), 373–380. https://doi.org/10.1016/j.coal.2009.03.007

Chen, G., Zhang, J., Lu, S., Pervukhina, M., Liu, K., Xue, Q., Tian, H., Tian, S., Li, J., Clennell, M. B., & Dewhurst, D. N. (2016). Adsorption Behavior of Hydrocarbon on Illite. Energy & Fuels, 30(11), 9114–9121. https://doi.org/10.1021/acs.energyfuels.6b01777

Cheng, Y., Jiang, H., Zhang, X., Cui, J., Song, C., & Li, X. (2017). Effects of coal rank on physicochemical properties of coal and on methane adsorption. International Journal of Coal Science & Technology, 4(2), 129–146. https://doi.org/10.1007/s40789-017-0161-6

Choi, J.-G., Do, D. D., & Do, H. D. (2001). Surface Diffusion of Adsorbed Molecules in Porous Media: Monolayer, Multilayer, and Capillary Condensation Regimes. Industrial & Engineering Chemistry Research, 40(19), 4005–4031. https://doi.org/10.1021/ie010195z

Clarkson, C. R., & Bustin, R. M. (1999). The effect of pore structure and gas pressure upon the transport properties of coal: A laboratory and modeling study. 1.

Isotherms and pore volume distributions. Fuel, 78(11), 1333–1344. https://doi.org/10.1016/S0016-2361(99)00055-1

Coenen, J., Glass, L.-M., & Sanderink, L. (2022). Two degrees and the SDGs: A network analysis of the interlinkages between transnational climate actions and the Sustainable Development Goals. Sustainability Science, 17(4), 1489–1510. https://doi.org/10.1007/s11625-021-01007-9

Corum, M. D., Jones, K. B., & Warwick, P. D. (2013). CO_2 Sequestration Potential of Unmineable Coal—State of Knowledge. Energy Procedia, 37, 5134–5140. https://doi.org/10.1016/j.egypro.2013.06.428

Cui, X., Bustin, R. M., & Dipple, G. (2004). Selective transport of CO_2, CH_4, and N_2 in coals: Insights from modeling of experimental gas adsorption data. Fuel, 83(3), 293–303. https://doi.org/10.1016/j.fuel.2003.09.001

Dąbrowski, A. (2001). Adsorption—From theory to practice. Advances in Colloid and Interface Science, 93(1–3), 135–224. https://doi.org/10.1016/S0001-8686(00)00082-8

Day, S., Duffy, G., Sakurovs, R., & Weir, S. (2008). Effect of coal properties on CO_2 sorption capacity under supercritical conditions. International Journal of Greenhouse Gas Control, 2(3), 342–352. https://doi.org/10.1016/S1750-5836(07)00120-X

Deevi, S., & Suuberg, E. (1987). Physical changes accompanying drying of western US lignites. Fuel, 66(4), 454–460. https://doi.org/10.1016/0016-2361(87)90147-5

Den Elzen, M., & Meinshausen, M. (2006). Meeting the EU 2°C climate target: Global and regional emission implications. Climate Policy, 6(5), 545–564. https://doi.org/10.1080/14693062.2006.9685620

Donnelly, C., Greuell, W., Andersson, J., Gerten, D., Pisacane, G., Roudier, P., & Ludwig, F. (2017). Impacts of climate change on European hydrology at 1.5, 2 and 3 degrees mean global warming above preindustrial level. Climatic Change, 143(1–2), 13–26. https://doi.org/10.1007/s10584-017-1971-7

Donohue, M. D., & Aranovich, G. L. (1998). Classification of Gibbs adsorption isotherms. Advances in Colloid and Interface Science, 76–77, 137–152. https://doi.org/10.1016/S0001-8686(98)00044-X

Dutta, P., Harpalani, S., & Prusty, B. (2008). Modeling of CO2 sorption on coal. Fuel, 87(10–11), 2023–2036. https://doi.org/10.1016/j.fuel.2007.12.015

Ediger, V. Ş. (2019). An integrated review and analysis of multi-energy transition from fossil fuels to renewables. Energy Procedia, 156, 2–6. https://doi.org/10.1016/j.egypro.2018.11.073

Edwards, G. (2020). Coal and climate change. WIREs Climate Change, 11(2). https://doi.org/10.1002/wcc.629

EIA. (2021). U.S. Energy Information Administration (EIA). https://www.eia.gov/tools/faqs/faq.php

Faiz, M., Saghafi, A., Sherwood, N., & Wang, I. (2007). The influence of petrological properties and burial history on coal seam methane reservoir characterisation, Sydney Basin, Australia. International Journal of Coal Geology, 70(1–3), 193–208. https://doi.org/10.1016/j.coal.2006.02.012

Figueroa, J. D., Fout, T., Plasynski, S., McIlvried, H., & Srivastava, R. D. (2008). Advances in CO2 capture technology—The U.S. Department of Energy's Carbon Sequestration Program. International Journal of Greenhouse Gas Control, 2(1), 9–20. https://doi.org/10.1016/S1750-5836(07)00094-1

Flores, R. M. (2014). Coalification, Gasification, and Gas Storage. In Coal and Coalbed Gas (pp. 167–233). Elsevier. https://linkinghub.elsevier.com/retrieve/pii/B9780123969729000045

Fuso Nerini, F., Sovacool, B., Hughes, N., Cozzi, L., Cosgrave, E., Howells, M., Tavoni, M., Tomei, J., Zerriffi, H., & Milligan, B. (2019). Connecting climate action with other Sustainable Development Goals. Nature Sustainability, 2(8), 674–680. https://doi.org/10.1038/s41893-019-0334-y

Gbenou, T., Fopah-Lele, A., & Wang, K. (2021). Recent Status and Prospects on Thermochemical Heat Storage Processes and Applications. Entropy, 23(8), 953. https://doi.org/10.3390/e23080953

Gensterblum, Y. (2013). CBM and CO2-ECBM related sorption processes in coal. RWTH Aachen University.

Goodman, A. L., Busch, A., Duffy, G. J., Fitzgerald, J. E., Gasem, K. A. M., Gensterblum, Y., Krooss, B. M., Levy, J., Ozdemir, E., Pan, Z., Robinson, R.

L., Schroeder, K., Sudibandriyo, M., & White, C. M. (2004). An Inter-laboratory Comparison of CO_2 Isotherms Measured on Argonne Premium Coal Samples. Energy & Fuels, 18(4), 1175–1182. https://doi.org/10.1021/ef034104h

Gray, I. (1987). Reservoir Engineering in Coal Seams: Part 1—The Physical Process of Gas Storage and Movement in Coal Seams. SPE Reservoir Engineering, 2(01), 28–34. https://doi.org/10.2118/12514-PA

Green, C. (1992). Economics and the ?greenhouse effect? Climatic Change, 22(4), 265–291. https://doi.org/10.1007/BF00142429

Gül, Y., & Küçükkarasu, O. (2020). Resource estimation for Alpagut—Dodurga coal field and determination of spatial distribution of coal quality parameters. TURKISH JOURNAL OF EARTH SCIENCES. https://doi.org/10.3906/yer-1910-17

Gumma, S. (2003). Gibbs Dividing Surface and Helium Adsorption. Adsorption, 9(1), 17–28. https://doi.org/10.1023/A:1023859112985

Guo, B., & Ghalambor, A. (2005). Properties of Natural Gas. In Natural Gas Engineering Handbook (pp. 13–33). Elsevier. https://linkinghub.elsevier.com/retrieve/pii/B9781933762418500095

Guodai, W., Linhua, P., Bingxiang, H., Jinhua, L., Ye, Z., Ruigang, Z., & Zheng, S. (2021). Adaption of Theoretical Adsorption Model on Coal: Physical Structure. Frontiers in Earth Science, 9, 691311. https://doi.org/10.3389/feart.2021.691311

Hadi Mosleh, M., Turner, M., Sedighi, M., & Vardon, P. J. (2018). Carbon dioxide flow and interactions in a high rank coal: Permeability evolution and reversibility of reactive processes. International Journal of Greenhouse Gas Control, 70, 57–67. https://doi.org/10.1016/j.ijggc.2018.01.002

Haenel, M. W. (1992). Recent progress in coal structure research. Fuel, 71(11), 1211–1223. https://doi.org/10.1016/0016-2361(92)90046-Q

Hanak, D. P., Anthony, E. J., & Manovic, V. (2015). A review of developments in pilot-plant testing and modelling of calcium looping process for CO_2 capture from power generation systems. Energy & Environmental Science, 8(8), 2199–2249. https://doi.org/10.1039/C5EE01228G

Haul, R. (1982). S. J. Gregg, K. S. W. Sing: Adsorption, Surface Area and Porosity. 2. Auflage, Academic Press, London 1982. 303 Seiten, Preis: $ 49.50. Berichte Der Bunsengesellschaft Für Physikalische Chemie, 86(10), 957–957. https://doi.org/10.1002/bbpc.19820861019

Hulme, M. (2016). 1.5 °C and climate research after the Paris Agreement. Nature Climate Change, 6(3), 222–224. https://doi.org/10.1038/nclimate2939

Humayun, R., & Tomasko, D. L. (2000). High-resolution adsorption isotherms of supercritical carbon dioxide on activated carbon. AIChE Journal, 46(10), 2065–2075. https://doi.org/10.1002/aic.690461017

IEA. (2013). Four energy policies can keep the 2°C climate goal alive—News. IEA. https://www.iea.org/news/four-energy-policies-can-keep-the-20c-climate-goal-alive

Iftekhar, S., Ramasamy, D. L., Srivastava, V., Asif, M. B., & Sillanpää, M. (2018). Understanding the factors affecting the adsorption of Lanthanum using different adsorbents: A critical review. Chemosphere, 204, 413–430. https://doi.org/10.1016/j.chemosphere.2018.04.053

International Energy Agency. (2009). CO_2 Emissions from Fuel Combustion 2009. OECD. https://www.oecd-ilibrary.org/energy/co2-emissions-from-fuel-combustion-2009_co2_fuel-2009-en-fr

IUPAC. (1976). MANUAL OF SYMBOLS AND TERMINOLOGY FOR PHYSICOCHEMICAL QUANTITIES AND UNITS, Appendix 2, Commison on Colloid and Surface Chemistry.

Izrael, Yu. A., Semenov, S. M., Anisimov, O. A., Anokhin, Yu. A., Velichko, A. A., Revich, B. A., & Shiklomanov, I. A. (2007). The fourth assessment report of the intergovernmental panel on climate change: Working group II contribution. Russian Meteorology and Hydrology, 32(9), 551–556. https://doi.org/10.3103/S1068373907090014

Kaliyavaradhan, S. K., & Ling, T.-C. (2017). Potential of CO 2 sequestration through construction and demolition (C&D) waste—An overview. Journal of CO2 Utilization, 20, 234–242. https://doi.org/10.1016/j.jcou.2017.05.014

Karimi, M., Rodrigues, A. E., & Silva, J. A. C. (2021). Designing a simple volumetric apparatus for measuring gas adsorption equilibria and kinetics of sorption. Application and validation for CO_2, CH_4 and N_2 adsorption in

binder-free beads of 4A zeolite. Chemical Engineering Journal, 425, 130538. https://doi.org/10.1016/j.cej.2021.130538

Keza, B. C. B. (2021). Measurement of CO2 Adsorption Capacity on Selected Turkish Coals for CO2 Sequestration Purposes. Middle East Technical University, Northern Cyprus Campus.

Keza, B. C. B., Argönül, A., & Alp, D. (2022). Measurement of carbon dioxide adsorption capacity on selected Turkish lignites. International Journal of Greenhouse Gas Control, 115, 103608. https://doi.org/10.1016/j.ijggc.2022.103608

Kim, H. J., Shi, Y., He, J., Lee, H.-H., & Lee, C.-H. (2011). Adsorption characteristics of CO_2 and CH_4 on dry and wet coal from subcritical to supercritical conditions. Chemical Engineering Journal, 171(1), 45–53. https://doi.org/10.1016/j.cej.2011.03.035

Király, Z., & Dékány, I. (1990). Interpretation of adsorption excess quantities: The absolute surface excess concentration. Colloid & Polymer Science, 268(7), 687–690. https://doi.org/10.1007/BF01410412

Klunk, M. A., Dasgupta, S., Das, M., & Shah, Z. (2018). System of Adsorption of CO_2 in Coalbed. Southern Brazilian Journal of Chemistry, 26(26), 2–9. https://doi.org/10.37633/sbjc.26(26)2018.2-9

Kumar, K. V., Gadipelli, S., Wood, B., Ramisetty, K. A., Stewart, A. A., Howard, C. A., Brett, D. J. L., & Rodriguez-Reinoso, F. (2019). Characterization of the adsorption site energies and heterogeneous surfaces of porous materials. Journal of Materials Chemistry A, 7(17), 10104–10137. https://doi.org/10.1039/C9TA00287A

Kumar, K. V., Porkodi, K., & Rocha, F. (2008). Comparison of various error functions in predicting the optimum isotherm by linear and non-linear regression analysis for the sorption of basic red 9 by activated carbon. Journal of Hazardous Materials, 150(1), 158–165. https://doi.org/10.1016/j.jhazmat.2007.09.020

Larsen, J. W. (2004). The effects of dissolved CO2 on coal structure and properties. International Journal of Coal Geology, 57(1), 63–70. https://doi.org/10.1016/j.coal.2003.08.001

Laubach, S. E., Marrett, R. A., Olson, J. E., & Scott, A. R. (1998). Characteristics and origins of coal cleat: A review. International Journal of Coal Geology, 35(1–4), 175–207. https://doi.org/10.1016/S0166-5162(97)00012-8

Leung, D. Y. C., Caramanna, G., & Maroto-Valer, M. M. (2014). An overview of current status of carbon dioxide capture and storage technologies. Renewable and Sustainable Energy Reviews, 39, 426–443. https://doi.org/10.1016/j.rser.2014.07.093

Li, W., Zhu, Y., Chen, S., & Zhou, Y. (2013). Research on the structural characteristics of vitrinite in different coal ranks. Fuel, 107, 647–652. https://doi.org/10.1016/j.fuel.2012.10.050

Linstrom, P. (1997). NIST Chemistry WebBook, NIST Standard Reference Database 69 [dataset]. National Institute of Standards and Technology. https://doi.org/10.18434/T4D303

Liu, H., Sang, S., Liu, S., Wu, H., Lan, T., Xu, H., & Ren, B. (2019). Supercritical-CO_2 Adsorption Quantification and Modeling for a Deep Coalbed Methane Reservoir in the Southern Qinshui Basin, China. ACS Omega, 4(7), 11685–11700. https://doi.org/10.1021/acsomega.9b00599

Liu, S., Sang, S., Ma, J., Wang, T., Du, Y., & Fang, H. (2019). Effects of supercritical CO_2 on micropores in bituminous and anthracite coal. Fuel, 242, 96–108. https://doi.org/10.1016/j.fuel.2019.01.008

Liu, Y., Zhu, Y., Liu, S., Chen, S., Li, W., & Wang, Y. (2018). Molecular structure controls on micropore evolution in coal vitrinite during coalification. International Journal of Coal Geology, 199, 19–30. https://doi.org/10.1016/j.coal.2018.09.012

Mangi, H. N., Chi, R., DeTian, Y., Sindhu, L., Lijin, He, D., Ashraf, U., Fu, H., Zixuan, L., Zhou, W., & Anees, A. (2022). The ungrind and grinded effects on the pore geometry and adsorption mechanism of the coal particles. Journal of Natural Gas Science and Engineering, 100, 104463. https://doi.org/10.1016/j.jngse.2022.104463

Martin. (2015, December 30). Sustainable Development Goals launch in 2016. United Nations Sustainable Development. https://www.un.org/sustainabledevelopment/blog/2015/12/sustainable-development-goals-kick-off-with-start-of-new-year/

Mathews, J. P., & Sharma, A. (2012). The structural alignment of coal and the analogous case of Argonne Upper Freeport coal. Fuel, 95, 19–24. https://doi.org/10.1016/j.fuel.2011.12.046

McCabe, P. J. (1984). Depositional environments ofcoal and coalbearing strata, in Sedimentology of Coal and Coalbearing Sequences: Vol. Special Publication 7 (Rahmani, R.A. and Flores, R.M., pp. 13–42). Blackwell Scientific Publications, Oxford.

Meng, M., Qiu, Z., Zhong, R., Liu, Z., Liu, Y., & Chen, P. (2019). Adsorption characteristics of supercritical CO_2/CH_4 on different types of coal and a machine learning approach. Chemical Engineering Journal, 368, 847–864. https://doi.org/10.1016/j.cej.2019.03.008

Metz, B. & Intergovernmental Panel on Climate Change (Eds.). (2005). IPCC special report on carbon dioxide capture and storage. Cambridge University Press, for the Intergovernmental Panel on Climate Change.

Miller, B. G. (2017). The Chemical and Physical Characteristics of Coal. In Clean Coal Engineering Technology (pp. 3–60). Elsevier. https://linkinghub.elsevier.com/retrieve/pii/B9780128113653000016

Mittal, M. L. (2012). Estimates of Emissions from Coal Fired Thermal Power Plants in India (p. 22). Department of Environmental and Occupational Health.

MTA. (2021). COAL EXPLORATION RESEARCH. https://www.mta.gov.tr/en/arastirmalar/komur-arama-arastirmalari

Murata, K., El-Merraoui, M., & Kaneko, K. (2001). A new determination method of absolute adsorption isotherm of supercritical gases under high pressure with a special relevance to density-functional theory study. The Journal of Chemical Physics, 114(9), 4196–4205. https://doi.org/10.1063/1.1344926

Nah, W. (2010). CO_2-ECBM optimization strategies and CO_2 storage capacity assessment of a European coalfield. Imperial College London.

NASA. (2023). Data.GISS: GISS Surface Temperature Analysis (v4): Analysis Graphs and Plots. https://data.giss.nasa.gov/gistemp/graphs_v4/

Nelson, C. R., Hill, D. G., & Pratt, T. J. (2000). Properties of Paleocene Fort Union Formation Canyon Seam Coal at the Triton Federal Coalbed Methane Well,

Campbell County, Wyoming. All Days, SPE-59786-MS. https://doi.org/10.2118/59786-MS

Nilsson, M., Chisholm, E., Griggs, D., Howden-Chapman, P., McCollum, D., Messerli, P., Neumann, B., Stevance, A.-S., Visbeck, M., & Stafford-Smith, M. (2018). Mapping interactions between the sustainable development goals: Lessons learned and ways forward. Sustainability Science, 13(6), 1489–1503. https://doi.org/10.1007/s11625-018-0604-z

NOAA. (2023, April 5). Greenhouse gases continued to increase rapidly in 2022. https://www.noaa.gov/news-release/greenhouse-gases-continued-to-increase-rapidly-in-2022

Ozdemir, E. (2004). Chemistry of the adsorption of carbon dioxide by argonne premium coals and a model to simulate CO_2 sequestration in coal seams. University of Pittsburgh.

Ozdemir, E. (2017). Dynamic nature of supercritical CO_2 adsorption on coals. Adsorption, 23(1), 25–36. https://doi.org/10.1007/s10450-016-9814-9

Ozdemir, E., Morsi, B. I., & Schroeder, K. (2004). CO_2 adsorption capacity of argonne premium coals. Fuel, 83(7–8), 1085–1094. https://doi.org/10.1016/j.fuel.2003.11.005

Ozdemir, E., & Schroeder, K. (2009). Effect of Moisture on Adsorption Isotherms and Adsorption Capacities of CO_2 on Coals. Energy & Fuels, 23(5), 2821–2831. https://doi.org/10.1021/ef801126a

Perera, M. (2018). A Comprehensive Overview of CO_2 Flow Behaviour in Deep Coal Seams. Energies, 11(4), 906. https://doi.org/10.3390/en11040906

Perera, M. S. A., Ranjith, P. G., Choi, S. K., Bouazza, A., Kodikara, J., & Airey, D. (2011). A review of coal properties pertinent to carbon dioxide sequestration in coal seams: With special reference to Victorian brown coals. Environmental Earth Sciences, 64(1), 223–235. https://doi.org/10.1007/s12665-010-0841-7

Pini, R., Marx, D., Burlini, L., Storti, G., & Mazzotti, M. (2011). Coal characterization for ECBM recovery: Gas sorption under dry and humid conditions, and its effect on displacement dynamics. Energy Procedia, 4, 2157–2161. https://doi.org/10.1016/j.egypro.2011.02.101

Purl, R., Evanoff, J. C., & Brugler, M. L. (1991). Measurement of Coal Cleat Porosity and Relative Permeability Characteristics. SPE Gas Technology Symposium. SPE Gas Technology Symposium, Houston, Texas. https://doi.org/10.2118/21491-MS

Ramasamy, S., Sripada, P. P., Khan, M. M., Tian, S., Trivedi, J., & Gupta, R. (2014). Adsorption Behavior of CO_2 in Coal and Coal Char. Energy & Fuels, 28(8), 5241–5251. https://doi.org/10.1021/ef500239b

Rice, D. D. (1993). Composition and Origins of Coalbed Gas. In B. E. Law & D. D. Rice, Hydrocarbons from Coal (pp. 159–184). American Association of Petroleum Geologists. https://pubs.geoscienceworld.org/books/book/1331/chapter/107170857

Rouquerol, J., Rouquerol, F., Llewellyn, P., & Denoyel, R. (2016). Surface excess amounts in high-pressure gas adsorption: Issues and benefits. Colloids and Surfaces A: Physicochemical and Engineering Aspects, 496, 3–12. https://doi.org/10.1016/j.colsurfa.2015.10.045

Sakurovs, R., Day, S., & Weir, S. (2009). Causes and consequences of errors in determining sorption capacity of coals for carbon dioxide at high pressure. International Journal of Coal Geology, 77(1–2), 16–22. https://doi.org/10.1016/j.coal.2008.07.001

Sakurovs, R., Day, S., Weir, S., & Duffy, G. (2007). Application of a Modified Dubinin−Radushkevich Equation to Adsorption of Gases by Coals under Supercritical Conditions. Energy & Fuels, 21(2), 992–997. https://doi.org/10.1021/ef0600614

Schmidt, L. D. (1945). Changes in coal during storage (In: Lowry, H.H.). Chemistry of Coal Utilization.

Seidle, J. (2011). Fundamentals of coalbed methane reservoir engineering. PennWell Corp.

Shojai Kaveh, N., Wolf, K.-H., Ashrafizadeh, S. N., & Rudolph, E. S. J. (2012). Effect of coal petrology and pressure on wetting properties of wet coal for CO2 and flue gas storage. International Journal of Greenhouse Gas Control, 11, S91–S101. https://doi.org/10.1016/j.ijggc.2012.09.009

Shukla, R., Ranjith, P., Haque, A., & Choi, X. (2010). A review of studies on CO_2 sequestration and caprock integrity. Fuel, 89(10), 2651–2664. https://doi.org/10.1016/j.fuel.2010.05.012

Song, Y., Xing, W., Zhang, Y., Jian, W., Liu, Z., & Liu, S. (2015). Adsorption isotherms and kinetics of carbon dioxide on Chinese dry coal over a wide pressure range. Adsorption, 21(1–2), 53–65. https://doi.org/10.1007/s10450-015-9649-9

Steele, William. (1993). Molecular interactions for physical adsorption. Chemical Reviews, 93(7), 2368–2372. https://doi.org/10.1021/cr00023a002

Stracher, G. B., Prakash, A., & Rein, G. (2015). Peat: Its Origins, Characteristics, and Geological Transformations. In Coal and Peat Fires: A Global Perspective (pp. 13–38). Elsevier. https://linkinghub.elsevier.com/retrieve/pii/B9780444595102000021

Sudibandriyo, M., Pan, Z., Fitzgerald, J. E., Robinson, R. L., & Gasem, K. A. M. (2003). Adsorption of Methane, Nitrogen, Carbon Dioxide, and Their Binary Mixtures on Dry Activated Carbon at 318.2 K and Pressures up to 13.6 MPa. Langmuir, 19(13), 5323–5331. https://doi.org/10.1021/la020976k

Sullivan, M., Rodosta, T., Mahajan, K., & Damiani, D. (2020). An overview of the Department of Energy's CarbonSAFE Initiative: Moving CCUS toward commercialization. AIChE Journal, 66(4). https://doi.org/10.1002/aic.16855

Talapatra, A. (2020). A study on the carbon dioxide injection into coal seam aiming at enhancing coal bed methane (ECBM) recovery. Journal of Petroleum Exploration and Production Technology, 10(5), 1965–1981. https://doi.org/10.1007/s13202-020-00847-y

Tambaria, T. N., Sugai, Y., & Anggara, F. (2023). Experimental measurements of CO_2 adsorption on Indonesian low-rank coals under various conditions. Journal of Petroleum Exploration and Production Technology, 13(3), 813–826. https://doi.org/10.1007/s13202-022-01569-z

The Engineering ToolBox. (2018). Carbon Dioxide—Thermophysical Properties. https://www.engineeringtoolbox.com/CO2-carbon-dioxide-properties-d_2017.html

Thomas, L. (2013). Coal geology (2nd ed). John Wiley & Sons.

Toprak, S. (2009). Petrographic properties of major coal seams in Turkey and their formation. International Journal of Coal Geology, 78(4), 263–275. https://doi.org/10.1016/j.coal.2009.03.006

United Nations. (2018). Global indicator framework for the Sustainable Development Goals and targets of the 2030 Agenda for Sustainable Development. https://unstats.un.org/sdgs/indicators/GlobalIndicatorFrameworkafterrefinement_Eng.pdf.

United Nations. (2015). Transforming our world: The 2030 Agenda for Sustainable Development | Department of Economic and Social Affairs. https://sdgs.un.org/2030agenda

U.S. Environmental Protection Agency. (n.d.). Coal Mine Methane Country Profiles. Global Methane Initiative. https://www.globalmethane.org/documents/toolsres_coal_overview_fullreport.pdf

Wang, H., & Hao, Y. (2017). Thermodynamic Study of Solar Thermochemical Methane Steam Reforming with Alternating H 2 and CO 2 Permeation Membranes Reactors. Energy Procedia, 105, 1980–1985. https://doi.org/10.1016/j.egypro.2017.03.570

Wang, J.-Y., Mangano, E., Brandani, S., & Ruthven, D. M. (2021). A review of common practices in gravimetric and volumetric adsorption kinetic experiments. Adsorption, 27(3), 295–318. https://doi.org/10.1007/s10450-020-00276-7

Weniger, S., Weniger, P., & Littke, R. (2016). Characterizing coal cleats from optical measurements for CBM evaluation. International Journal of Coal Geology, 154–155, 176–192. https://doi.org/10.1016/j.coal.2015.12.005

White, C. M., Smith, D. H., Jones, K. L., Goodman, A. L., Jikich, S. A., LaCount, R. B., DuBose, S. B., Ozdemir, E., Morsi, B. I., & Schroeder, K. T. (2005). Sequestration of Carbon Dioxide in Coal with Enhanced Coalbed Methane RecoveryA Review. Energy & Fuels, 19(3), 659–724. https://doi.org/10.1021/ef040047w

Witkowski, A., Majkut, M., & Rulik, S. (2014). Analysis of pipeline transportation systems for carbon dioxide sequestration. Archives of Thermodynamics, 35(1), 117–140. https://doi.org/10.2478/aoter-2014-0008

Wojtacha-Rychter, K., & Smoliński, A. (2017). Sorption characteristic of coal as regards of gas mixtures emitted in the process of the self-heating of coal. E3S Web of Conferences, 19, 01010. https://doi.org/10.1051/e3sconf/20171901010

Yohe, G. R. (1958). OXIDATION OF COAL. ILLINOIS STATE GEOLOGICAL SURVEY; 2012.

Zhang, L., Zeng, Y., & Cheng, Z. (2016). Removal of heavy metal ions using chitosan and modified chitosan: A review. Journal of Molecular Liquids, 214, 175–191. https://doi.org/10.1016/j.molliq.2015.12.013

Zhao, Y., Cao, S., Li, Y., Yang, H., Guo, P., Liu, G., & Pan, R. (2018). Experimental and numerical investigation on the effect of moisture on coal permeability. Natural Hazards, 90(3), 1201–1221. https://doi.org/10.1007/s11069-017-3095-9

Zhou, X., Weber, J., & Yuan, J. (2019). Poly(ionic liquid)s: Platform for CO2 capture and catalysis. Current Opinion in Green and Sustainable Chemistry, 16, 39–46. https://doi.org/10.1016/j.cogsc.2018.11.014

APPENDICES

A. Approximation of the system's void volume (V_{void})

The void volume is determined by employing the helium displacement method, which involves injecting gas into the reference cell and allowing the gas to expand in the sample cell after opening the expansion valve. Void volume is calculated once the coal sample is placed in the sample cell, ensuring the absence of any leaks in the volumetric system. The process is carried out at a constant temperature of 313.15 K. Once equilibrium is reached, the pressure readings in the reference cell (P_{RC}) and the equilibrium pressure (P_{Eq}) are recorded.

Sequential injections are performed without venting the gas out of the system, incrementing the pressure up to 80 bars. To ensure consistency in the void volume (V_{Void}) estimation, a minimum of 8 readings are taken at each pressure increment, which are then averaged to obtain the most accurate estimate, as presented in Table A.1 to A.3.

The derivation of the formula for V_{Void} involves the application of gas law and mass balance equations. For the first He injection before equilibrium, the following equation describes the moles of gas injected (n_{inj1}).

$$n_{RC1} = n_{inj1} = injected\ moles$$

$$P_{RC1} * V_{RC} = Z_{RC1} * n_{RC1} * R * T \qquad \text{A.1}$$

Where P_{RC1} represents the pressure in the reference cell during the initial injection, while V_{RC} denoted the volume within the reference cell at that point. Z_{RC1} signifies

the compressibility factor corresponding to P_{RC1}. Here, R stands for the universal gas constant, and T symbolizes the temperature, specifically set at 313.15 K.

Moles for 1st injection once equilibrium is reached:

$$n_{Eq1} = n_{RC1} = Equlibrium\ moles$$

$$P_{Eq1} * (V_{RC} + V_{Void}) = n_{Eq1} * Z_{Eq1} * R * T \quad \text{A.2}$$

$$V_{\text{Void}} = V_{SC} - V_{\text{ske}}$$

where, V_{SC} is the volume of the sample cell calculated initially by helium expansion and V_{ske} is the volume of the coal sample added to the sample cell before each experiment.

Similar principles apply to the second injection and subsequent injections, as residual gas from previous injections remains in the system.

For the second injection before equilibrium, the moles of injected gas (n_{inj2}) are:

$$n_{RC2} = n_{inj2} = injected\ moles$$

$$P_{RC2} * V_{RC} = n_{RC2} * Z_{RC2} * R * T \quad \text{A.3}$$

For the equilibrium after the 2nd injection, mass conservation is employed since the gas from the previous injection is retained in the system. The remaining mole of gas is referred to as residual moles (n_{Res1}).

$$P_{Eq2} * (V_{RC} + V_{Void}) = n_{Eq2} * Z_{Eq2} * R * T \quad \text{A.4}$$

Where equilibrium moles for the second injection is:

$$n_{Eq2} = n_{inj2} + n_{Res1}$$

$$n_{inj2} = \frac{P_{RC2} * V_{RC}}{Z_{RC2}}$$

$$n_{Res1} = \frac{P_{Eq1} * V_{Void}}{Z_{Eq1}}$$

Combining the equations, the void volume (V_{Void}) can be expressed in terms of the known quantities:

$$n_{Eq2} = \frac{P_{RC2} * V_{RC}}{Z_{RC2}} + \frac{P_{Eq1} * V_{Void}}{Z_{Eq1}}$$

Making V_{Void} the subject in the above equation:

$$V_{Void} = \left(\frac{\frac{P_{RC2}}{Z_{RC2}} - \frac{P_{Eq2}}{Z_{Eq2}}}{\frac{P_{Eq2}}{Z_{Eq2}} - \frac{P_{Eq1}}{Z_{Eq1}}} * V_{RC} \right) \quad \text{A.5}$$

For multiple injections (n) Equation A.5, the equation becomes:

$$\boxed{V_{Void(n)} = \left(\frac{\frac{P_n}{Z_n} - \frac{P_{Eq(n)}}{Z_{Eq(n)}}}{\frac{P_{Eq(n)}}{Z_{Eq(n)}} - \frac{P_{Eq(n-1)}}{Z_{Eq(n-1)}}} * V_{RC} \right)}$$

Table A.1 through Table A.3 presents the results of estimated void volume for the three coal samples obtained from individual experimental trials, each having different sample weight.

Table A.1. Çankırı sample results for the V_{Void}

Exp #	Sample weight (g-daf)	P_{RC} (bars)	P_{EQ} (bars)	V_{Void} (cc)	Avg V_{void} (cc)
1	29.99	14.7	10.8	49.09	50.43
		23.8	18.5	49.38	
		30.7	25.6	51.54	
		37.4	32.5	50.95	
		46.2	40.6	49.60	
		54.2	48.6	50.23	
		70.2	61.1	52.23	
2	33.71	13.3	9.7	48.74	48.49
		22	17	49.14	
		31	25.4	47.83	
		40.2	34.2	48.92	
		48.6	42.8	48.39	
		59.4	52.7	48.56	
		72.2	64.4	47.83	
3	38.88	11.8	8.6	47.83	45.37
		19.3	15.2	44.57	
		28.4	23.3	45.18	
		35.5	30.8	44.96	
		47.8	41.3	44.41	
		61.7	53.8	45.34	
		82.5	71.4	45.25	

Table A.2. Elazığ Sivrice sample results for the V_{Void}

Exp #	Sample weight (g-daf)	P_{RC} (bars)	P_{EQ} (bars)	V_{Void} (cc)	Avg V_{void} (cc)
1	33.75	13.7	9.4	46.75	46.58
		22.8	17.6	45.50	
		30.3	25.3	46.59	
		40.7	34.6	47.06	
		49.3	43.5	46.6	
		59.3	53.1	46.34	
		74.3	65.9	47.09	
2	31.94	12.6	9.1	49.24	48.21
		20.5	16	46.79	
		28.8	23.6	49.09	
		35.7	30.8	48.83	
		42.4	37.7	48.87	
		52.2	46.4	47.83	
		62.1	55.9	46.83	
3	33.6	10.6	7.9	46.13	46.93
		18.9	14.6	46.05	
		24.5	20.6	46.64	
		35	29.3	47.01	
		43.4	37.8	47.27	
		55.5	48.5	46.94	
		66.6	59.3	48.50	

Table A.3. Amasya Merzifon sample results for the V_{Void}

Exp #	Sample weight (g-daf)	P_{RC} (bars)	P_{EQ} (bars)	V_{Void} (cc)	Avg V_{void} (cc)
1	32.80	12.2	8.5	56.48	54.79
		18.8	14.4	53.51	
		27.4	21.8	54.30	
		39.5	31.9	53.99	
		47	40.5	54.23	
		57.4	50.1	54.56	
		68.9	60.7	55.50	
		83.8	73.7	55.74	
2	35.60	17.9	12.7	52.55	52.37
		26.9	20.9	52.50	
		38.2	31	51.15	
		43.8	38.4	52.36	
		49.7	44.9	52.98	
		61.3	54.4	52.11	
		80.3	69.3	52.97	
3	36.10	16.3	11.5	52.18	51.25
		26.4	20.2	51.13	
		36.7	29.9	50.30	
		48.3	40.6	51.63	
		56.1	49.7	50.46	
		64.4	58.2	52.34	
		79.7	70.8	50.68	

B. Derivation of RC and SC volumes using graphical approach

The volume of the reference cell (V_{RC}) and the sample cell (V_{SC}) is determined by the He expansion method. The process is carried out in two stages at a constant temperature of 313.15K. Firstly, helium gas is sequentially injected into empty cells in increments up to 100 bars. The gas expands in the sample cell, and pressure readings, P_{RC} and P_{SC}, are recorded at each incremental stage. Then, the sample cell is loaded with a cylindrical disk of the known volume, and similar pressure readings are recorded. The constant volume of the cylindrical disk (V_{disk}) used in this study is 7.713 cc.

The equations derived for the unknown parameters V_{RC} and V_{SC} are based on the gas equation of state.

When the gas is in the reference cell, the following equation holds:

$$P_1 V_{RC} = Z_1 n_1 R T_1 \qquad \text{B.1}$$

When the gas is expanded into the sample cell, the equation becomes:

$$P_2 (V_{RC} + V_{SC}) = Z_2 n_1 R T_1 \qquad \text{B.2}$$

When the disk is present in the sample cell, the equation is expressed as:

$$P_3 (V_{RC} + V_{SC} - V_{disk}) = Z_3 n_1 R T_1 \qquad \text{B.3}$$

Manipulating Equations B.1 and B.2, we can express Z_1 and Z_2 in terms of the other variables:

$$\frac{P_1}{P_2} * \frac{V_{RC}}{V_{RC}+V_{SC}} = \frac{Z_1}{Z_2}$$

By rearranging the equation, we obtain a straight-line equation: $y = m_A * x$

$$P_2 Z_1 = \left(\frac{V_{RC}}{V_{RC} + V_{SC}}\right) * P_1 Z_2$$

Similarly, manipulating Equations B.1 and B.3, we can express Z_1 and Z_3 in terms of the other variables:

$$\frac{P_1}{P_3} * \frac{V_{RC}}{V_{RC}+V_{SC}-V_{disk}} = \frac{Z_1}{Z_3}$$

By rearranging the equation, we obtain a straight-line equation: $y = m_B * x$

$$P_3 Z_1 = \left(\frac{V_{RC}}{V_{RC}+V_{SC}-V_{disk}}\right) * P_1 Z_3$$

By plotting P_2*Z_1 versus P_1*Z_2 and P_3*Z_1 versus $P1*Z_3$, we can observe linear relationship with slopes m_A and m_B, respectively. These slopes can be calculated.

From the graphical line equations, the gradients are:

$$m_A = \frac{V_{RC}}{V_{RC}+V_{SC}}$$

$$V_{RC} = m_A * (V_{RC}+V_{SC}) \longrightarrow \text{eqn (i)}$$

$$m_B = \frac{V_{RC}}{V_{RC}+V_{SC}-V_{disk}}$$

$$V_{RC} = m_B * (V_{RC}+V_{SC}-V_{disk}) \longrightarrow \text{eqn (ii)}$$

By substituting Equation (i) into Equation (ii), we can solve it simultaneously. The resulting equation for the reference cell volume (V_{RC}) is:

$$V_{RC} = \frac{m_A * m_B}{m_B - m_A} * V_{disk} \qquad \text{B.4}$$

To derive the equation for the sample cell volume (V_{SC}), we substitute Equation (i) into the final V_{RC} equation:

$$V_{RC} = m_A * (V_{RC}+V_{SC})$$

$$V_{RC} = \frac{m_A * V_{SC}}{1-m_A} \longrightarrow \text{eqn (iii)}$$

Substituting Equation (iii) into the final V_{RC} equation, we find:

$$\frac{m_A * V_{SC}}{1 - m_A} = \frac{m_A * m_B}{m_B - m_A} * V_{disk}$$

The resulting equation for sample cell volume (V_{SC}) is:

$$V_{SC} = \frac{m_B * V_{disk}}{m_B - m_A} * (1 - m_A) \qquad \text{B.4}$$

Table B. 2. Estimation of reference cell (RC) and sample cell (SC)

Pressure readings for an empty system			**Pressure readings with disk in SC**		
P_{RC}, bars	P_{EQ}, bars	m_A	P_{RC}, bars	P_{EQ}, bars	m_B
11.6	5.7	0.491	10.8	5.6	0.518
22.4	11.1	0.495	20.8	10.9	0.52
30.6	15.2	0.496	30.5	16	0.524
40.4	20	0.495	42	21.9	0.521
52.4	25.9	0.494	52.1	27.2	0.522
60.5	29.9	0.494	61.4	32	0.521
70.5	34.8	0.493	71.9	37.5	0.521
81	39.9	0.492	87	45.4	0.521
92.6	45.5	0.491	95	49.2	0.517
From the line eqn m_A:		**0.493**	**From the line eqn m_B:**		**0.521**
V_{RC} = 71.75 cc and **V_{SC}** = 73.76 cc					

C. Adsorbed moles calculation

Real gas law states:

$$P * V = Z * n * R * T \quad \text{C.1}$$

At the first injection before equilibrium:

$$P_1 * V_{RC} = Z_1 * n_{inj} * R * T \quad \text{C.2}$$

First injection after equilibrium:

$$P_{Eq1} * (V_{RC} + V_{Void}) = Z_{Eq1} * n_{free} * R * T \quad \text{C.6}$$

The mass balance after the first injection:

$$n_{inj} = n_{free} + n_{adsorbed} \quad \text{C.7}$$

Adsorbed moles after the first injection:

$$n_{ads} = n_{inj} - n_{free} \quad \text{C.8}$$

$$n_{ads} = \frac{V_{RC}}{R * T} * \left(\frac{P_1}{Z_1} - \frac{P_{Eq1}}{Z_{Eq1}}\right) - \left(\frac{P_{Eq1}}{Z_{Eq1}}\right) * \frac{V_{Void}}{R * T} \quad \text{C.9}$$

Similarly, the mass balance at the second injection:

$$n_{inj} + n_{res} = n_{free} + n_{ads}$$

Where, n_{res} are the residual moles, n_{ads} are the adsorbed moles.

Equation for the second injection before equilibrium and after equilibrium are as follows:

$$P_2 * V_{RC} = Z_2 * n_{inj} * R * T \quad \text{C.10}$$

$$P_{Eq2} * (V_{RC} + V_{Void}) = Z_{Eq2} * n_{free} * R * T \quad \text{C.11}$$

Moles present from the previous injection:

$$P_{Eq1} * V_{Void} = Z_{Eq1} * n_{res} * R * T \quad \text{C.12}$$

Moles adsorbed after the second injection:

$$n_{ads} = n_{inj} + n_{res} - n_{free}$$

$$n_{ads} = \left(\frac{V_{RC}}{R * T}\right) * \left(\frac{P_2}{Z_2} - \frac{P_{Eq2}}{Z_{Eq2}}\right) - \left(\frac{P_{Eq2}}{Z_{Eq2}} - \frac{P_{Eq1}}{Z_{Eq1}}\right) * \left(\frac{V_{Void}}{R * T}\right) \quad \text{C.13}$$

Similar procedure will be followed at each sequentially higher pressure. Final equation at any injection pressure will be as follows:

$$n_{ads} = \left(\frac{V_{RC}}{R * T}\right) * \left(\frac{P_n}{Z_n} - \frac{P_{Eq(n)}}{Z_{Eq(n)}}\right) - \left(\frac{P_{Eq(n)}}{Z_{Eq(n)}} - \frac{P_{Eq(n-1)}}{Z_{Eq(n-1)}}\right) * \left(\frac{V_{Void}}{R * T}\right) \quad \text{C.14}$$

D. Adsorbed phase density determination (ρ_a)

The calculation of the adsorbed density (ρ_a) is obtained by employing Equation 3.12, displayed below. According to the existing literature, it has been proposed that if the adsorbed phase extends beyond the surface of the coal to a measurable distance, the excess adsorbed amount (n_{ex}) can be mathematically expressed in relation to the adsorbed phase density and free gas phase density (Song et al., 2015).

$$n_{ex} = n_{abs} - \rho_g \left(-\frac{n_{abs}}{\rho_a}\right)$$

This study utilizes a graphical approach to estimate the adsorbed phase density. This is achieved by plotting excess adsorption (n_{ex}) against free gas density (ρ_g), as demonstrated in Figure D.1. The graph shown clearly demonstrates a linear relationship between n_{ex} and ρ_g (P,T) at higher densities. This indicates that a constant density is achieved for the adsorbed phase after a certain point, when the excess adsorption (n_{ex}) gradually diminishes until it reaches zero. Therefore, by employing a linear equation to model this linear segment, it is possible to determine the exact point of intersection at which the number of moles becomes zero, which serves as an indicator of the adsorbed density (ρ_a).

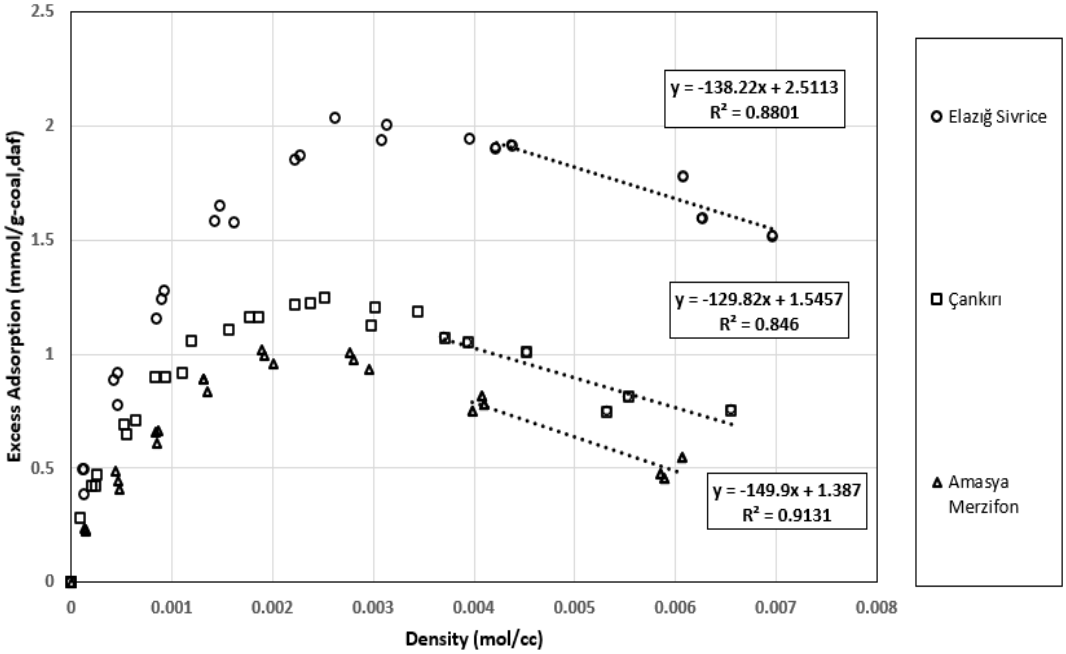

Figure D.1. Graphical estimation of adsorbed phase density

E. Estimation of Z factor and free gas density for CO_2

Isothermal properties for CO_2 are generated at 313.15 K from National Institute of Standard and Technology chemistry webbook. (Linstrom, 1997). Required parameters such as compressibility Z-factor, Figure E.1, and free gas density (ρ_g), Figure E.2, are obtained for CO_2 from the graph below.

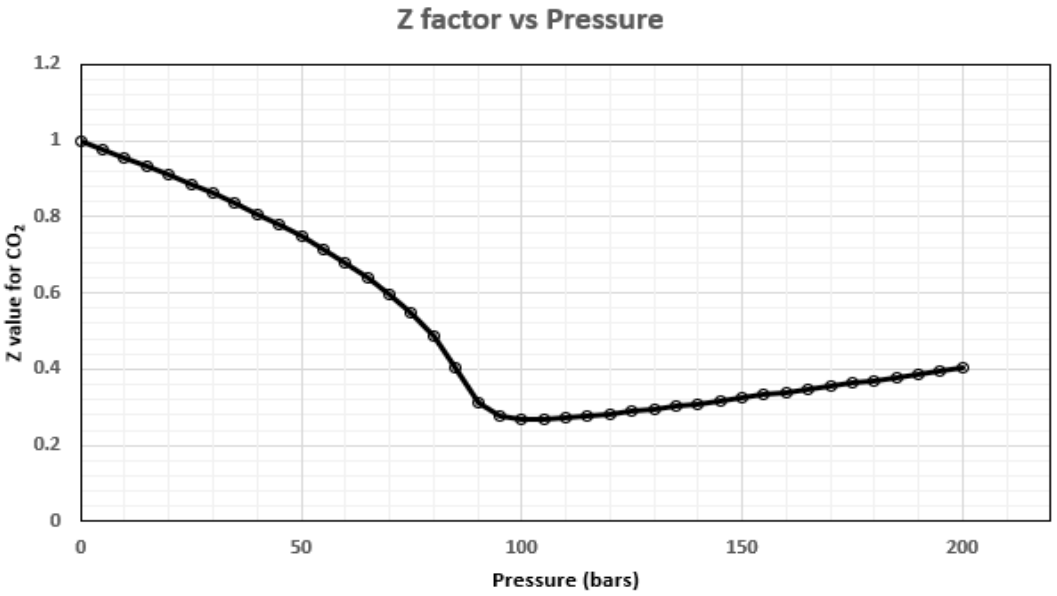

Figure E.1. Z factor for CO_2 at 313.15 K

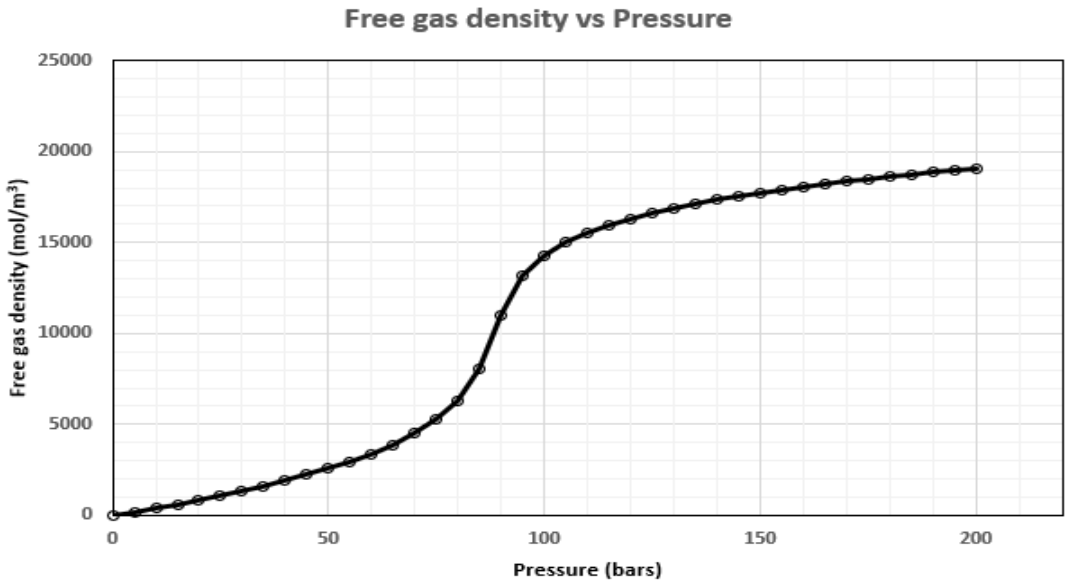

Figure E.2. Free gas density of CO_2 at 313.15 K

F. Thermophysical properties for CO_2

Thermophysical properties used in this study and the phase diagram for CO_2 are provided in Table F.1 and Figure F.1 respectively.

Table F. 2. Thermophysical properties for CO_2 (Linstrom, 1997)

Property	**Value**
Molecular Formula	CO_2
Molecular Weight (M)	Approximately 44.01 g/mol
Critical Temperature (T_c)	304.21 K (31.04°C)
Critical Pressure (P_c)	73.8 bars (72.9atm)
Critical Density (ρ_c)	0.467 g/cc
Tripple Point Temperature (T_p)	216.59 K (-56.56°C)
Tripple Point Pressure (P_p)	5.18kPa
Compressibility Factor (Z)	Varies with T and P; Z=1 at T_c and P_c
Specific Volume at 1atm	547 cc/g

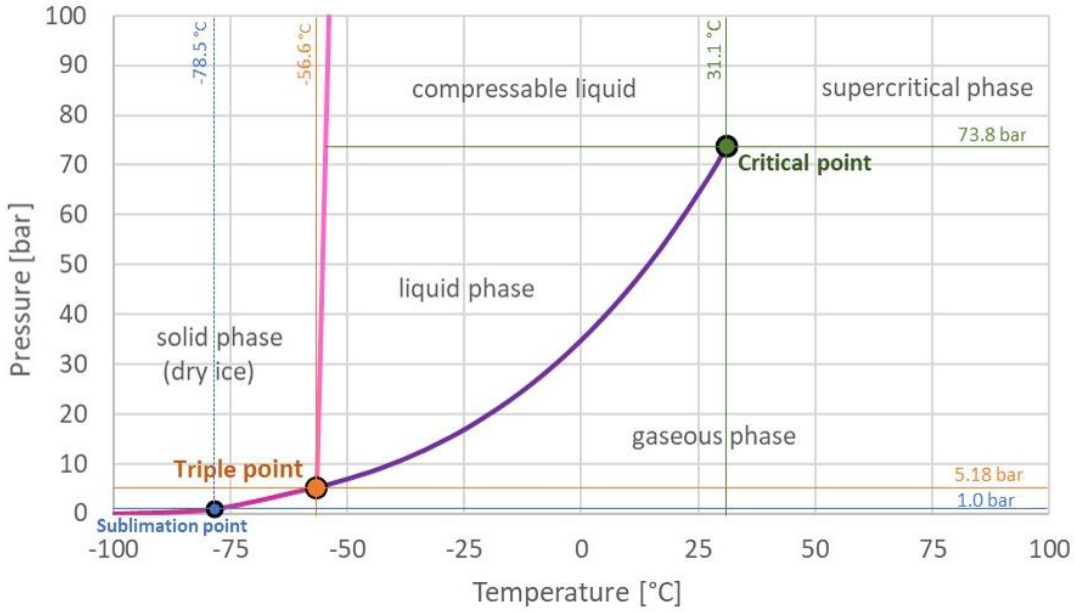

Figure F.1. Phase diagram for CO_2 (The Engineering ToolBox, 2018)

G. Experimental results for excess adsorption (n_{ex})

The following tables from G.1-G.3 present the aggregated findings of excess adsorption obtained from volumetric adsorption experiments conducted on three coal samples at a temperature of 313.15 K. The studies were carried out using varied weights of the coal samples in each trial.

Table G. 4. Çankırı sample results for excess adsorption

Exp#	P_{RC}, bars	P_{EQ}, bars	Excess adsorption (n_{ex}), mmol/g
Trial 1 Weight=29.99 g	0	0	0
	6.8	2.3	0.280
	11.4	6.6	0.470
	19.7	13.5	0.648
	26.4	20	0.897
	33.3	27.3	1.058
	45.1	37.9	1.161
	53.2	47.2	1.220
	60.7	55.7	1.203
	68.4	63.2	1.069
	80	75.3	0.747
Trial 2 Weight=33.71 g	13.4	5.3	0.421
	20.8	13.1	0.692
	29.4	22	0.896
	43.1	34.3	1.105
	51.9	45	1.215
	60.6	55.3	1.123
	70.4	65.4	1.048
	80.5	76.3	0.810
Trial 3 Weight=38.88 g	15.4	6.3	0.422
	24.1	15.5	0.705
	33.2	25.4	0.915
	48.8	39.4	1.160
	55.4	49.4	1.246
	65.9	60.6	1.183
	74.1	70.2	1.006
	84	80.7	0.752

Table G. 5. Elazığ Sivrice sample results for excess adsorption

Exp#	P_{RC}, bars	P_{EQ}, bars	Excess adsorption (n_{ex}), mmol/g
Trial 1 Weight=33.75 g	0	0	0
	11	3.3	0.493
	20.8	11.5	0.913
	31	21.7	1.274
	45.1	35.3	1.578
	53.6	45.9	1.870
	63.6	57.1	2.004
	72.5	67.7	1.902
	83.5	79.8	1.591
Trial 2 Weight=31.94 g	10.5	3.1	0.496
	19.2	10.6	0.887
	30.7	21.2	1.240
	42.3	32.6	1.647
	53.2	45	1.853
	63.1	56.5	1.937
	74.8	69	1.912
	82.6	78.9	1.775
Trial 3 Weight=33.6 g	10.1	3.5	0.384
	20.4	11.5	0.774
	29	20.2	1.157
	41.5	31.6	1.583
	62.4	50.8	2.031
	71.9	65.5	1.944
	86.2	81.9	1.517

Table G. 6. Amasya Merzifon sample results for excess adsorption

Exp#	P_{RC}, bars	P_{EQ}, bars	Excess adsorption (n_{ex}), mmol/g
Trial 1 Weight=32.8 g	0	0	0.227
	8.8	3.6	0.409
	19.3	11.7	0.610
	28	20.2	0.837
	38.8	30.2	0.960
	50	41.7	0.935
	62.8	55	0.751
	71.2	65.7	0.456
	82.7	78	0.227
Trial 2 Weight=35.6 g	8.5	3.3	0.235
	19.4	11.5	0.447
	27.8	20	0.657
	37.9	29.6	0.889
	47.7	40.2	0.996
	60.4	53	0.976
	73	66.7	0.780
	82	77.8	0.478
Trial 3 Weight=36.1 g	9.1	3.5	0.231
	18.6	11.5	0.487
	28.4	20.2	0.667
	37.5	31.6	0.890
	47.3	50.8	1.022
	59.7	65.5	1.005
	72.8	81.9	0.817
	83.1	78.8	0.548

TEZ İZİN FORMU / THESIS PERMISSION FORM

PROGRAM / PROGRAM

Sürdürülebilir Çevre ve Enerji Sistemleri / Sustainable Environment and Energy Systems ☑

Siyaset Bilimi ve Uluslararası İlişkiler / Political Science and International Relations ☐

İngilizce Öğretmenliği / English Language Teaching ☐

Elektrik Elektronik Mühendisliği / Electrical and Electronics Engineering ☐

Bilgisayar Mühendisliği / Computer Engineering ☐

Makina Mühendisliği / Mechanical Engineering ☐

YAZARIN / AUTHOR

Soyadı / Surname : Alvi

Adı / Name : Syed Muhammad Hussain Turab

Programı / Program : Sustainable Environment and Energy Systems

TEZİN ADI / TITLE OF THE THESIS (İngilizce / English) :

Experimental Investigation of CO2 Adsorption on Selected Turkish Lignite Coals

TEZİN TÜRÜ / DEGREE: **Yüksek Lisans / Master** ☑ **Doktora / PhD** ☐

1. **Tezin tamamı dünya çapında erişime açılacaktır. /** Release the entire work immediately for access worldwide. ☐

2. **Tez iki yıl süreyle erişime kapalı olacaktır. /** Secure the entire work for patent and/or proprietary purposes for a period of **two years.** * ☐

3. **Tez altı ay süreyle erişime kapalı olacaktır. /** Secure the entire work for period of **six months.** * ☑

Yazarın imzası / Author Signature ..... **Tarih / Date** 31st - August - 2023

Tez Danışmanı / Thesis Advisor Full Name: Assist.Prof.Dr Doruk Alp

Tez Danışmanı İmzası / Thesis Advisor Signature: .....

Eş Danışmanı / Co-Advisor Full Name: Dr.-Ing. Aykut Argönül

Eş Danışmanı İmzası / Co-Advisor Signature: .....

Program Koordinatörü / Program Coordinator Full Name: Canras Batunlu

Program Koordinatörü İmzası / Program Coordinator Signature: .....